TECHNISCHE UNIVERSITÄT MÜNCHEN

Fakultät für Medizin

Klinikum rechts der Isar

Nuklearmedizinische Klinik und Poliklinik

Relationship between in-vivo [^{11}C]PiB PET Signal and Amyloid-β Plaque Pathology in different transgenic Mouse Models of Alzheimer's Disease

Boris Gerhard Jaroslav von Reutern

Vollständiger Abdruck der von der Fakultät für Medizin der Technischen Universität München zur Erlangung des akademischen Grades eines

Doctor of Philosophy (Ph.D.)

genehmigten Dissertation.

Vorsitzende: Univ.-Prof. Dr. G. Multhoff

Prüfer der Dissertation:

1. apl. Prof. Dr. S. Ziegler

2. Priv.-Doz. Dr. A. Beer

Die Dissertation wurde am 17.09.2012 bei der Fakultät für Medizin der Technischen Universität München eingereicht und durch die Fakultät für Medizin am 24.09.2012 angenommen.

Abstract in English:

The quantitative relationship between the in-vivo signal of amyloid-β (Aβ) positron emission tomography (PET) imaging with [^{11}C]6-OH-BTA-1 (PiB) in transgenic mouse models of Alzheimer's disease and the underlying histopathology is so far ill-defined. In this study we compared a single transgenic APP (Tg2576) and a double transgenic APP/PS1 (ARTE10) mouse model. We performed PiB PET imaging followed by an automated quantification of Aβ plaque histopathology using three different stainings: Thioflavin S (TfS), immunofluorescence against full-length Aβ peptide, and against N3-pyroglutamate-Aβ peptide (N3pE-Aβ). PET images were analysed with a region-of-interest-based and a voxel-based approach. We found the highest correlation between TfS plaque load and PET results. Voxel-based analysis revealed a pattern of significant voxels which resembles the pattern of Aβ plaque distribution in the mouse brain. Our results suggest that the amount of highly-dense TfS positive plaques but not the amount of diffuse TfS negative plaques is the determining factor for in-vivo PiB imaging. The presence of N3pE-Aβ did not relevantly influence the PET signal.

Abstract in Deutsch:

Der quantitative Zusammenhang zwischen dem in-vivo Signal der Amyloid-β (Aβ) Bildgebung mittels Positronen-Emissions-Tomographie (PET) mit [^{11}C]6-OH-BTA-1 (PiB) in transgenen Mausmodellen der Alzheimer Erkrankung und der zugrunde liegenden Histopathologie ist bisher nicht ausreichend geklärt. Diese Arbeit vergleicht ein einfach-transgenes APP (Tg2576) und ein doppelt-transgenes APP/PS1 (ARTE10) Mausmodell. Nach einem PiB PET-Scan wurde mittels drei histologischer Färbungen die Aβ-Plaque-Pathologie quantifiziert: Thioflavin S (TfS), Immunofluoreszenz gegen unmodifiziertes Aβ-Peptid und gegen N3-Pyroglutamat-Aβ-Peptid (N3pE-Aβ). Das PET-Signal wurde region-of-interest- und voxel-basiert ausgewertet. Die höchste Korrelation zwischen PET-Signal und Histopathologie wurde für TfS gemessen. Das Muster signifikanter Voxel in der voxel-basierten Analyse ähnelte der Aβ-Plaque-Verteilung im Maushirn. Unsere Ergebnisse legen nahe, dass die Menge der dichten TfS-positiven und nicht die der diffusen TfS-negativen Plaques maßgebend für die in-vivo PiB-Bildgebung ist. N3pE-Aβ beeinflusste das PET-Signal unwesentlich.

Table of Contents:

1. Introduction

1.1 Alzheimer's - a neurodegenerative disorder

1.1.1 Definition and characteristics of neurodegenerative diseases

Neurodegenerative diseases (ND) is an umbrella term for a group of primary diseases of the neuron with the defining feature of a progressive loss of functioning neurons[1]. Diseases primarily affecting not the neuron per se but rather attributes, such as the myelin sheath as seen in multiple sclerosis, are not regarded as neurodegenerative. The same applies to a loss of neurons secondary to an exposure to hypoxia, poison, infection, trauma or other external factors. In contrast, the term dementia does not refer to a primary disease but to a syndrome affecting various higher cognitive functions such as memory, orientation, language, attention and problem solving. This syndrome can be caused by a large group of neurological disorders. ND involve different specific groups of neurons and therefore different functional systems with multifaceted pathological and clinical expressions. Dementia and movement disorders are the most commonly observed symptoms of ND[2]. In general, ND show a sporadic occurrence but multiple hereditary forms are known[3]. Either form progresses relentlessly and so far, there is no effective treatment stopping the process after it has been triggered once[4].

Great progress towards a better understanding of the pathogenesis of ND has been achieved over the past decades[5]. However, the underlying reasons for triggering a ND remain as well in the dark as the reasons for the consecutive cell damage[4]. This uncertainty is reflected in the classification of the assumingly more than hundred ND with none of the already refined classifications being entirely satisfactory[6]. Different classifications were proposed[7] of which for a long time the most popular categorization was based on histopathological hallmarks, such as the presence and topography of particular inclusions or deposits, together with the predominant clinical symptoms[8]. A new school of thought arose with advancing research technologies and successive enlightening of the

molecular characteristics of the ND[9,10]. This leads to classifications based on the observation that most ND share the feature of misfolded proteins, leading to the concept of ND as "proteinopathies"[11-14]. Of these proteinopathies, Alzheimer's disease (AD) is far the most frequent[15].

1.1.2 Brief history of Alzheimer's disease

With respect to the publications of Alois Alzheimer in 1906 and 1907, AD is regarded a disease that was discovered more than a century ago. However, for several decades, the condition described by Alois Alzheimer received only little attention in the scientific community. It was widely accepted that AD was a very rare pre-senile disorder and entirely different from senile dementia[16]. This situation changed dramatically in the 1970s when evidences accumulated that the senile dementia was indeed that described by Alzheimer [17,18] and the major cause of dementia in the elderly population[19]. Most of our knowledge about AD was gathered within the last three decades and the little attention that was formerly given to this disease turned into the complete opposite with great efforts and research resources being invested in this field[20].
There are at least more than 50 different diseases that can lead to dementia[21] but by far the most common cause of dementia is AD[22,23]. Today, the awareness of AD reaches beyond the scientific communities and medical professionals. In certain contexts, AD even became a winged word and is sometimes used synonymously or being confounded with dementia by non-professionals and public media. The impact of the disease on aging societies becomes more and more subject of public discussion[24].

1.1.3 Epidemiology and social impact of Alzheimer's disease

The estimated lifetime risk of developing AD adds to 10-11% in males and 14-17% in females by the age of 85[25]. Hereby the prevalence rates for AD rise exponentially with age, increasing markedly after the age of 65[26,27]. In 2005, *Alzheimer's Disease International*, the international federation of Alzheimer

associations around the world, estimated that 24.2 million people lived with dementia at that time, with 4.6 million new cases arising every year[28].

AD and dementia have substantial economic consequences for aging societies[29]. Studies on disability found that dementia was the most important contributor to disability in the elderly and contributed more years-of-disability in people aged at least 65 years than stroke, musculoskeletal disease or cancer[30]. AD is also a major determinant of mortality[31,32]. While AD is a major cause leading to nursing home placement[22,33,34], most patients with dementia live at home and receive unpaid help from family members or members of the same household[35]. This informal care is an important part of the burden of AD on a society and estimated in value of several milliard Euros per year[22]. Those AD caregivers carry a significant cost, not only financial, but also concerning their own health[36].

In light of this development, there is a high need for causal treatments or at least remedies to decrease the pace at which clinical symptoms progress. Our understanding of the pathogenesis and risk factors as well as advances in our ability to early and specifically diagnose AD will play a pivotal role for extenuating the economic and social consequences of AD[37].

1.1.4 Pathogenesis and symptoms of Alzheimer's disease

Neuropathologically, AD is defined by the presence of two cardinal lesions[38]: extracellularly deposited Aβ and intracellularly deposited neurofibrillary tangles (NFT) consisting of hyperphosphorylated and aggregated tau protein, a protein that stabilizes microtubules. The predominant hypothesis of the pathogenesis of AD is ostensible simple. The Aβ peptide is the result of two sequential enzymatic cleavages of the amyloid precursor protein (APP) by the β-secretase and then the γ-secretase. Aβ shows a disposition to aggregate as β-sheet-pleated protein and exists at least intermediately as soluble oligomers before it forms highly insoluble fibrils that eventually deposit as plaques in the brain parenchyma[39]. There is evidence that the soluble forms are the main neurotoxins[40] which damage the neurons and stimulate the formation of NFT,

thereby linking the two major AD pathologies[41,42]. This hypothesis is usually called the amyloid (cascade) hypothesis and is backed by an enormous amount of evidence from multiple areas of biological research[43]. According to Braak[44], this cascade begins in the temporal lobe in transentorhinal region (clinically silent stages I and II), proceeds into cortical and subcortical components of the limbic system (stages III and IV - incipient AD), and eventually extends into association areas of the neocortex (stages V and VI - fully developed AD) leading to atrophy primarily of the frontal and temporal association cortices. Interestingly, the sequential appearance of AD pathology resembles, but in reverse order, the cortical myelination process and thus the maturation process of the human brain[45]. While the affection of the limbic system causes the prominent symptom of memory deficits, the further course involves also non-amnestic symptoms[46] affecting language[47], spatial cognition, executive function, mood and troublesome and disruptive behaviours[48]. Also psychosis[49] and motor dysfunction such as parkinsonism[50] lie within the spectrum of symptoms.

However, at a closer look, several pitfalls challenge our model of the AD pathogenesis of which only a few will be mentioned here. Foremost, the exact mechanism of how the cell damage by both of the cardinal lesions occur is still not known[39]. Several mechanism potentially play a role[51] such as synaptic failure, oxidative stress, metabolic and mitochondrial dysfunction, but the direct relation remains in question and also the linkage of Aβ to tau pathology is far from being well understood[52]. The complexity further unfolds through the observation that Aβ on the one hand seems to play the leading part of the pathophysiologic cascade[53], but on the other hand might not be necessary for the progression of the disease. For instance, it has been suggested that tau pathology, once triggered, can propagate within the brain and does not require the presence of Aβ[54]. Furthermore there is growing evidence that even after removal of a great portion of the Aβ deposits, clinical symptoms neither improve nor are stopped from progression[52,55]. To further complicate things, NFT pathology seems indeed to better reflect the clinical severity than Aβ pathology[56], but observations in mouse models[57] as well as human data[58]

suggest that the link between NFT and cell death is also not as strong as it has been supposed.
In light of these evidences, other hypotheses for the pathogenesis of AD have been suggested but struggle also with open questions and contradicting evidences[52]. Together, this illustrates our still fragmentary knowledge of AD pathogenesis.

1.1.5 Genetics and risk factors for Alzheimer's Disease

AD is commonly classified according to family history and age of onset[59,60]. Table 1 summarises these classifications and gives the definitions. Genetic risk factors influencing family history and age of onset are being studied intensively and may be divided into three categories[59]: (1) rare autosomal dominant mutations, (2) common mutations or variants with a moderate effect and (3) common mutations or variants with a small effect. However, the relationship between genetic factors, age of onset and family history is complex and often not well understood.
Mutations of three genes are held responsible for more than 80% of autosomal dominant inherited AD: Amyloid precursor protein (APP), Presenilin1 (PS1 or PSEN1) and rather rarely Presenilin 2 (PS2 or PSEN2). These mutations show an almost complete penetrance for causing AD and are all connected to the cleavage of the APP and thus to the production of Aβ. Together more than one hundred mutations of these loci have been reported so far[61]. Autosomal dominant forms account for the majority of early onset cases[62], though it has been estimated that up to 40% of early onset cases are sporadic i.e. have a negative family history[63]. In turn, not all of these mutations necessarily lead to an early onset of the disease[64].
Moderate effects relative to the autosomal dominant mutations are mainly seen in carriers of the allele ε4 of the APOE gene. Albeit moderate in effect, it is regarded as major susceptibility gene for late onset forms of AD[65]. The lifetime risk of developing AD rises significantly for APOE ε4 carriers and that in a dose-dependent manner (higher risk for homozygous carriers)[25].

Table 1. Common classifications of AD based on medical history*.

	Categories	Definition
Family history	Autosomal dominant (< 5%)	AD that occurs in ≥ three individuals in ≥ two generations, with two of the individuals being first-degree relatives of the third.
	Familial (~15-25%)	AD that occurs in ≥ two individuals and ≥ two of the affected individuals are third-degree relatives or closer.
	Sporadic (~75%)	Isolated case in the family or cases separated by > three degrees of relationship.
Age of onset	Early onset (~6-7%)[63,66]	<60-65 years
	Late onset (~93-94%)[63,66]	>60-65 years

*according to the *American College of Medical Genetics* and the *National Society of Genetic Counselors* - Guidelines 2011.

At least nine further gene loci have been identified to account for a higher risk of developing AD. Though individually small in effect, it was estimated that accumulated, they may account for a population attributable risk of up to 35%[67]. These gene loci are suspected to influence e.g. the immune system function, the cholesterol metabolism, synaptic functions and cell membrane processes[68].

Interestingly it has been hypothesised[69] that familial early onset AD and late onset AD show different patterns in the pathogenesis of Aβ peptide accumulation with an emphasis on overproduction in early onset AD and an emphasis on decreased clearance in late onset AD[70]. Of note, the fact that so far no mutations in the tau gene have been associated to hereditary forms of AD is one of the strongest arguments for the amyloid cascade hypothesis.

Non-genetic risk factors, especially modifiable risk factors receive increasing attention and include alcohol intake, blood pressure, diabetes, education[71,72], inflammation, hormone therapy, head injury and others. An up-to-date overview including meta-analyses can be accessed for free at http://www.alzrisk.org.

In summary, early onset[73] as well as late onset AD[74] has a substantial genetic component, but vulnerability for developing AD is seen as a complex

association between environmental, lifestyle and genetic factors[75], leading to today's concept of AD as a multifactorial disease.

1.1.6 Mouse models of Alzheimer's disease

A starting point for the creation of transgenic animal models of AD was offered with the identification of the responsible genes for hereditary forms of AD. Transgenic models with Aβ plaque pathology were first[76] produced using APP carrying a missense mutation known from autosomal dominant forms of AD. Today, a large array of mouse models of AD exists (for a comprehensive list see http://www.alzforum.org - Research Models) making it the most widely used species to model AD. A condensed overview of a commonly used classification[77] of transgenic mouse models provides table 2.

Mouse models of AD have been providing valuable insights into the disease process[78]. For instance, the crossing of transgenic mice carrying mutated tau into APP transgenic mice were used to convincingly show that Aβ controls the rate of development of tangle pathology[79], further providing evidence for the current amyloid cascade hypothesis which regards tau pathology as a downstream event in the pathogenesis. However, one should be cautious to extrapolate results from transgenic animals to humans. This becomes apparent by the fact that APP single transgenic mice, despite the presence of abundant Aβ plaques, do not show considerable neuronal loss or tangle pathology. Furthermore, single transgenic mice for PS1 or PS2 do not develop Aβ pathology, although these genes are known to be responsible for hereditary forms of AD.

Other species than mice are used as well and include rats, rabbits, dogs, primates[80] and invertebrates[81]. Despite great progress in modelling AD, it is important to bear in mind that none of the currently available models emulates the full spectrum of AD pathology.

Table 2. Common classification of transgenic mouse models of AD.

Category		Pathology	Important limitation
Single transgenic models	APP	Aβ pathology*, synaptic dysfunction, cognitive decline, behavioural alterations	No development of NFT, limited neuronal loss despite extensive Aβ pathology
	PS**	Increased Aβ42/Aβ40 ratio in some models, only few cognitive and behavioural abnormalities	No development of NFT, no Aβ pathology, no neuronal loss
	Tau	NFT pathology, neuronal loss, cognitive decline, behavioural alterations	No Aβ pathology
Double transgenic models	APP PS**	Accelerated Aβ pathology in APP/PS compared to single transgenic APP model	No NFT pathology, limited neuronal loss
	APP Tau	Accelerated tau pathology in APP/Tau models compared to single transgenic tau model	

* depending on promoter[82] and mutation[83], ** PS1 or PS2

1.1.7 Treatment of Alzheimer's Disease

To date, treatment approaches to AD are merely symptomatic, modest in efficacy and often subject of controversial discussion[37]. Much attention is given to pharmacological treatments aiming to improve cognition and functional deficits. This treatment approach consists only of a small group of approved drugs, namely the cholinesterase inhibitors Donepezil, Rivastigmine, Galantamine, and the NMDA receptor antagonist Memantine. Though studies on the pathophysiology of the cholinergic system in AD patients suggest that the cholinergic deficit occurs in rather late stages and that in early stages an intrinsic up-regulation of cholinergic activity can be observed[84], cholinesterase inhibitors are nevertheless regarded as standard treatment for mild to moderate AD (usually Mini-Mental-State-Examination 16 to 26[85]). However, its efficacy in patients with mild cognitive impairment and mild AD has been questioned[86]. The administration of Memantine bases on the hypothesis that neurodegeneration is

in part due to excitotoxic cell damage mediated by excessive Ca^{2+} influx through NMDA receptors. As it failed to show beneficial effects in mild AD[87], Memantine should be offered as therapeutic option for moderate to severe AD but also this is supported only by meagre evidence for its efficacy[85].

Taken together, notable level of evidence for this group of drugs exists to stabilize cognition and function in certain stages of the disease. However the average duration of effect is estimated to range within six to twelve months before the patient's condition starts to degrade again[88,89]. Furthermore, based on the different combination of symptoms and variable courses observed among AD patients, the effects of these drugs vary intra- and inter-individually, with no possibility to predict the individual response to these medications beforehand.

Further treatment of the symptoms of AD consists of a wide range of unspecific pharmacological[59] and non-pharmacological interventions[90], but can only mitigate the burden of symptoms for patients and caregivers, encounter behavioural and psychological symptoms of the disease, and help to sustain activities of daily living as long as possible[91].

Aside from treatments for symptomatic relief, much hope lies in the emerging so called disease modifying drugs with several of them already being studied in late phases of clinical trials. These drugs pursue different strategies to stop or alter the course of the disease which fall in three basic categories: (1) altering Aβ metabolism, (2) targeting hyperphosphorylated tau and (3) other strategies. Most drugs in on-going phase 2 or phase 3 clinical trials belong to the first category[92] and aim to reduce Aβ production, to prevent Aβ aggregation or to promote Aβ clearance. They include drugs that were primarily developed for other diseases such as diabetes[93] or hypertension[94], as well as drugs that are specifically designed e.g. to alter the β- or γ-secretase activity[95,96], to induce an immune response to Aβ peptides[97] or to prevent the formation of Aβ oligomers[98] which are suspected to pose an important neurotoxin[99]. Analogue to strategies against Aβ, much effort is also being invested in drugs that inhibit tau-phosphorylation[100], or prevent tau aggregation[101]. Other strategies being investigated involve protein growth factors[102], mitochondrial function[103], the

receptor for advanced glycation endproducts (RAGE)[104] and deep brain stimulation[105].

Despite promising preliminary results for many of these drugs, none of them has succeeded in phase 3 clinical trials so far[106]. In the contrary, several later phase clinical trials had to be terminated due to severe adverse effects[96] or because no clinical improvement was detectable[107]. Not only that none of these drugs is close to be officially approved, the observation that Aβ clearing in symptomatic AD patients is not necessarily accompanied by cognitive improvement has challenged our understanding of AD pathophysiology[52,55].

There is growing consensus that mild to moderate AD might be too late in the disease process to improve substantively the outcome with the currently pursued strategies. This leads to a revaluation of preventive strategies in AD drug development[108]. This shift in focus is supported by recently updated criteria for the diagnosis of AD[46] that pay increased attention to the detection of early stages of the disease[109,110]. Implementing these criteria in the design of future trials is expected to have an important impact on drug development[37,106,111].

1.1.8 Diagnosis of Alzheimer's Disease

For many years, the NINCDS-ADRDA criteria[112] and the DSM-IV-TR criteria[113] were among the most used for diagnosing AD. Both criteria require deficits in memory and at least one other cognitive domain. The DSM-IV-TR criteria additionally stipulate that the cognitive impairment must have an impact on social life or activities of daily living. NINCDS-ADRDA criteria classify the diagnosis as *definite* (typical symptoms and histologic confirmation), *probable* (typical symptoms without histologic confirmation) or *possible* (atypical symptoms but no alternative diagnosis at least equally likely). These criteria are regarded as fairly reliable reaching a sensitivity of 81% and a specificity of 70%[114]. However they allow a diagnosis only at late stages of the disease, as it is broadly accepted that the onset of the pathologic process occurs years before the onset of clinical symptoms[110,115]. Therefore criteria for mild cognitive impairment (MCI) were defined[116], a stage in which activities of daily living are

basically unimpaired. But MCI is an unspecific stage and precedes also dementia of other types than AD. This led to an revision of the NINCDS-ADRDA criteria proposing the concept of *prodromal AD*[117], essentially a subtype of MCI. In order to diagnose prodromal AD, these criteria require a consistent episodic memory deficit plus at least one supportive biomarker. In 2011, the NIA-AA workgroup also published new recommendations concerning the definition and diagnosis of preclinical stages of AD[46,109,110], recognizing the importance of biomarkers for the early diagnosis of AD and dementia of other causes.

Biomarkers can be defined as variables (physiological, biochemical or anatomical) that can be measured *in-vivo* and that indicate specific features of disease-related pathological changes[118]. Regarding AD, five biomarkers earned most of the attention and have been studied widely over the past years: decreased $A\beta_{42}$ in the cerebrospinal fluid (CSF), increased CSF tau, decreased [^{18}F]fluorodeoxyglucose uptake on PET (FDG-PET), PET Aβ imaging, and structural MRI measures of cerebral atrophy[118]. A good level of evidence suggests that abnormal biomarker findings precede the onset of clinical symptoms by years, possibly more than a decade[118]. Figure 1 shows a hypothetical model of the course of biomarker findings in relation to clinical symptoms (taken from Sperling et al. 2011).

However, these biomarkers likely do not reflect the full pathophysiologic process. For example, CSF and Aβ PET are thought to be an estimation of Aβ deposition, but do not provide information on Aβ oligomers, which are suspected to be an important neurotoxin in the pathophysiologic cascade. Abnormal tau findings which seem to relate to the extent of neuronal injury[119] and brain atrophy are both not specific for AD and are found in certain other ND as well. Furthermore, asymptomatic individuals who are biomarker positive do not necessarily progress to clinical dementia[110].

Despite these limitations, the establishment of biomarkers for AD mark an important step in AD diagnostic research. As Aβ accumulation seems to emerge early in the disease process[120], in-vivo imaging of Aβ might play an prominent role in detecting early stages of the disease and in identifying individuals who are at higher risk of developing AD.

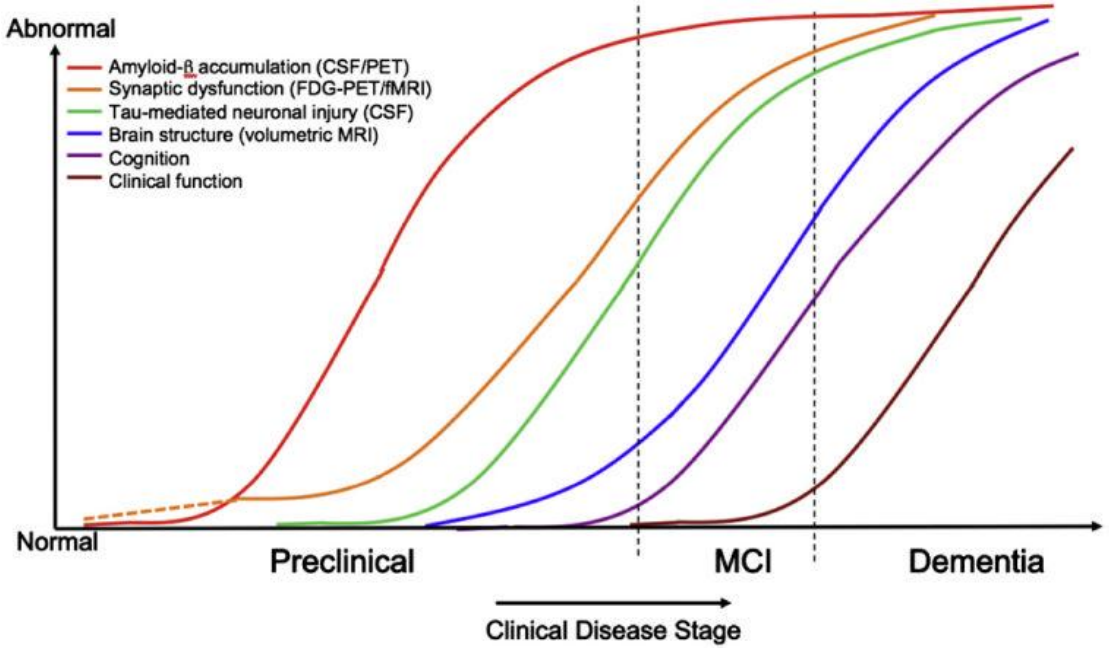

Figure 1. Hypothetical course of biomarker findings in relation to clinical stages of AD (taken from Sperling et al. 2011). Abnormal Aβ is identified by measuring $A\beta_{42}$ in the cerebrospinal fluid (CSF) or by Aβ PET imaging. Synaptic dysfunction is evidenced by [^{18}F]fluorodeoxyglucose PET (FDG-PET) or functional magnetic resonance imaging (fMRI). The dashed line indicates that synaptic dysfunction may be detectable in carriers of the APOE ε4 allele before detectable Aβ deposition. Neuronal injury is evidenced by CSF tau or CSF phospho-tau. Abnormal brain structure is evidenced by structural magnetic resonance imaging (MRI). MCI stands for mild cognitive impairment.

1.2 *In-vivo* Amyloid-β imaging

1.2.1 Clinical Aβ imaging with Aβ PET tracers

In order to liberate the confirmation of AD pathology from analysis of brain tissue gained by autopsy or biopsy, efforts are being made to design agents for in-vivo detection of AD pathology since the late 1990s. Using techniques from nuclear medicine is regarded as one of the more promising approaches. Therefore efforts are focused on agents that would fulfil basically three major criteria[121]. These agents should: (1) allow the labelling with a radionuclide, (2) cross the blood-brain-barrier to enter the brain parenchyma and (3) bind specifically to cerebral amyloid deposits. [^{18}F]FDDNP was the first reported PET

tracer to image AD pathology in-vivo[122] in 2003, but turned out to exhibit relatively high non-specific binding. Shortly after, two further tracers were published, [^{11}C]SB-13[123] and [^{11}C]PiB[124] (PiB), which both show high affinity to Aβ, high initial brain uptake and relatively rapid washout. However due to a short half-life of 20 minutes, [^{11}C]-labelled tracers are available only in or within the proximity of cyclotron-equipped PET centres. In order to make Aβ imaging tracers broader available, current research focuses on developing [^{18}F]-labelled Aβ tracers with kinetics and metabolism properties comparable to PiB[125-127], as [^{18}F] has a half-life of nearly two hours.

The following sections focus on studies that used PiB, because PiB has been employed in most clinical studies so far and contributed the lion's share of our knowledge about the relevance of Aβ imaging in the diagnosis of AD and preclinical stages of AD[128]. The objectives of these clinical Aβ imaging studies fall into three basic categories: (1) association of PiB retention and clinical diagnosis, (2) PiB retention as disease predictor and (3) association of PiB retention and underlying pathology.

Results from studies on the association of PiB retention and clinical diagnosis were encouraging. For example, the accuracy of a merely clinical diagnosis of AD (i.e. without Aβ imaging) in highly specialised centres reaches over 95% (confirmed by autopsy)[129]. Among these clinically diagnosed AD patients about 96% were determined to be Aβ positive by PiB PET[128]. However, the ability to "diagnose" AD merely by Aβ imaging is limited, as several studies identified even cognitive normal individuals in up to 24% as Aβ positive[128]. Furthermore, there were studies conducted which tried to distinguish cognitive normal individuals from MCI patients, or MCI patients from AD patients based on PiB retention. Also, some studies aimed to correlate PiB retention with clinical symptomatology (e.g. measured with Clinical Dementia Rating (CDR)). Although the results of both approaches have been overall positive, they were far away from univocal[128]. With respect to these findings, it was argued that disease staging is not a particular strength of Aβ imaging[128]. However, it might proof to be a valuable tool to increase the accuracy of a clinical diagnosis of AD in less specialised centres, for which an accuracy near 70% was reported[114].

Furthermore, rather than helping in staging a disease, Aβ imaging can dichotomize patients with none or unspecific symptoms (e.g. patients with MCI) into those who are Aβ positive and those who are Aβ negative.

Determining the Aβ status of cognitive normal individuals and patients with MCI raised the question about the quality of Aβ imaging as predictor for converting from cognitive normal to prodromal symptoms of dementia or from there to AD dementia. In this context, it is important to note that MCI patients do not necessarily progress to dementia of any type. Studies suggested that nearly a half[130] or more[131] remain cognitive stable even after 10 years of follow-up. Some studies reported that a portion of MCI patients even converts back to cognitive normal[132,133]. A meta-analysis[128] of five studies that followed in total 155 MCI patients for 1 to 3 years after PiB scan, reported that over a third converted to a clinical diagnosis of AD in this period of time and of these converters, about 93% had been PiB positive (conversion rate of all PiB positive MCI patients was 53%, however this rate might increase with prolonged follow-up). Given the long period of probably over 10 years of Aβ accumulation before clinical symptoms occur, data on the rate of conversion from cognitive normal to MCI is yet very limited with only one study published so far. This study reported that PiB is a stronger predictor for progression than other factors including age and ApoE status[134]. Taken together, studies available so far suggest that PiB positivity is probably a good predictor for the likelihood of converting from MCI to AD, and potentially also for the likelihood of converting from cognitive normal to MCI.

The focus in diagnosing AD shifts more and more towards the prodromal and pre-symptomatic stages. However, the earlier one moves into the disease stages of AD, the lesser accurate clinical diagnostic tools become, and clinical assessment eventually becomes useless in cognitive normal individuals. Therefore, the higher an evaluation of a patient relies on Aβ imaging and the lesser it can be flanked by a clinical assessment of the symptomatology, the more important it becomes to understand the basic principles of PiB binding to pathologic changes in the brain. This important relationship of Aβ plaque histopathology and PiB binding has been studied in two ways: post-mortem PiB-

labelling without in-vivo PiB data and in-vivo PiB data with post-mortem neuropathologic analysis. In a widely-noticed post-mortem PiB-labelling study without in-vivo data, Lockhart et. al reported that PiB is a nonspecific marker for fibrillar Aβ deposits, binding to classic plaques (compact/cored), diffuse plaques, and CAA[135]. The other type of study, correlating in-vivo PiB data with post-mortem analysis, is naturally limited and therefore, it's not surprising that the literature only reports on a total of 17 cases of autopsy following a PiB scan. In these cases, the time intervals of imaging to autopsy ranged from few months to 1 to 3 years[136-144]. Additional there is one study correlating in-vivo PiB imaging with histopathology in ten cases that underwent biopsy due to suspected normal pressure hydrocephalus[145]. Overall, for all individuals determined to be PiB positive the presence of significant Aβ deposition was confirmed, meaning a specificity 100%. However, the more interesting finding was that few cases among these studies where found with some degree of Aβ pathology but negative PiB scan (of note, these cases met only the criteria for possible AD by CERAD[146]). It was suggested that these cases present an example of non-fibrillar diffuse Aβ deposits[128] and thus decreased PiB binding may be caused by a predominance of Aβ40 over Aβ42[144] as Rosen et al. suggested that insoluble Aβ40 may present in high quantities without significant PiB binding[147]. Usually Aβ42 is the prevalent Aβ species in AD patients[148,149]. However, the reasons for these mismatches of PiB and pathologic findings are not yet clear. Taken together, questions remain about the sensitivity of clinical PiB imaging for different forms of Aβ deposits. Also a potential threshold of Aβ pathology for PiB positivity has yet to be determined[144].

In conclusion, since the publication of PiB in 2004, clinical Aβ imaging studies contributed a significant body of our knowledge about AD. Aβ PET tracers allowed for the first time to noninvasively image disease specific pathologic changes in living subjects and thus provide information that were formerly restricted to histological analysis of brain tissue. The more important Aβ imaging becomes as a predictor for disease progression or as a biomarker indicating early pathologic changes, the more important is a fundamental understanding of the relationship of imaging results and underlying pathology. However, those

analyses are naturally limited in human studies. A promising approach to help filling the gaps of knowledge in this matter are preclinical studies which allow direct correlations of in-vivo PiB data with histopathologic evaluation.

1.2.2 Preclinical Aβ imaging in mouse models of Alzheimer's disease

In the context of the (early) detection of AD pathology, preclinical Aβ imaging techniques that parallel the one from human studies are of particular interest. The aim is to study the complex relationship of pathology and imaging signal and thus provide implications for clinical diagnostic procedures. Different techniques were suggested and investigated to image Aβ deposits *in-vivo* in animal models of AD. However, invasive imaging techniques that visualised individual Aβ deposits such as multi-photon microscopy through a skull window[150,151] are not transferrable to a clinical setting. MRI-based techniques[152-156] were also shown to be able to image even individual Aβ deposits in-vivo[155] in mouse models of AD. MRI offers a number of advantages such as high spatial resolution of MRI scanners and the absence of exposure to radiation. But MRI-based imaging of Aβ pathology has not largely penetrated into the field of clinical studies so far[157].

With the emergence of clinical Aβ imaging by means of PET, transferring this methodology into a preclinical setting was highly desirable. However, small animal PET imaging has a number of limitations to consider. Foremost, the rather low spatial resolution of small animal PET scanners in relation to tissue sample size makes the analysis of PET signal susceptible to biasing effects such as spill-over or motion. The analysis is further complicated by the minimal anatomical information that PET images often provide. Therefore additional imaging and co-registration procedures are usually necessary.

Rodents are preferred animals for modelling a disease. Rat models of AD as well as mouse models of AD exist. With respect to the limitations of small animal PET, rats would be the favourable candidate over mice for small animal PET, as they offer a better relation of scanner resolution to brain size (the rat brain is about six times larger than the mouse brain). Unfortunately, rats

carrying APP transgenes demonstrated only low and unsteady expression of Aβ[158] and only recently, a rat model was introduced that reliably produces Aβ deposits[158,159]. On the contrary, mouse models of AD are widely available since the mid-1990s. They are the most often used animal model for AD[160] and also routinely employed for preclinical in-vivo studies on disease modifying drugs[161]. Therefore, most preclinical Aβ imaging studies in rodents relied on mouse models of AD.

Soon after the initial report on the successful application in AD patients, PiB was applied in a double transgenic APP/PS1 mouse model of AD[162]. Unexpectedly, this initial study could not detect significant cerebral tracer retention, even in a 12 months old mouse. The authors concluded that Aβ deposits of transgenic mouse models of AD provide far less high-affinity binding sites for PiB than the Aβ deposits found in AD patients, due to differences in the secondary structure. Shortly after, another study employed PiB in a single transgenic APP mouse model named Tg2576[163]. In neocortical brain regions, they detected statistically significant PiB retention in Tg2576 animals compared to control animals. However the authors concluded that their findings are not based on specific PiB binding to Aβ deposits.

The first successful Aβ imaging study with PiB demonstrated significant PiB retention in aged mice of a single transgenic APP mouse model named APP23[164]. The authors attributed their success to the usage of PiB with a very high specific activity and thus to an optimal exploitation of the limited amount of high-affinity binding sites on the Aβ deposits which were postulated by the initial study mentioned above[162]. To further investigate potential reasons for the low amount of high-affinity binding sites, they measured a truncated subtype of the Aβ peptide, regarded as a post-translational modified form of Aβ, the N3-pyroglutamate-Aβ (N3pE-Aβ). N3pE-Aβ was reported to constitute the major type of deposited Aβ peptide in AD patients[165]. Mouse models were also reported to hold N3pE-Aβ in their deposits but to a lower extend than AD patients[166,167]. The authors concluded that the amount of N3pE-Aβ is responsible for high-affinity PiB binding and that the lower amount of N3pE-Aβ

in mouse models of AD would thereby explain the results of the previous studies.

These findings were contrasted by a study from our group[168] that demonstrated specific retention of PiB in a double transgenic APP/PS1 mouse model named ARTE10. Importantly, this study employed a specific activity that ranged within values that most clinical PET centres routinely produce. This study further suggested that PiB retention strongly correlates with the level of overall Aβ plaque load in this mouse model and that old homozygous ARTE10 carry high-affinity binding sites for PiB comparable to AD patients. The value of this mouse model of AD was further demonstrated in another study, in which ARTE10 was successfully employed for in-vivo validation of a newly developed Aβ PET tracer[169]. Recently, a comparable mouse model (APP/PS1) was also used for preclinical in-vivo validation[170] of a [^{18}F]-labelled Aβ PET tracer being currently under development. However, neither study reported on the amount of N3pE-Aβ in the Aβ deposits.

Taken together, after overcoming initial problems, preclinical Aβ imaging studies in mouse models of AD are regarded more and more as a powerful tool for diagnostic and therapeutic research on AD. However, preclinical Aβ imaging studies published so far used different methodology for the analysis of histopathology and PET signal and employed mouse models of different transgenic configuration and of different age. No direct comparison of mouse models exists in this matter and the hypotheses on the reasons for the disappointing outcome of the initial studies are still based on a limited level of evidence. Therefore, several open questions remain of which we regard the following as most eminent: What are the key differences between the mouse models that influence PET tracer binding to Aβ and therefore in-vivo Aβ PET signal? What role do the different types of Aβ peptides play? And, to what extend can results and methodology be translated between clinical and preclinical studies?

1.3 Objectives of research

For the preclinical study on hand, we employed the Aβ PET tracer PiB in two different mouse models of AD: Tg2576 and ARTE10. The objectives of research of this preclinical study fall in three basic categories:

(1) Comparing the two mouse models regarding PiB PET imaging results and plaque pathology: There has been only one study employing Tg2576 for Aβ imaging with PiB so far and this study suggested that Tg2576 was potentially not suitable for Aβ imaging despite a high age of the animals and the presence of Aβ plaques. In contrast, ARTE10 was shown to be well suitable for Aβ imaging even at a younger age. For ARTE10, a strong correlation between in-vivo PiB signal and Aβ plaque load was shown, for Tg2576 no equivalent in-vivo data exists. We wanted to investigate potential reasons for the previous failure of Tg2576 through a direct comparison of the two mouse models.

(2) Investigating the relationship of Aβ pathology and PiB PET imaging results: The key difference between the two mouse models is the transgenic configuration with Tg2576 being a single APP transgenic mouse model and ARTE10 being an APP/PS1 double transgenic mouse model of AD. It was shown that the transgenic configuration of a mouse model influences the morphology of their Aβ plaques[171]. We employed stainings that allow to differentiate between diffuse and highly-dense Aβ plaques. As diffuse plaques are thought to emerge early in the disease process of AD[172] and can also be found in the absence of any associated evidence of cognitive impairment[173], our results could potentially have implication for humans studies. Furthermore, it was suggested that a key factor for high-affinity PiB binding to Aβ deposits is the amount of truncated Aβ peptide, particular N3-pyroglutamate-Aβ (N3pE-Aβ). In order to address this hypothesis, we employed a highly sensitive and specific staining against N3pE-Aβ to assess the portion of this subtype of Aβ peptide among our mouse models and correlated it with the corresponding PiB PET imaging results.

(3) Assessing the feasibility of a voxel-based analysis of in-vivo PiB PET signal in mouse models of AD: Voxel-based analysis of PiB PET studies in humans

becomes more and more popular as voxel-based approaches offer a number of advantages. As the feasibility of this analysis method has not been shown for in-vivo cerebral tracer uptake in mice, we want to investigate the possibility of transferring this analysis method to preclinical Aβ imaging studies in mouse models of AD.

2. Materials and Methods

2.1 General information

2.1.1 Animals employed

For this study we employed two different transgenic mouse models of Alzheimer's disease: ARTE10[174] and Tg2576[175].

1. ARTE10 (short: A10) (exact description: C57Bl/6J genetic background, CB-Tg(Thy1-PSEN1*M146V/Thy1-APP*swe)-10Arte, Artemis Pharmaceuticals, Cologne, Germany) is a double transgenic mouse model with two human transgenes: Amyloid Precursor Protein (APP) containing the Swedish mutation[176] (position 670 Lysin → Asparagin and position 671 Methionin → Leucin) and Presenilin 1 (PS1 or PSEN1) containing a mutation at position 146 with Methionin → Valin[177]. ARTE10 mice can be hemizygous (tg/-) or homozygous (tg/tg).
2. Tg2576 (exact description: 129S6 genetic background, Cg-Tg(APP*swe)2576Kha, Taconic Farms, Hudson, New York, USA) is a single transgenic mouse model with one human transgene of APP containing also the Swedish mutation.

As controls, we employed non-transgenic mice with corresponding genetic background to ARTE10 (referred to as A10 wildtypes or ARTE10 wildtypes in the text) and Tg2576 (referred to as Tg2576 wildtypes in the text).

In total we performed experiments on 80 animals of which 4 animals were excluded from analysis. Details on number of animals per study group, sex, mean age and mean body weight and reasons for exclusion are summarized in table 3 on page 22.

All animals were kept under temperature-controlled environmental conditions and fed a standard diet with access ad libitum until the start of experiments and after. Animal husbandry followed the regulations of European Union (EU) guideline No. 86/609. The Committee on Animal Health and Care of the local government (Regierung von Oberbayern, Munich, Germany) approved all

experimental procedures (Tierversuchsantrag: 211-2531-35/06), which were carried out in accordance with the German Animal Welfare Act (Deutsches Tierschutzgesetz).

Table 3. Overview of details of the six study groups.

Study group	**N** (♀, ♂)	Mean **age** ± SD (Min-Max) in months	♀: Mean weight ± SD (Min-Max) in g	♂: Mean weight ± SD (Min-Max) in g
A10 tg/-	**17*** (17,0)	**24.7** ± 0.4 (24.10 - 25.5)	30.2 ± 5.2 (24.1 - 44.8)	Ø
A10 tg/tg young	**13** (8,5)	**12.8** ± 0.7 (12.2 - 14.0)	29.0 ± 4.1 (26.1 - 37.7)	35.9 ± 1.9 (33.8 - 38.0)
A10 tg/tg old	**13** (9,4)	**24.6** ± 0.5 (23.6 - 25.4)	24.2 ± 2.4 (20.8 - 28.4)	33.6 ± 4.1 (27.6 - 36.3)
A10 wildtype	**10** (5,5)	**25.1** ± 0.8 (24.1 - 26.7)	31.5 ± 10.4 (21.4 - 48.6)	37.7 ± 2.8 (34.7 - 31.1)
Tg2576 tg	**16**** (16,0)	**24.9** ± 0.6 (23.8 - 25.8)	24.0 ± 3.2 (17.2 - 29.1)	Ø
Tg2576 wildtype	**7***** (7,0)	**24.6** ± 0.2 (24.4 - 25.0)	29.7 ± 3.7 (23.5 - 33.6)	Ø

* 19 animals, 2 excluded due to a macroscopic visible brain tumour.
** 17 animals, 1 excluded due to heavy motion during PET scan, especially during the last minutes of the scan.
*** 8 animals, 1 excluded due to a macroscopic visible brain tumour.

2.1.2 Sequence of experiments

Animals were housed until they reached the target age of 1 year (A10 tg/tg young), respectively 2 years (all others). Once an animal reached the target age in a justifiable state of health for experimental procedures, it went through a standardised sequence of experiments, of which a flowchart is given in figure 2 on page 23. The following chapters 2.2 to 2.5 describe the details of the particular steps in chronological order. The experimental protocols for PiB PET and MRI imaging were an adaptation of previously published protocols by Manook et al.[168]. The experimental protocol for plaque load analysis was an adaptation of a previously published protocol by Willuweit et al.[174].

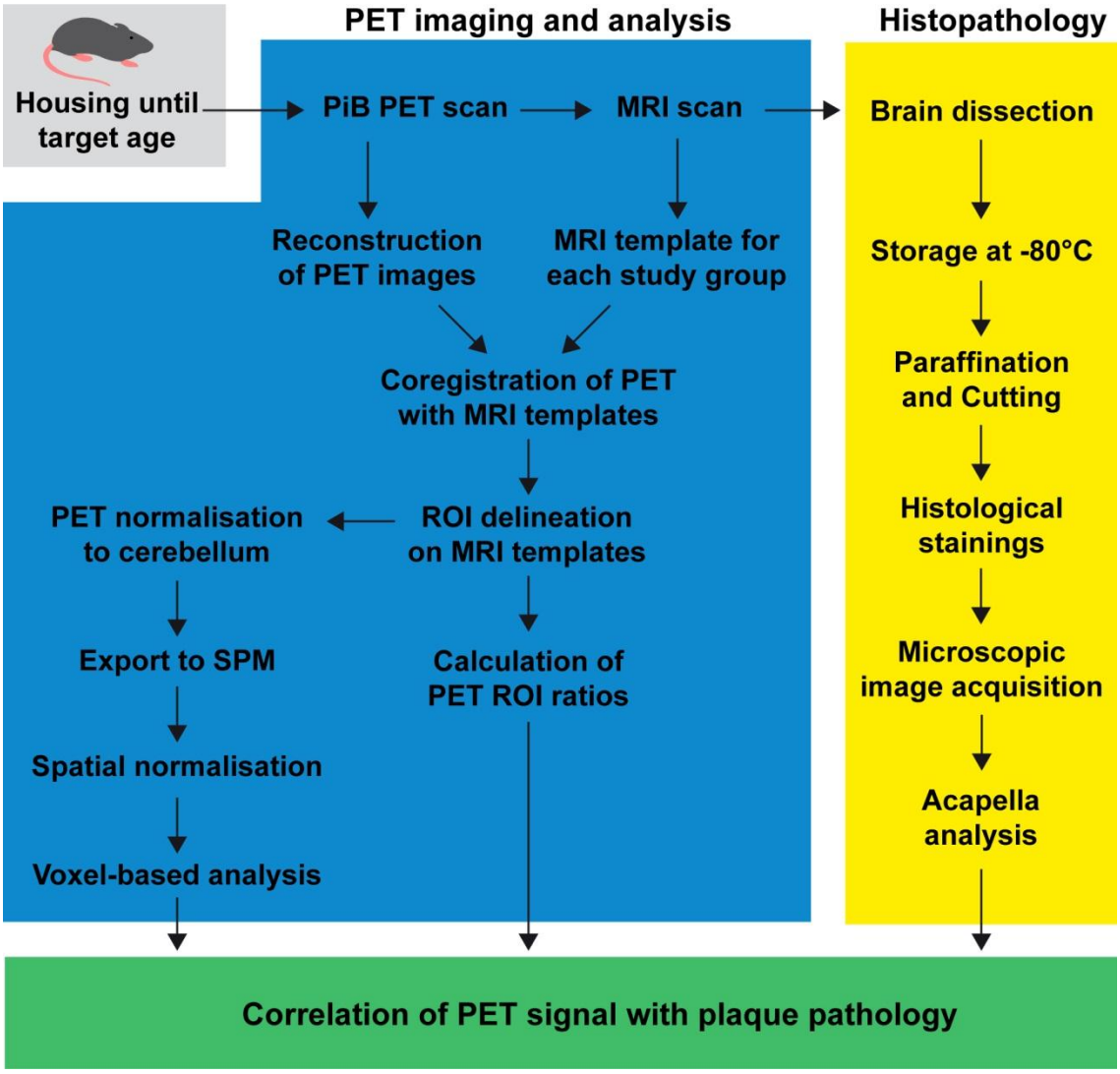

Figure 2. Flowchart giving an overview of conducted experiments and analysis steps.

2.2 PET and MRI imaging of the animals

2.2.1 Animal Preparation and Anaesthesia

We initiated anaesthesia at least 10 min before the scan with 1.0% to 2.0% isoflurane in a 2l/min oxygen flow. Isoflurane anaesthesia continued throughout the whole experiment with the amount of isoflurane adapted according to the situation (e.g. increased during i.v. injection). Throughout the whole experiment an electric heating pad prevented hypothermia and dexpanthenol ointment protected the eyes.

For i.v. injection we inserted a home-made catheter, comprising of 30 gauge needles, an elastic hollow vessel-loop and a 1ml syringe, into the lateral tail vein and affixed it with superglue.

2.2.2 Radiosynthesis

The radiosynthesis of *N*-[^{11}C-*methyl*]6-OH-BTA-1 (PiB) was performed according to the standard protocol of our facility, described in detail in Manook et al.[168]. Noteworthy details: Radiochemical and chemical purities were >98.5 % as determined by analytical HPLC. The radiochemical yield averaged at 35 % at the end of synthesis (EOS) based on [^{11}C]CH_3OTf, resulting in a mean of 3.6 GBq of PiB. The specific activity averaged at 76.7 GBq/µmol at EOS. In most cases we used one synthesis for two sequential PET scans. In order to align specific activity of PiB within the two scans, we added an amount of authentic standard N-methyl-6-OH-BTA-1 to the first injectate. This resulted in a specific activity in the range 300-400 mCi/µmol (11.1 – 14.8 GBq/µmol). We formulated the resulting solution with isotonic sodium chloride solution prior to injection to reduce ethanol content to less than 2%.

2.2.3 Tracer administration and PET scan

PET scans were performed on a Siemens Inveon PET/CT system (Siemens Healthcare, Erlangen, Germany) with an axial FOV of 12.7 cm, a bore diameter of 12 cm and ~1.5 mm FWHM spatial resolution at the centre of the FOV[178].
Simultaneously with a slow bolus injection of approximately 50 to 200 µl of PiB solution, we started the PET scan with a duration of 45 minutes in 3D listmode. After tracer injection we flushed the catheter with 50 µl to 100 µl isotonic sodium chloride solution.
Before and after tracer injection, we measured the activity in the syringe with a dose calibrator (Capintec Inc., Ramsey, NJ, USA) to calculate the injected dose. After the PET scan we removed the catheter and measured the body weight. After removal, the catheter was also measured with the dose calibrator in order

to assess the fraction of the injected dose that did not enter the circulation of the animal. We corrected the activity measured in the catheter for decay and subtracted it from the calculated injected dose. Details on mean injected activity and times for PiB injection and flushing per study group are summarized in table 4 on page 25.

Animals were allowed to awake and recover from the PET scan before we proceeded to the MRI scan.

Table 4. Overview of injected PiB doses and injection times per study group.

Study group	Mean **injected dose*** ± SD (Min-Max) in MBq	Mean duration of PiB injection ± SD (Min-Max) in min:sec	Mean duration of flushing ± SD (Min-Max) in min:sec
A10 tg/-	**18.4** ± 4.0 (8.8 - 24.2)	01:37 ± 00:37 (00:34 - 02:35)	00:24 ± 00:12 (00:05 - 00:46)
A10 tg/tg young	**22.4** ± 6.3 (11.8 - 30.6)	01:10 ± 00:50 (00:18 - 02:49)	00:21 ± 00:11 (00:07 - 00:50)
A10 tg/tg old	**15.9** ± 5.4 (8.9 - 27.0)	01:49 ± 00:40 (00:40 - 03:10)	00:23 ± 00:11 (00:10 - 00:50)
A10 wildtype	**17.3** ± 6.6 (4.3 - 25.6)	01:20 ± 01:04 (00:20 - 03:15)	00:18 ± 00:08 (00:04 - 00:27)
Tg2576 tg	**23.5** ± 6.8 (9.6 - 35.5)	01:19 ± 00:48 (00:18 - 02:44)	00:25 ± 00:12 (00:06 - 00:46)
Tg2576 wildtype	**20.8** ± 4.8 (11.6 - 28.0)	01:52 ± 01:04 (00:33 - 03:29)	00:11 ± 00:05 (00:05 - 00:19)

* corrected for activity measured in the catheter after the scan.

2.2.4 MRI scan of the animal brain

Similar to the PET scans we initiated anaesthesia at least 10 minutes before the scan and kept the animals under continuous 1.0% to 1.8% isoflurane in a 2l/min oxygen flow. Dexpanthenol ointment protected the eyes. Throughout the MRI scan a heat storing gel pack (COLDHOT, 3M, St. Paul, Minnesota, USA) preheated in a microwave oven prevented hypothermia.

In cases of a waiting period between the PET scan and the MRI scan of greater than 1 week), we omitted the MRI scan and sacrificed the animal immediately after the PET scan. Reasons for such waiting periods were mostly scanner malfunction and maintenance works. This resulted in a total number of 51 out of 80 animals that received a MRI scan of the brain (A10 tg/- 8 mice, A10 tg/tg young 9 mice, A10 tg/tg old 8 mice, A10 wildtype 8 mice, Tg2576 tg 11 mice, Tg2576 wt 7 mice).

MRI scans were performed on a Philips Achieva 1.5 T clinical MRI system with a 23 mm microscopy receive-only coil. We acquired T1 weighted brain images using a 3D fast gradient echo (3D-TFE) sequence with an inversion pre-pulse (TR: 12ms, TE: 3.9ms, TI: 800ms, TFE Factor: 120, flip angle: 8°, number of signal averages (NSA): 12, acquired matrix MxP: 248x120, partitions: 60, FOV: 64x32x16mm, resolution: 0.26x0.27x0.26mm, reconstructed resolution: 0.13x0.13x0.13mm). Acquisition duration was 46 minutes 11 seconds.

2.3 Tissue recovery and histological staining

2.3.1 Brain dissection and tissue preservation

Immediately after the MRI scan (respectively the PET scan for the animals that did not receive a MRI scan) the animal was sacrificed per cervical dislocation. The skull was dissected and opened mid-sagittally with fine scissors starting from the cerebellum and ending at the osseous vicinity of the olfactory bulbs. The brain was carefully removed, halved in left and right hemisphere and frozen with fine crushed dry ice. After a few minutes the frozen brain was transferred to a pre-cooled plastic tube and stored in a refrigerator at -80°C.

2.3.2 Paraffination of the brain and cutting

For paraffination, the right hemisphere of each animal was thawed and incubated overnight in a 75% 2-propanol solution (2-propanol, Merck, 109634, diluted with aqua dest.) at room temperature, followed by 4h in a 90% 2-

propanol solution. Each hemisphere was then para-sagittally cut in two halves and incubated in 100% 2-propanol (solution exchanged after 1h, 2h, overnight and again after 1h). The brain material was then transferred to a mixture of 50% 2-propanol / 50% paraffin (Histowax, Histolab Products AB, Gothenburg, Sweden) and kept at 60°C in a rotation stove. After 7h the 2-propanol / paraffin mixture was replaced with 100% paraffin. The 100% paraffin was exchanged after 7h, 16h and again after 7h.

Both halves of each hemisphere were then embedded side by side (Paraffin Embedding Center EG1150, Leica Microsystems GmbH, Wetzlar, Germany) in such a way that the cut surfaces from the para-sagittal cut faced towards the later sectional area.

The resulting paraffin blocks were then cut with a thickness of 5 µm with a manual rotary microtome (RM2165, Leica Microsystems GmbH, Wetzlar, Germany and Feather microtome blades type A35) and mounted on microscopic glass slides (SuperFrost Ultra Plus, Gerhard Menzel GmbH, Braunschweig, Germany), 3 sections per slide. The slides were stored at room temperature in conventional slide boxes.

2.3.3 Deparaffination and rehydration

Before staining, the sections were deparaffinated and rehydrated. This was done by incubating the slides in 100% xylol for 3 times 5 minutes, followed by 3 times 5 minutes in 100% ethanol, 5 minutes in 96% ethanol, 5 minutes in 70% ethanol and 3 times 2 minutes in aqua dest.

2.3.4 Thioflavin S staining

The deparaffinated and rehydrated sections were incubated in a 1% (1 g per 100 ml aqua dest.) solution of Thioflavin S (T1892, Sigma-Aldrich, St. Louis, Missouri, USA) for 30 minutes. The sections were then washed with aqua dest. 3 times 2 minutes, incubated in 80% Ethanol for 6 minutes, washed again and coverslip mounted with 22x50 mm cover glasses and VectaShield as mounting

medium (H-1500 with DAPI, Vector Laboratories Inc., Burlingame, California, USA). The slides were stored in conventional slide boxes in a refrigerator at 4°C until microscopic image acquisition.

2.3.5 Immunohistochemistry stainings

We performed two separate immunofluorescence (IF) stainings:

1. with a monoclonal primary antibody binding specifically to the full length Amyloid-β peptide (Aβ 1-40/42) (3A5, Affiris AG, Vienna, Austria)[179] and
2. with a monoclonal primary antibody binding specifically to N3-pyroglutamate-Amyloid-β (D129, Affiris AG, Vienna, Austria)[179].

The full length Aβ is further referred to as Aβ or N1-Aβ, N3-pyroglutamate-Aβ is further referred to as pyroglutamate Aβ or N3pE-Aβ.

The deparaffinated and rehydrated sections were first treated with an antigen retrieval solution (10x concentrate, diluted 1:10 with aqua dest., S2367 pH 9.0 used for 3A5 and S1699 pH 6.0 used for D129, DAKO, Glostrup, Denmark) by heating the solution with the sections in a microwave oven for 15 minutes followed by a cooling off period of 20 minutes. The sections were then washed 2 times 3 minutes with PBT (0,1% Tween-20 added to PBS). Afterwards the sections were blocked with 4% NGS-PBT (normal goat serum diluted in PBT) and kept for 30 minutes in a humidified chamber at room temperature. The sections were then probed with the primary antibody diluted 1:200 (3A5 and D129) in 4% NGS-PBT and kept in a humidified chamber for 30 minutes at room temperature. The sections were washed 2 times 3 minutes in PBT and incubated with a Fluorescein-conjugated anti-mouse IgG secondary antibody (FI-2000, Vector Laboratories Inc., Burlingame, California, USA) diluted 1:100 in 4% NGS-PBT for 30 minutes and kept in a humidified chamber at room temperature. The sections were then washed 2 times 3 minutes with PBT and 2 times 3 minutes with aqua dest. and then coverslip mounted in the same way as the Thioflavin S stained sections. The slides were then stored in conventional slide boxes in a refrigerator at 4°C until microscopic image acquisition.

2.4 Analysis of histological sections

2.4.1 Digital image acquisition of histological sections

We acquired digital images by using an automated whole-slide-scanner (Mirax Scan, Carl Zeiss MicroImaging GmbH, Jena, Germany) using filter sets for DAPI, GFP and TexasRed. The DAPI (contained in the mounting medium) fluorescence was used by the scanner to set the optical focus, GFP contained the specific signal through the Fluorescein-conjugated secondary antibody, and TexasRed delivered unspecific fluorescence such as tissue auto-fluorescence. Exposure times were 10ms for DAPI, 50ms for GFP and 200ms for TexasRed for all slide of all stainings. Acquired images were saved in the MRXS (.mrxs) file format.

2.4.2 Pre-processing of histological images

MRXS files were processed using the MIRAX Viewer software (Version 1.12.22.1, Carl Zeiss MicroImaging GmbH, Jena, Germany). Rectangular ROIs comprising the whole sagittal brain section were manually defined to export each tissue section to a TIFF-file (RedGreenBlue, uncompressed, with a 1:8 down-sampling in resolution) in such a way that the GFP signal was copied into the green channel and the TexasRed signal into the red channel. The blue channel remained blank (value 0 for all pixels).

As we stained 2 slides per tg mouse and staining (1 slide per wildtype mouse respectively), and each slide usually had 3 paraffin sections mounted, and each paraffin section contained 2 tissue sections due to the para-sagittal cut, the image export to TIFF-files resulted in 8 to 12 TIFF-files per tg mouse and staining and 3 to 6 TIFF-files per wildtype mouse. In total, exporting images resulted in 2184 TIFF-files.

TIFF-files were then loaded in Photoshop CS4 (Adobe Systems, San Jose, California, USA) in order to define regions of interest for plaque load analysis. Defining regions of interest was done by assigning pixels the value 100 in the

formerly empty blue channel. In our study this was done manually using the polygonal lasso tool. The neocortex and hippocampus were defined as regions of interest in accordance with the anatomical delineations given by Paxinos mouse atlas[180].

2.4.3 Image analysis with Acapella Software

To measure the relative plaque load in a region of interest of each section, we used the Acapella™ analysis software (PerkinElmer Inc., Waltham, Massachusetts, USA) applying a special script (developed by Evotec AG, Hamburg, Germany). This script allows quantitative assessment of the relative plaque load (sum of pixels representing plaque signals divided by the sum of all pixels representing the regions of interest). Furthermore this script provides details such as mean plaque count (relative per 10,000 pixel of ROI) and plaque size (area expressed as number of pixel) for each section.

A frequent difficulty of automatic image analysis is the identification of false positive structures arising from background staining and tissue artefacts, thereby lowering the specificity and reliability of object recognition. The employed script is able to discriminate and eliminate contaminations or otherwise interfering signals (e.g. resulting from dust particles or folds in the tissue).

We carefully inspected each section after Acapella analysis. Minor detection deficits were tolerated (e.g. failure to detect < 5 plaques); larger deficits (e.g. failure to detect a group of plaques) lead to exclusion of the particular image. In cases of a large contamination detected as plaque specific signal (e.g. a tissue fold or dust particle), we adjusted the region of interest and ran the script for the particular section again.

We analysed at least 8, maximal 12 sections per tg mouse per staining (respectively 3 to 6 sections per wildtype mouse) and calculated mean values of plaque load, plaque size and plaque count for each individual.

2.5 Analysis of PET and MRI imaging data

2.5.1 Creation of MRI templates

For the creation of study group specific MRI templates we first loaded all MRI images in Pmod 3.1 and manually coregistered them. Hereby special attention was given to structures which are easy to recognise in our MRI images such as the arbor vitae of the cerebellum, the corpus callosum, the ventricles, the hippocampus, the thalamus and the overall brain contour. Structures outside of the brain were mostly not in the field of view or are subject to higher variability e.g. through muscle tonus and therefore not considered in the manual coregistration process. The brains of the mice with the same genetic background (transgenic and non-transgenic) showed a remarkably low anatomic variability. Therefore coregistered MRI images of mice of the same study group were averaged to create a study group specific MRI template.

2.5.1 PET data reconstruction

PET images were reconstructed with the following parameters: 2D FBP, Nyquist: 0.5, zoom factor: 1, voxel size (x,y,z): 0.776,0.776,0.796 mm, size (x,y,z): 128,128,159 voxels, time framing: 10x60 seconds, 7x300 seconds, correction for scatter (Inveon Acquisition Workplace, Siemens Healthcare, Erlangen, Germany). We cropped the PET images to head and neck and corrected them manually frame-wise for motion using the Pmod 3.1 Fusion Tool (required in two cases).

2.5.2 Coregistration of PET data with MRI templates

We manually coregistered the PET images with the group specific MRI-template using the brain contours from a summed frame of the initial tracer uptake (2 to 4 min). PET images were scaled in such a way that the assumed brain signal matched the brain contour of the MRI template. The quality of the coregistration

was then checked in a summed frame of minute 1 to 5 and again in a summed frame of minutes 36 to 45 (last two frames). The final step of the coregistration process was the comparison of all coregistered PET images of a study group. Hereby we first scaled the PET images to percentage of injected dose per cc, normalised to body weight in kg (%ID*kg/cc) and then created a summed frame of the minutes 36 to 45 (last two frames). The coregistration of these final PET images was corrected if necessary. Final PET images were eventually saved to the database and used for all further analysis steps.

2.5.3 ROI definition and ratio calculation

For traditional ratio-based PET data analysis we drew two regions of interest (ROI) on the group specific MRI templates, one comprising the neocortex and hippocampus, the other comprising the cerebellum. This was done using Pmod 3.1. We then applied these ROIs to the coregistered PET images and exported the ROI values to Microsoft Excel 2003 in order to calculate neocortex + hippocampus to cerebellum ratios (further referred to as PET ratios).

2.5.4 Creation of brain masks for spatial normalisation of PET images

As noted previously, brains of mice with the same genetic background (transgenic as well as non-transgenic) showed a remarkably low anatomic variability (see figure 13 on page 23). Therefore we averaged the coregistered MRI images of all mice with the same genetic background, resulting in two MRI templates, one for ARTE10 mice, the other for Tg2576 mice. Therefore two brain masks were created by defining ROIs on these two MRI templates. The following ROIs were defined: the whole brain, the neocortex, the subcortical grey matter, the olfactory bulbs, the thalamus, the hippocampus, the brainstem and the cerebellum. Values from 10 to 100 were assigned to these ROIs, and 0 to voxels outside of the whole brain ROI (see figure 14 on page 51). This was done using Pmod 3.1. The two brain masks were then exported to SPM8

(Statistical Parametric Mapping, Welcome Trust Centre for NeuroImaging, University College London, GB) via Analyze-formatted files.
In SPM8, the Tg2576 specific brain mask was normalised to the ARTE10 specific brain mask with the following parameters: source image smoothing: 0.4 mm, template image smoothing 0.4 mm, nonlinear frequency cut-off 1.75, nonlinear iterations 14, nonlinear regularisations 1, preserve concentration, 7th degree B-Spline interpolation. This resulted in a transformation matrix that was then used to spatially normalise the PET images of the Tg2576 mice.

2.5.5 Normalisation of PET images and exporting to SPM

Before export for spatial normalisation and voxel-based analysis, PET images were normalised to the individual mean value of the cerebellum ROI in Pmod 3.1 using the scale tool. All cerebellum normalised PET images were then exported from the Pmod DICOM database to Analyze-formatted files.

2.5.6 Spatial normalisation of Tg2576 PET images.

The transformation matrix created with the two brain masks was then applied to all Tg2576 PET images using the Deformations tool in SPM8 with interpolation set to trilinear. The spatially normalised PET images of the Tg2576 mice were used for all further analysis steps.

2.5.7 Voxel-based group comparison with SPM

For voxel-based group comparisons we assigned all tg mice to one of four groups based on their Thioflavin S plaque load and tested them against the group of 17 wildtype animals. These groups were: group 1 with 14 animals and a plaque load from 0% to 3.2%, group 2 with 15 animals and a plaque load from >3.2% to 6.5%, group 3 with 15 animals and a plaque load from >6.5% to 9.0% and group 4 with 15 animals and a plaque load above 9.0%. Voxel-based group comparison was done with SPM8 using a two-sample t-test design with the

following parameters: assuming independence and unequal variance, no grand mean scaling, implicit masking and global calculation omitted. The resulting t-maps were thresholded at $p < 0.05$ with FWE-correction. The t-maps were saved as Analyze-formatted files, loaded in Pmod 3.1 and superimposed to the ARTE10 MRI template for identifying brain regions that show significant voxels.

2.6 Correlation of in-vivo PET signal with histological findings

2.6.1 Plotting and statistical analysis of PET ratios and histological findings

PET ratios and mean values of plaque load, plaque count and plaque size were loaded in GraphPad Prism (Version 6.0, GraphPad Software Inc., California, USA). GraphPad Prism were used for plotting diagrams and provided the tools to calculate statistical parameters such as curve fitting (least squares), r (Pearson's correlation coefficient) and to test whether the correlation coefficient was statistically significant, with p (two-tailed) ≤ 0.05 regarded as significant.
ΔPET signal per plaque load percentage point as used e.g. in figure 12 on page 48 was calculated by subtracting the mean cerebellar signal from the neocortex + hippocampus signal (i.e. PET ratio - 1) divided by plaque load.

2.6.2 Voxel-based regression analysis with plaque load with SPM

Voxel-based regression analysis with Thioflavin S plaque load was done with SPM8 using a multiple regression design with the individual Thioflavin S plaque load as covariate vector and the following parameters: centring to the overall mean, include intercept, implicit masking, global calculation omitted and no global normalisation. The resulting t-map was thresholded at $p \leq 0.05$ with FWE-correction. The t-map was saved as Analyze-formatted file, loaded in Pmod 3.1 and superimposed to the ARTE10 MRI template for identifying brain regions that show significant voxels.

3. Results

3.1 Ratio-based analysis of PET signal and histological findings

3.1.1 Overview of PET results

Figure 3 on page 36 provides a comparative overview of the actual PET images. In contrast to wildtype mice, tg mice showed higher tracer retention in cortical and hippocampal brain regions than in other brain regions. Higher tracer retention in the thalamus was observed mostly in old homozygous ARTE10 mice. All study groups showed only low tracer retention in the cerebellum. High tracer retention in retro-orbital structures and structures neighbouring the olfactory bulb was another common feature of all study groups. Beyond that, no other structures outside of the brain showed constantly another distinct focus of tracer retention, neither within a study group nor across study groups.

An overview of PET ratios sorted by study group is given in figure 5 a) on page 38. In general, transgenic mice of all study groups showed PET ratios of greater 1.0 with the highest PET ratios found in old homozygous ARTE10 mice. In contrast, most wildtype mice showed PET ratios of 1.0 and below, but some wildtype mice presented with a PET ratio as high as 1.08.
Given the low PET ratios in some mice from the study groups ARTE10 tg/- and Tg2576 tg there is a potential overlap of PET ratios between transgenic and wildtype mice. Therefore transgenic animals that showed low PET ratios were not unambiguously distinguishable from wildtype mice merely by PET imaging.

3.1.2 Overview of histological plaque load results

We employed three different stainings to histologically measure the plaque load: Thioflavin S (TfS) staining against Aβ deposits and two immunofluorescence (IF) stainings, one against full length Aβ peptide (N1-Aβ) and the other against the N3-truncated pyroglutamate Aβ peptide (N3pE-Aβ).

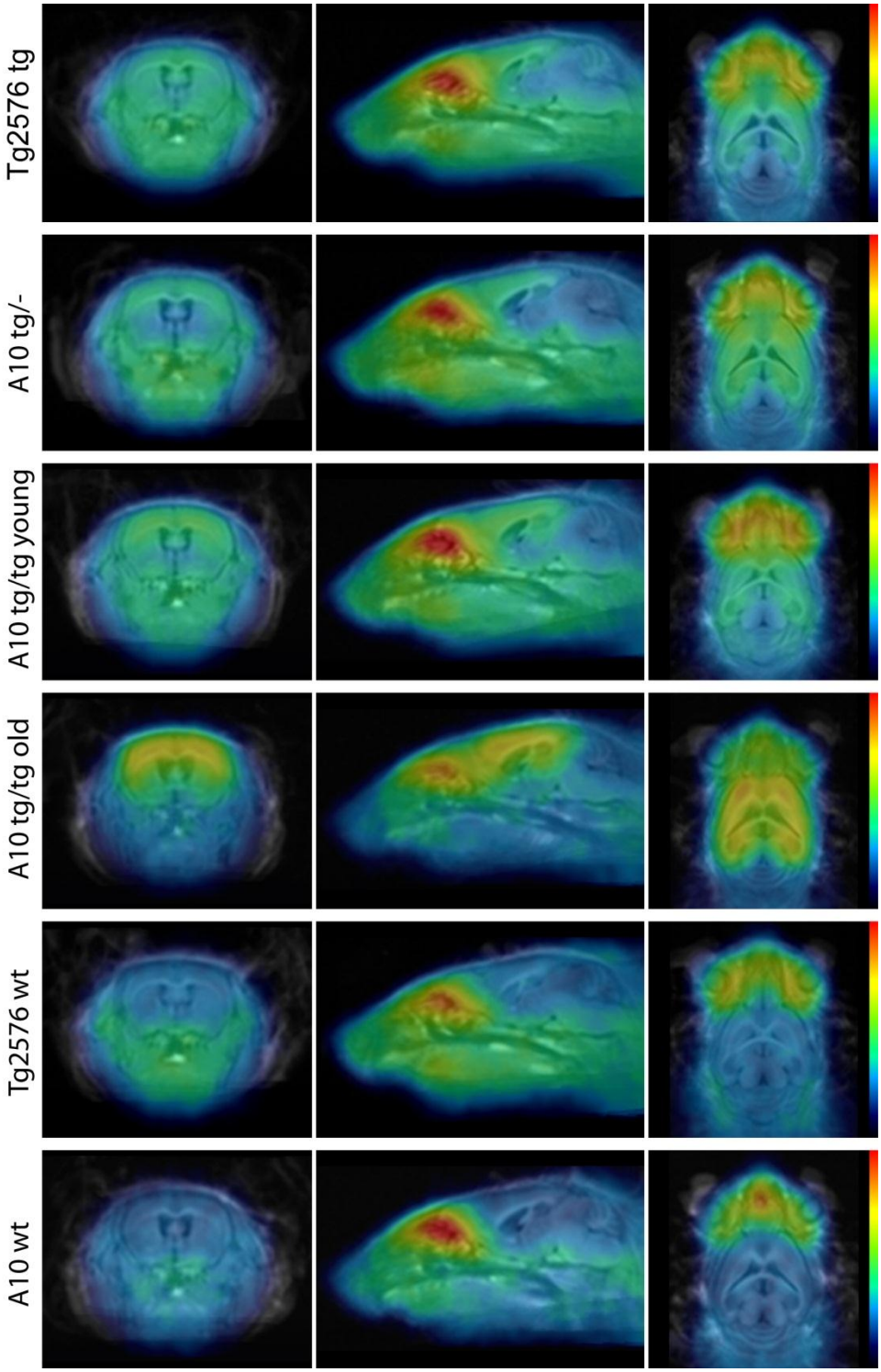

Figure 3. Overview of PiB PET images sorted by study group. Each row represents a mean of all PET images of the study group in coronal view (left column), sagittal view (middle column) and horizontal view (right column). Colour scale bar represents (from black to red) 0 to 0.06 %ID*kg/cc (percentage of injected dose per cc, normalised to body weight in kg). PET images are superimposed on their study group specific MRI template.

Figure 4 on page 37 demonstrates the different spectrum of Aβ visualised by the three stainings. Thioflavin S positive plaques appeared as mostly densely packed Aβ aggregates or Aβ deposits within the blood vessel walls (not shown in the figure). The staining against full length Aβ peptide additionally revealed Aβ deposits with lower density. These lower density Aβ deposits were spread over large parts of the brain but not the cerebellum. In contrast, the stainings against N3pE-Aβ were mostly found as small fractions of larger Aβ deposits of higher density and hereby rather in the centres than outer parts of these deposits.

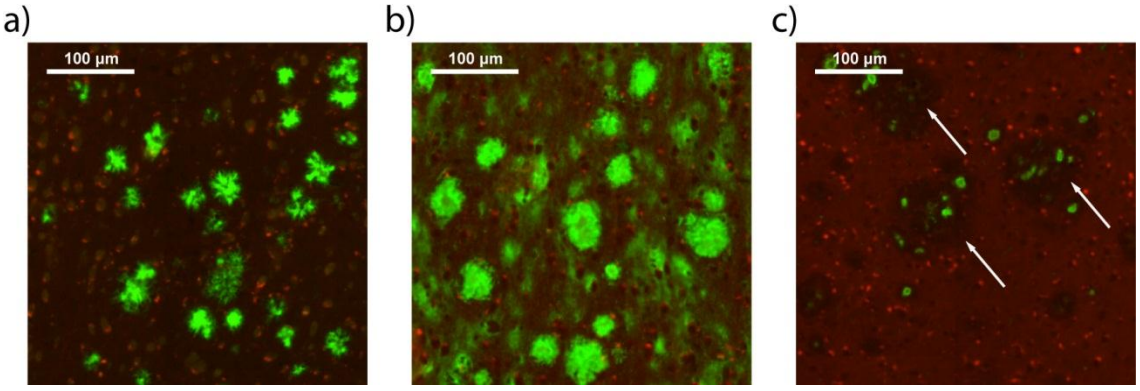

Figure 4. Visual comparison of the stainings. Detail of the frontal cortex of an A10 tg/- mouse (sections not corresponding). For better illustration, DAPI staining (blue channel) was removed and unspecific tissue background (red channel) was enhanced. The green channel with specific staining signal was not altered. a) Thioflavin S staining, b) immunofluorescence staining against full length Aβ and c) immunofluorescence staining against N3-pyroglutamate-Aβ (N3pE-Aβ). Arrows in c) point at shadows in the tissue background caused by plaque deposits. N3pE-Aβ positive staining signal was found mainly in the middle of those plaque shadows.

An overview of individual plaque load results of the three stainings sorted by study group is given in figure 5 b), c) and d) on page 38. Figure 6 on page 39 illustrates exemplarily the spectrum of Thioflavin S plaque load found in the tg animals and the visual results of plaque detection by Acapella.

Measuring plaque load with Thioflavin S or IF against Aβ allowed to undoubtedly distinguish between transgenic and wildtype animals. Even the lowest TfS plaque load found in transgenic mice was still more than 13 fold higher than the highest value in wildtype mice. For the IF staining against Aβ, this relation was greater than 15 fold. This is contrasted by the plaque load results of the IF stainings against N3pE-Aβ for which we found values of several

tg mice within the range of wildtype mice. Hereby the values found in wildtype mice (i.e. the rate of false positive signal) in the IF stainings against N3pE-Aβ were in the same range as the values found with the IF staining against Aβ (mean plaque load value for wildtype in the IF staining against Aβ: 0.30%, mean plaque load value for wildtype in the IF staining against N3pE-Aβ: 0.16%). Therefore the overlap of wildtype mice with transgenic mice observed in the results of the IF stainings against N3pE-Aβ was not based on a higher unspecific signal in this staining.

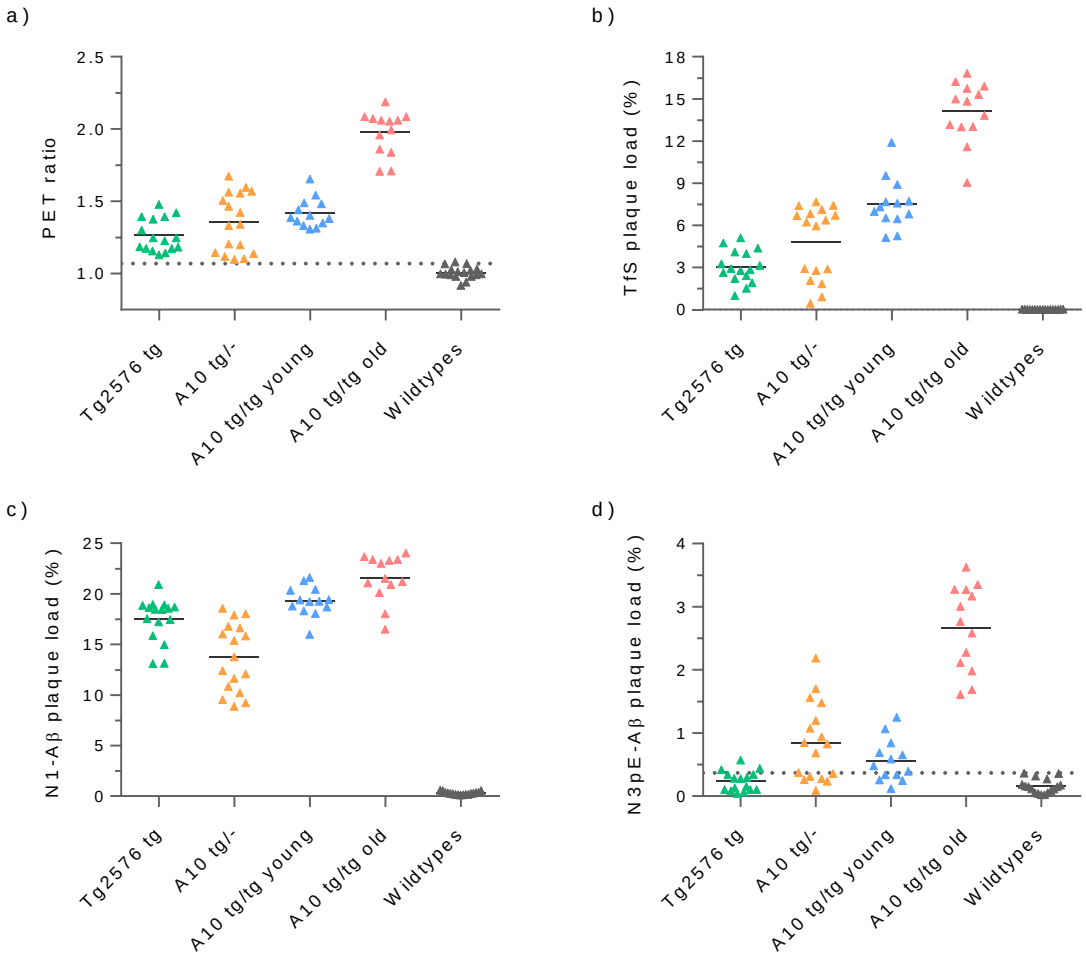

Figure 5. Overview of PET and histological determined plaque load sorted by study group (A10 wt and Tg2576 wt combined in the group *Wildtypes*). (a) Individual PiB PET ratios during the last 10 minutes of the scan (36-45 min). Values represent the ratio of the signal measured in a VOI comprising the neocortex and hippocampus to the signal measured in a VOI comprising the cerebellum. (b) Individual Thioflavin S plaque load. (c) Individual plaque load in the immunofluorescence staining against full length Aβ (N1-Aβ). (d) Individual plaque load in the immunofluorescence staining against N3-pyroglutamate-Aβ (N3pE-Aβ). All plaque load values are given as percentage of stained area relative to a ROI comprising the neocortex and hippocampus. Dotted lines mark the highest value measured in wildtype mice.

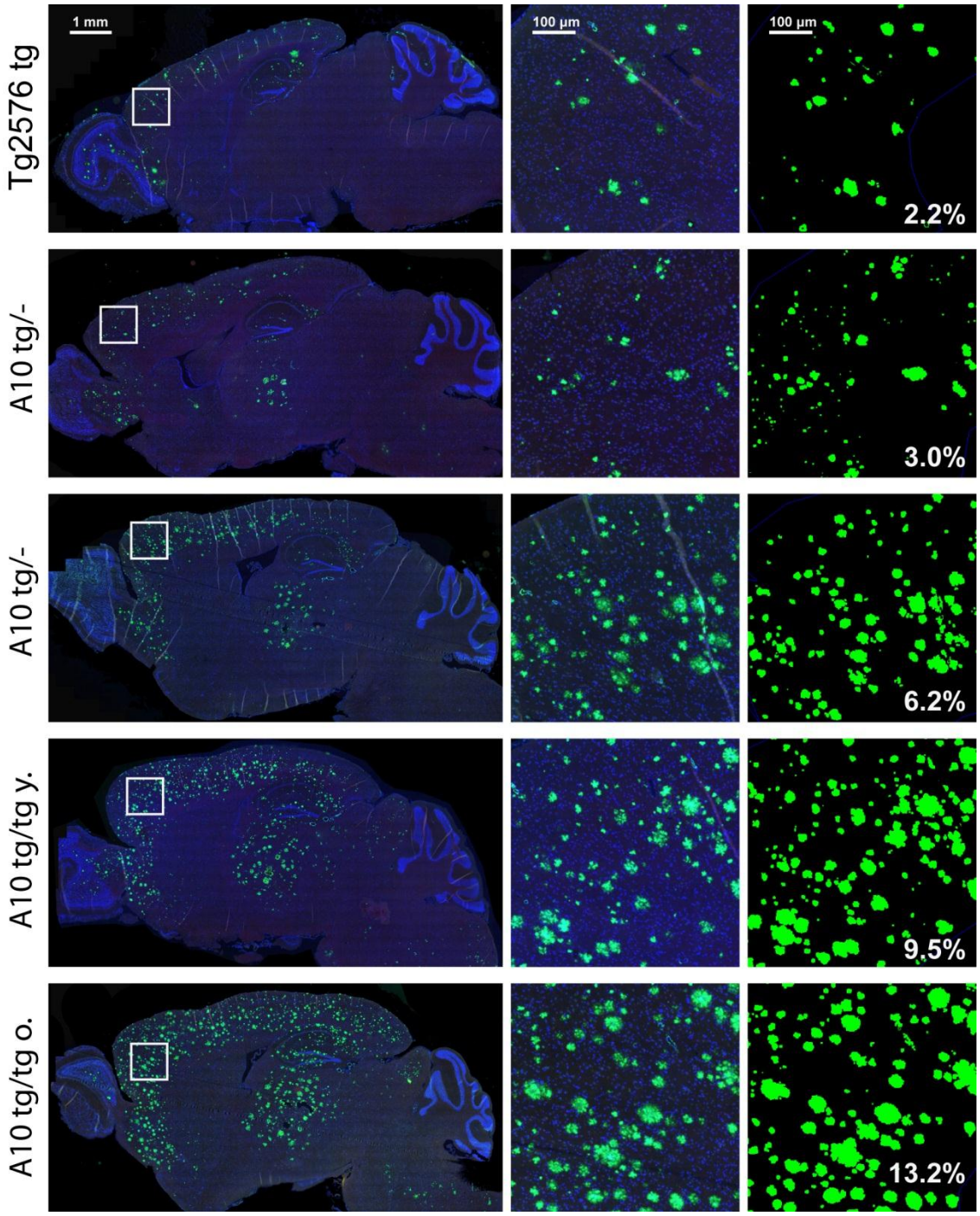

Figure 6. Overview of Thioflavin S stainings and Acapella results of exemplary sections with one mouse per row. Its particular group affiliation is given on the left. Left column shows a full view of the sections in the way they were acquired by the slide scanner, with DAPI (blue channel), Thioflavin S (green channel) and unspecific tissue background (red channel). Middle column shows the zoom (10x) of the area indicated in the full view section by the white rectangle. Right column shows Acapella results of that area. Percentage value in the right column represents the mean Thioflavin S plaque load value measured in the particular mouse, not the value of the zoomed area. Scale bars in the first row apply to all rows.

Interestingly, the Thioflavin S plaque load did not simply constitute a constant fraction of Aβ plaque load. This was especially true for Tg2576 tg animals compared to ARTE10 tg/- animals. ARTE10 tg/- mice showed a higher mean Thioflavin S plaque load than Tg2576 tg mice, but the opposite was true regarding Aβ plaque load. Likewise, old homozygous ARTE10 animals showed higher Thioflavin S plaque load values with a low overlap with young homozygous ARTE10 animals, but this clear discrimination between the groups could not be found in the Aβ plaque load results.
Noteworthy as well, N3pE-Aβ plaque load values of most Tg2576 tg animals ranged within the spectrum of false positive values found in wildtype mice. Also, ARTE10 tg/- mice showed higher N3pE-Aβ values than young homozygous ARTE10, though ARTE10 tg/- mice had a lower mean Thioflavin S plaque load and Aβ plaque load.

3.1.3 Formation of plaque load by plaque size and plaque count

Besides overall plaque load, Acapella analyses mean plaque size and mean plaque count within a given ROI. Figure 8 on page 42 illustrates the course of these two measures in relation to increasing plaque load for each staining.
Additional production of Aβ peptide can deposit in two ways. It can either deposit as a new plaque i.e. increasing plaque count, or leading to a growth of existing plaques i.e. increasing plaque size. In principle, both processes were observed in our transgenic animals with increasing plaque load but with differing emphasis among the study groups and stainings.
For Thioflavin S positive plaques, Tg2576 tg animals showed a higher tendency towards a growth in plaque size than transgenic ARTE10 animals. For the Aβ staining, the opposite is true with a higher tendency towards an increase in plaque count in Tg2576 tg animals than in transgenic ARTE10 animals. Hereby, we even observed a decrease in plaque count with increasing Aβ plaque load in homozygous ARTE10 animals. This seemingly contradictory result can be explained by our observation that with increasing Aβ plaque load, groups of plaques with low density Aβ deposits in between tended to be detected as one

large entity by Acapella. In turn, N3pE-Aβ plaque load grew almost exclusively in count and only marginal in size. This observation applied primarily to transgenic ARTE10 animals as the N3pE-Aβ plaque load values of Tg2576 tg animals ranged mostly within the values of unspecific signal found in wildtype animals.

3.1.4 Mutual relationships between histological findings

As mentioned before, Thioflavin S positive plaque load did not seem to be merely a constant fraction of Aβ plaque load. Though a significant correlation between Thioflavin S plaque load and Aβ plaque load existed (figure 9 a) on page 44), the relationship of Aβ plaques to Thioflavin S positive plaques was better described looking at Aβ plaque size and Thioflavin S plaque count (figure 9 b) and c) on page 44). Aβ plaque size rather than Aβ plaque load showed a better correlation with Thioflavin S plaque load and in turn, Thioflavin S plaque count rather than Thioflavin S plaque load showed a better correlation with Aβ plaque load.

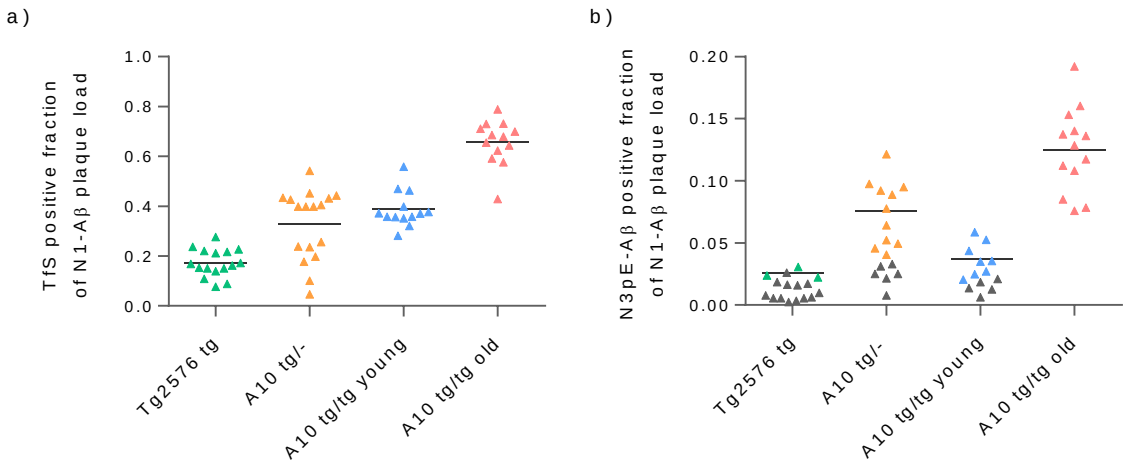

Figure 7. Fraction of full length Aβ (N1-Aβ) plaque load that is positive for Thioflavin S plotted in a) and N3-pyroglutamate-Aβ (N3pE-Aβ) plotted in b). Transgenic mice with N3-pyroglutamate-Aβ values within the range of wildtype values were regarded as false positive and greyed in b) and excluded from mean calculation (grey line).

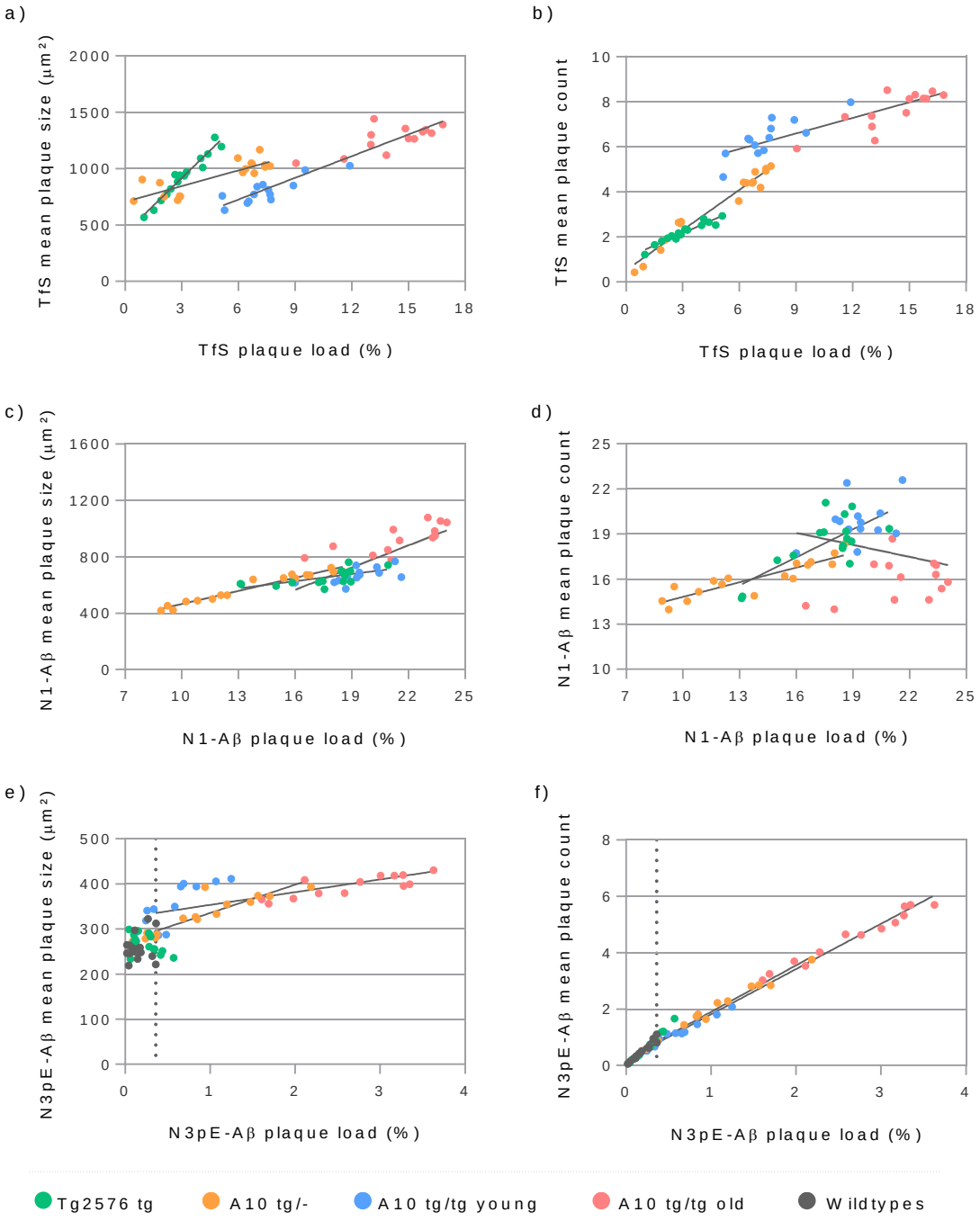

Figure 8. Mean plaque size and count for a) and b) Thioflavin S, c) and d) immunofluorescence staining against full length Aβ (N1-Aβ), e) and f) immunofluorescence staining against N3-pyroglutamate-Aβ (N3pE-Aβ). All plaque load values are given as percentage of stained area relative to an area of a ROI comprising the neocortex and hippocampus. All plaque count values refer to 10,000 ROI-pixels (approx. 68,540 µm²). Grey lines represent a linear fit of each group with A10 tg/tg young and old fitted as one group. Dotted grey line represents highest N3pE-Aβ plaque load value measured in wildtype mice. Transgenic mice with N3pE-Aβ plaque load values within the range of wildtypes were excluded from curve fitting.

In both considerations, Tg2576 tg animals distinguished themselves from transgenic ARTE10 animals. With about the same Aβ plaque load, Tg2576 tg animals tended to have a lower Thioflavin S plaque load. Analogously, at the same Aβ plaque size, Thioflavin S plaque load of Tg2576 tg animals also ranged below transgenic ARTE10 animals. This means in turn, that with about the same Thioflavin S plaque count, Aβ plaque load ranged higher in Tg2576 animals than in transgenic ARTE10 animals. Therefore the fraction of Aβ peptide turned into Thioflavin S positive deposits was lower in Tg2576 tg animals than in transgenic ARTE10 animals (see also figure 7 a) on page 41). The relative amount of Aβ plaque load that is not positive for Thioflavin S is therefore increased in Tg2576 tg animals compared to transgenic ARTE10 animals. Additionally, unlike transgenic ARTE10 animals, it showed a tendency to further increase with higher Aβ plaque load (figure 9 d) on page 44). N3pE-Aβ plaque load constituted only a minor fraction of total Aβ plaque load (figure 7 b) on page 41) and correlated well with Thioflavin S plaque load (figure 9 e) on page 44), and less with Thioflavin plaque size (figure 9 f) on page 44) or count (data not shown).

3.1.5 Correlation of PET results with histological plaque load

All three stainings revealed high correlations with ratio-based PET results (figure 10 on page 45). The highest correlation with PET ratios was found with Thioflavin S plaque load. The correlation of PET ratios with Aβ plaque load showed the lowest correlation and also a tendency of separating groups with Tg2576 tg animals showing high Aβ plaque load levels but relatively low PET ratios compared to ARTE10 tg/- animals with about the same Aβ plaque load. To a lower extend the same is true for Tg2576 tg animals compared to young homozygous ARTE10 animals. Correlating N3pE-Aβ with PET ratios showed a high correlation among animals that were found with a N3pE-Aβ plaque load value above the values of wildtype animals. However transgenic animals with unspecific N3pE-Aβ plaque load values showed PET ratios as high as 1.44.

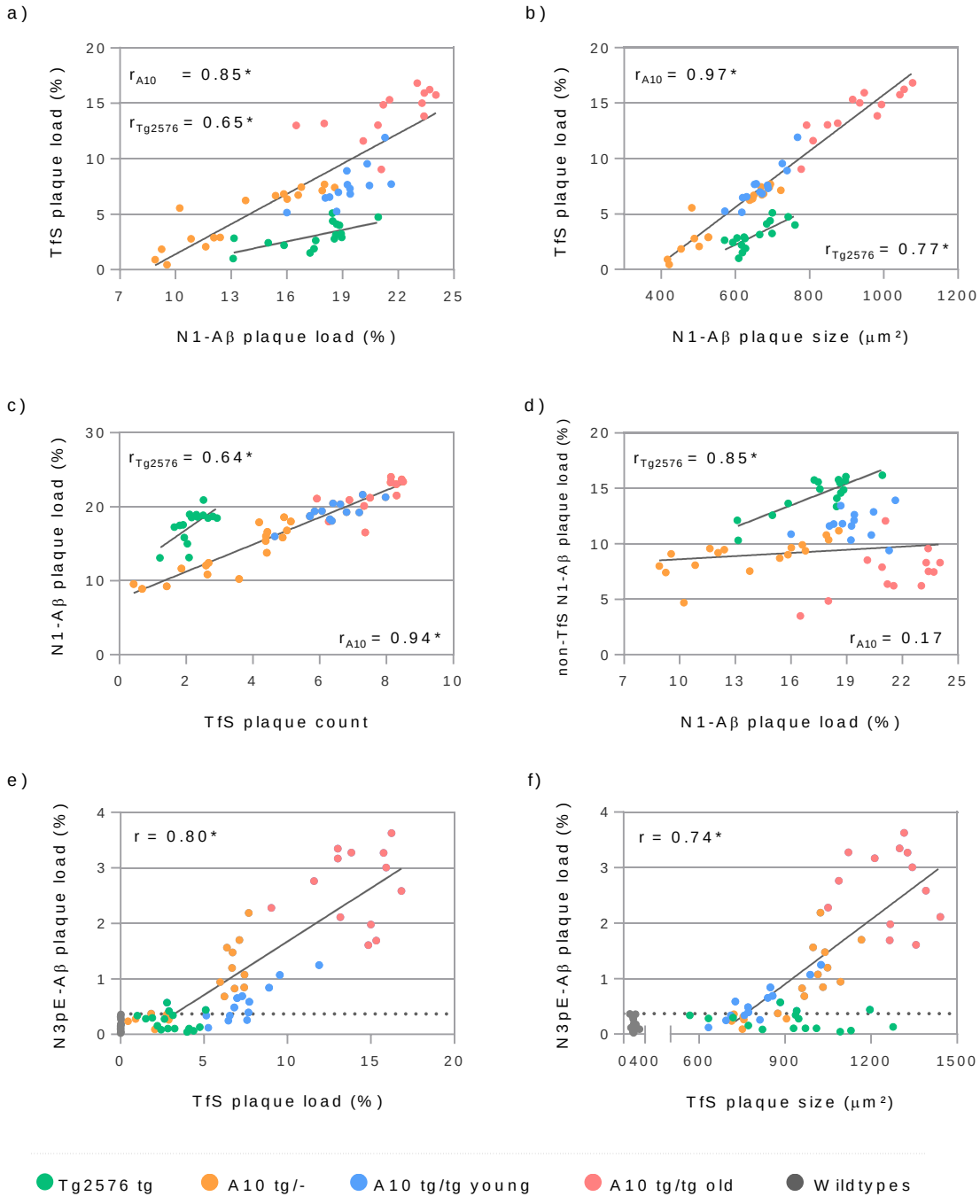

Figure 9. Mutual relationship of histological findings for: a) Thioflavin S plaque load with plaque load measured with immunofluorescence against full length Aβ (N1-Aβ), b) Aβ plaque size and TfS plaque load, c) TfS plaque count and N1-Aβ plaque load, d) non-TfS N1-Aβ plaque load (i.e. N1-Aβ plaque load - TfS plaque load representing an estimate of low density Aβ plaque load) with N1-Aβ plaque load, e) TfS plaque load and N3pE-Aβ plaque load and f) TfS plaque size and the amount of N3pE-Aβ plaque load found. All ARTE10 animals were fitted together. Animals within the range of wildtypes in e) and f) were excluded from fit calculation.

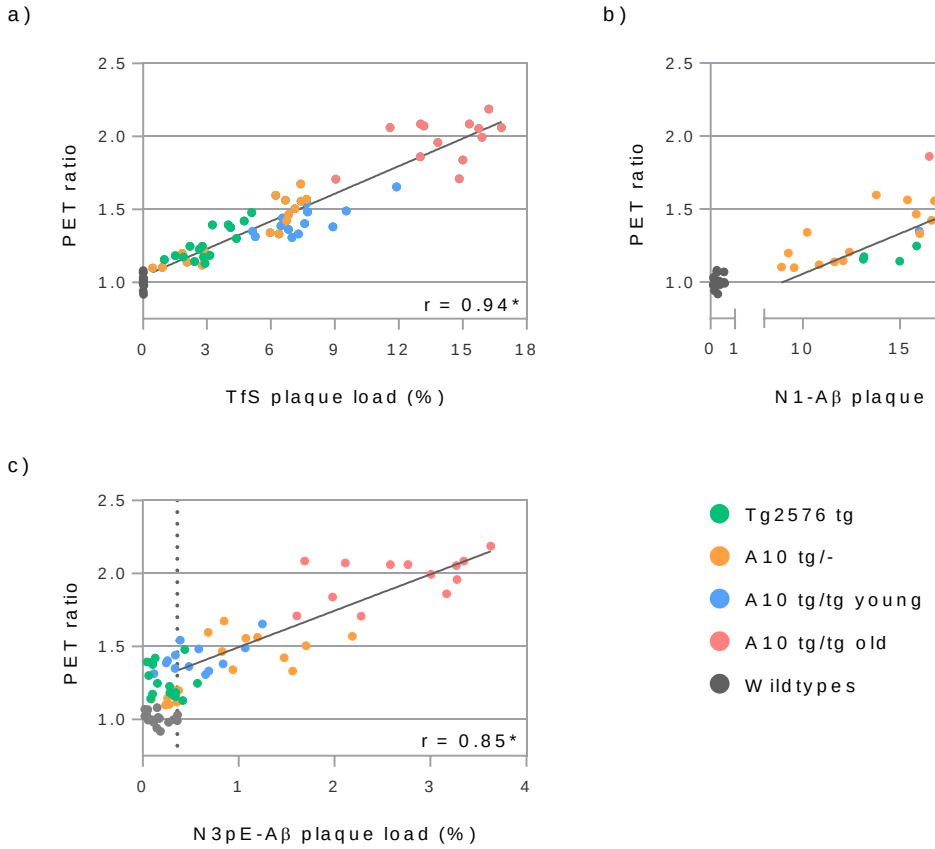

Figure 10. Correlation of PET ratio with plaque load measured with a) Thioflavin S, b) IF against Aβ and c) IF against N3pE-Aβ. Grey lines represent a linear fit of all transgenic animals. Dotted grey line represents highest N3pE-Aβ plaque load value measured in wildtype mice. r values represent Pearson's correlation coefficients (including outliers), * indicates significance for p(two-tailed) < 0.05. Transgenic mice with N3pE-Aβ plaque load values within the range of wildtypes were excluded from fit and r calculation.

3.1.6 Correlation of PET results with plaque size and plaque count

The high correlation of PET results with Thioflavin S plaque load could not be attributed to one of the two plaque load forming quantities, i.e. plaque size and load correlated less with PET results than plaque load (figure 11 a) and b) on page 47). A different finding can be observed in the Aβ staining results: Aβ plaque size showed a higher correlation with PET results than the Aβ plaque load (figure 11 c) on page 47). Hereby transgenic ARTE10 animals and Tg2576 tg animals showed about the same slope of the fitted curve with similar

correlations but Tg2576 tg animals ranged at a lower level i.e. lower PET ratios at the same range of Aβ plaque size, which is analogue to the correlation of Aβ plaque size and Thioflavin S plaque load (figure 9 b) on page 44).
Aβ plaque count correlated even negatively with PET results for transgenic ARTE10 animals, and shows no correlation in Tg2576 tg animals. The opposite is true for N3pE-Aβ plaque size and N3pE-Aβ plaque count with N3pE-Aβ plaque count correlated far better with PET results than N3pE-Aβ plaque size.

3.1.7 Yield of PET signal in relation to plaque load and plaque formation

The gain of PET signal (relative to the cerebellum) per Aβ plaque load percentage point increased with growing Aβ plaque size. Hereby the calculated fits of transgenic ARTE10 animals and Tg2576 tg animals showed about the same slope of the fitted curve with the same correlations but Tg2576 tg animals ranged at a lower level i.e. a lower gain of PET signal per Aβ plaque size (figure 12 a) on page 48). This is analogue to the observation that Tg2576 tg animals showed a lower tendency to turn Aβ plaque load into Thioflavin S positive plaque load (figure 9 b) on page 44) and that Tg2576 tg animals showed a lower PET ratio at a certain average Aβ plaque size (figure 11 c) on page 47).
Across study groups we observed different gain of PET signal (relative to the cerebellum) per Thioflavin S plaque load percentage point (figure 12 b) on page 48). Analysing the correlation of gain of PET signal and Thioflavin s plaque size, plaque count and the quotient of plaque size to plaque count, we observed a significant negative correlation for plaque count and a significant positive correlation for the quotient of plaque size to plaque count (figure 12 c), d) and e) on page 48). Plaque size and non-TfS Aβ plaque load correlations were not significant. We observed one outlier in the Tg2576 tg study group and two outliers in the ARTE10 tg/- study group. These three outliers showed very low Thioflavin S plaque load values of ≤ 1%. The analysis given in figure 12 includes these three outliers. To test whether these three outliers significantly influenced our findings we calculated the correlation coefficients without them.

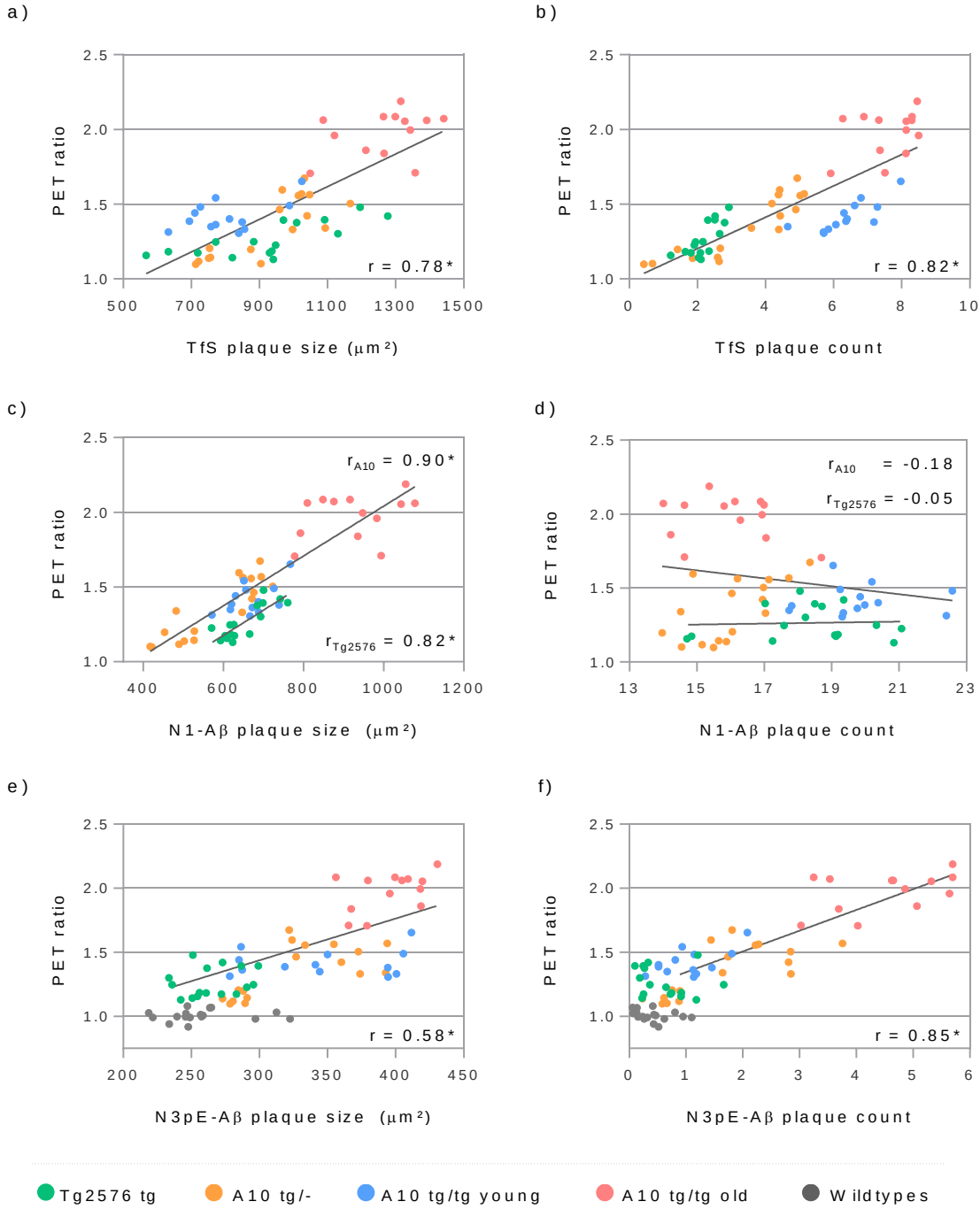

Figure 11. Correlation of PET ratio with plaque size and plaque count for a) and b) Thioflavin S stainings, c) and d) immunofluorescence stainings against full length Aβ (N1-Aβ), e) and f) immunofluorescence stainings against N3-pyroglutamate-Aβ (N3pE-Aβ). For N1-Aβ plaque size and plaque count in c) and d), transgenic ARTE10 animals and Tg2576 tg animals were fitted separately. r values represent Pearson's correlation coefficients (including outliers), * indicates significance for p(two-tailed) < 0.05. Transgenic animals with N3pE-Aβ plaque load within the range of wildtype animals were excluded from fit and r calculation in e) and f).

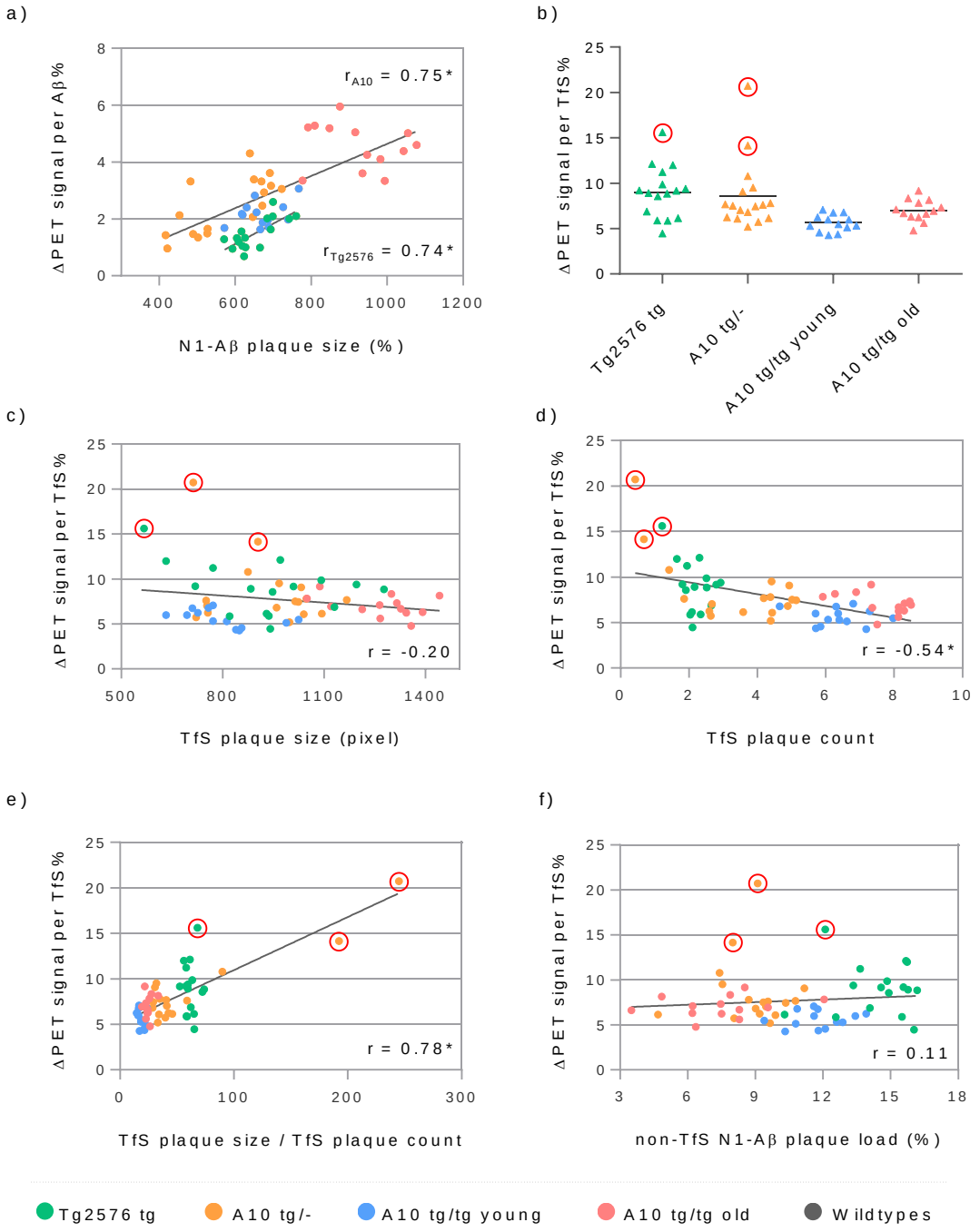

Figure 12. Yield of PET signal per plaque load and its formation. a) PET signal gain per full length Aβ (N1-Aβ) plaque load percentage point to N1-Aβ plaque size. b) PET signal gain per Thioflavin S plaque load percentage point sorted by study group. Graphs c) to f) plot PET signal gain per Thioflavin S plaque load percentage point to the c) Thioflavin S plaque size, d) Thioflavin S plaque count, e) quotient of Thioflavin plaque size to Thioflavin S plaque count and f) N1-Aβ plaque load that is not Thioflavin S positive (N1-Aβ plaque load - Thioflavin S plaque load). r values represent Pearson's correlation coefficients (including outliers), * indicates significance for p(two-tailed) < 0.05. Red circled data points indicate outliers which were excluded in an alternative analysis (see main text).

Excluding the three outliers, the correlation of the gain of PET signal per Thioflavin S percentage point with Thioflavin S plaque size was reduced to a coefficient of 0.01, correlated with Thioflavin S plaque count was reduced to a coefficient of -0.44 (remains significant), correlated with plaque size to plaque count quotient was reduced to 0.54 (remains significant) and correlated with non-TfS Aβ plaque count was increased to 0.26 (does not reach significance). Therefore the three outliers did not alter significantly our findings.

3.2 Voxel-based analysis of PET signal

3.2.1 Spatial normalisation of PET images

During the creation of the study group specific MRI templates necessary for the ROI-ratio-based analysis of the PET images, we already observed a very low variability of anatomical measures of the brains of mice with the same genetic background (i.e. among ARTE10 animals or among Tg2576 animals), but a high difference between the animals with a different genetic background (i.e. ARTE10 animals compared with Tg2576 animals).

Before we analysed the PET images on a voxel-basis, we measured the anatomical differences of the brains of the animals to clarify the need to spatially normalise the PET images across study groups. We regarded a difference of anatomical brain measures within the range or above small animal PET resolution (~1.5 mm FWHM at the centre of the FOV[178]) as critical value to necessitate spatial normalisation.

Analysis of anatomical brain measures is illustrated in sagittal view in figure 13 on page 50. Most prominent differences include the total length of the brain with a difference of 0.8 mm, length of the neocortex with a difference of 1.4 mm and the length of the cerebellum with a difference of 0.6 mm.

We decided to spatially normalise the PET images based on the different length of the neocortex, a brain region of high importance in our analysis as most of the Aβ plaque deposits are found here.

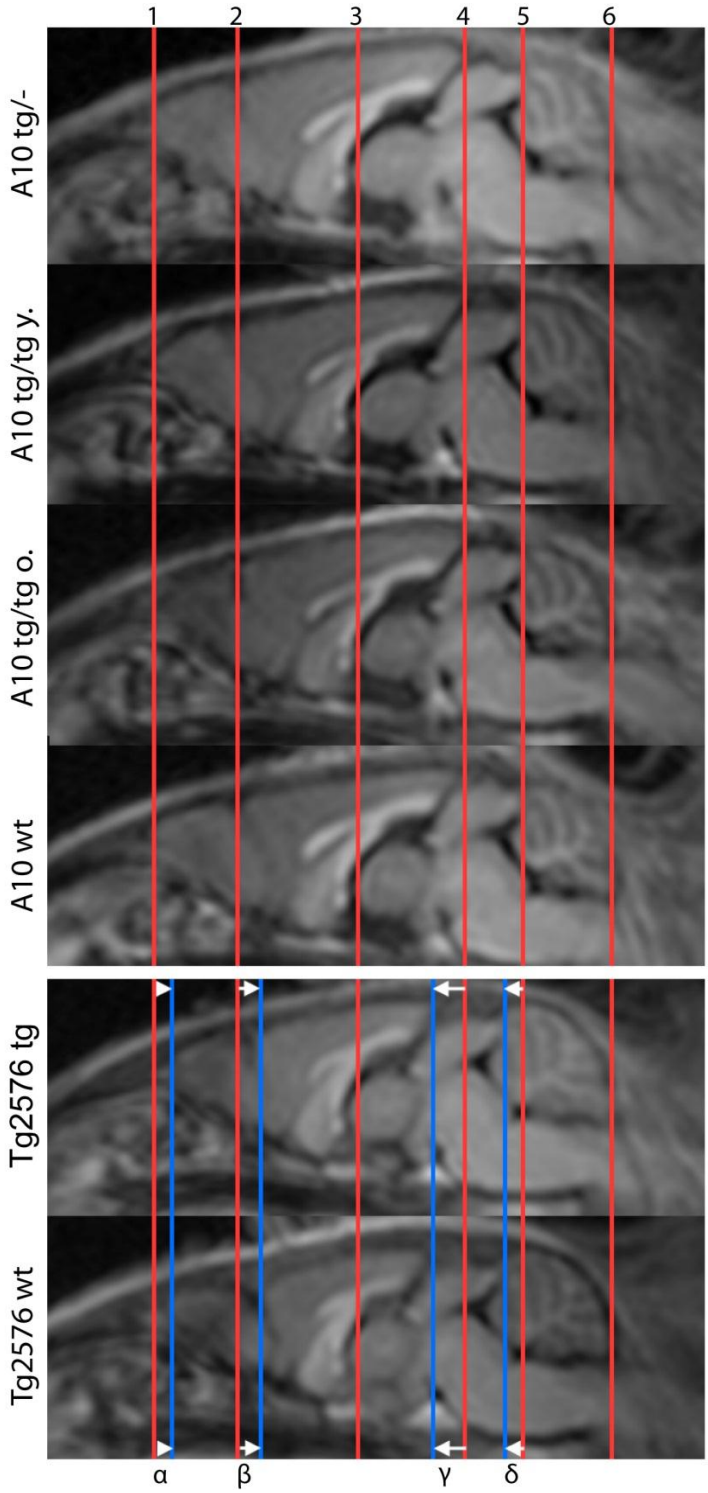

Figure 13. Group-wise comparison of measures of MRI templates. Each row represents the mean of all brain MRI scans acquired in that group. Position of structures are marked with lines for A10 mice (red) and Tg2576 mice (blue) with 1 rostral tip of the olfactory bulb, 2 frontal neocortex, 3 thalamus, 4 caudal tip of the neocortex, 5 caudal tip of the colliculus, 6 caudal tip to the cerebellum. Differences in measures between A10 and Tg2576 mice are α ≈ 0.8 mm, β ≈ 0.7 mm, γ ≈ 0.7 mm, δ ≈ 0.6 mm. Total length of line 1 to 6 ≈ 16.0 mm, line 2 to 6 ≈ 12.6 mm.

PiB PET images of brains of mice cannot be spatially normalised on the basis of information provided by the PET images themselves. There are not enough cerebral structures distinguishable that could serve as markers for spatial transformation. A possible work-around is to use the MRI images to create a transformation matrix and apply it to the coregistered PET images. However our MRI images were acquired using a clinical MRI scanner and did not provide the necessary contrast for satisfying normalisation results. We circumvented this problem by manually creating brain masks based on the MRI templates for ARTE10 animals and Tg2576 animals. These brain masks provided sharp contrasts between important brain structures. Figure 14 on page 51 demonstrates the workflow of creating the MRI masks and consecutive spatial normalisation of the MRI masks (Tg2576 normalised to ARTE10). The resulting transformation matrix was applied to all PET images of the Tg2576 tg and Tg2576 wildtype animals.

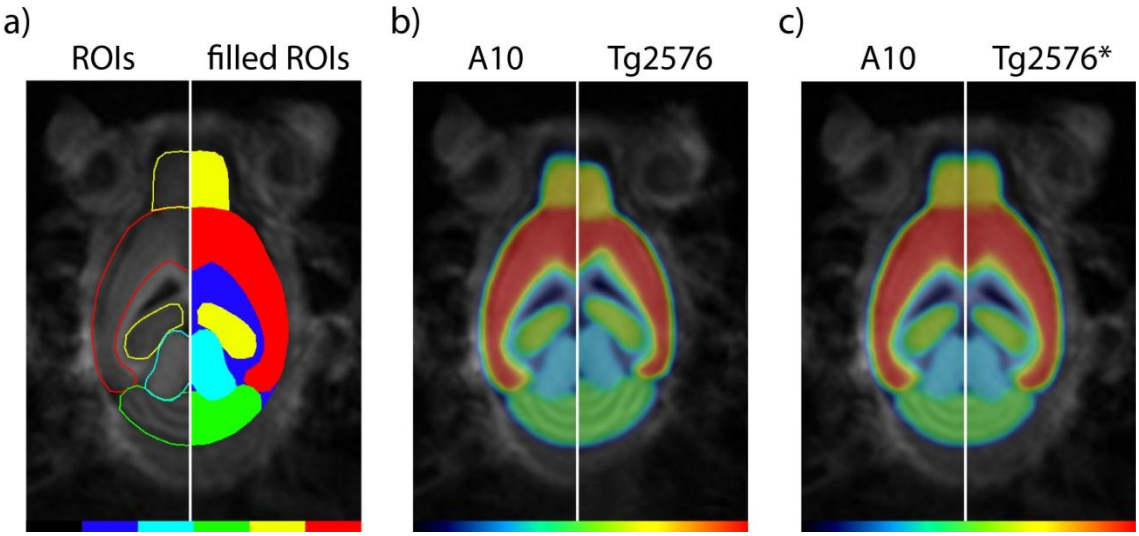

Figure 14. Creation and Comparison of MRI masks for spatial normalisation of PET images. a) Creation of the MRI Mask via ROI drawing (left) and filling (right) with values from 0 (black, outside of the brain) to 100 (red, cortex). The resulting mask was created twice, one fitting to the ARTE10 mouse model and one fitting to the Tg2576 mouse model. b) Comparison of the two resulting MRT masks for all ARTE10 mice (left) and all Tg2576 mice (right), both superimposed to a group specific MRT template c) Mask for ARTE10 mice unchanged, MRT mask of Tg2576 mice after spatial normalisation to the ARTE10 mask (Tg2576*), both superimposed to the ARTE10 MRT template. Colour sale bar represents values assigned to the ROIs (black to red: 0 to 100). Masks in b) and c) are smoothed with 0.4 mm Gaussian Filter.

3.2.2 Voxel-based analysis of PiB retention

Analysing regional PiB tracer retention on a voxel-basis served two questions. First, identifying significant voxels of tracer retention and their corresponding brain regions and second, analysing the course of distribution of significant voxels across the brain with increasing plaque load.

In order to study these two questions, we divided all transgenic animals in 4 different groups based on their Thioflavin S plaque load value. We chose the Thioflavin S plaque load value for group allocation as ratio-based analysis of the PET images showed the best correlation of PET ratios with Thioflavin S plaque load (see figure 10 on page 45). When defining plaque load ranges for group allocation of the transgenic animals to four groups, we had to compromise between comparable share of plaque load spectrum and group size. This resulted in the first three groups covering each a plaque load spectrum of around 3% (n = 14, 15 and 15) and the fourth group covering plaque load values of greater than 9% (n = 15).

Figure 15 on page 53 illustrates the resulting t-maps of the four analysis groups in coronal view thresholded at $p \leq 0.05$ with FWE correction.

Group 1 with a Thioflavin S plaque load of 0% to 3.2% showed significant voxels mainly in the neocortex with highest t-values found in frontal regions. Group 2 with a Thioflavin S plaque load of >3.2% to 6.5% showed an increase in significant voxels compared to group 1 with most voxels found still in the neocortex but reaching further caudal. Additional voxel were identified in dorsal parts of the hippocampus. The focus of t-values remained on frontal parts of the neocortex. Group 3 with a Thioflavin S plaque load of >6.5% to 9% showed a further increase in voxels with significant voxels reaching further caudal in the neocortex compared to group 2 and now covering larger parts of the dorsal hippocampus. The focus of t-values shifted slightly to more caudal parts of the neocortex with a second focus in the most dorsal regions of the hippocampus. Group 4 with a Thioflavin S plaque load of >9% showed again an increase in voxels now covering almost the entire neocortex and hippocampus and additionally large parts of the dorsal thalamus. A clear regional focus could not

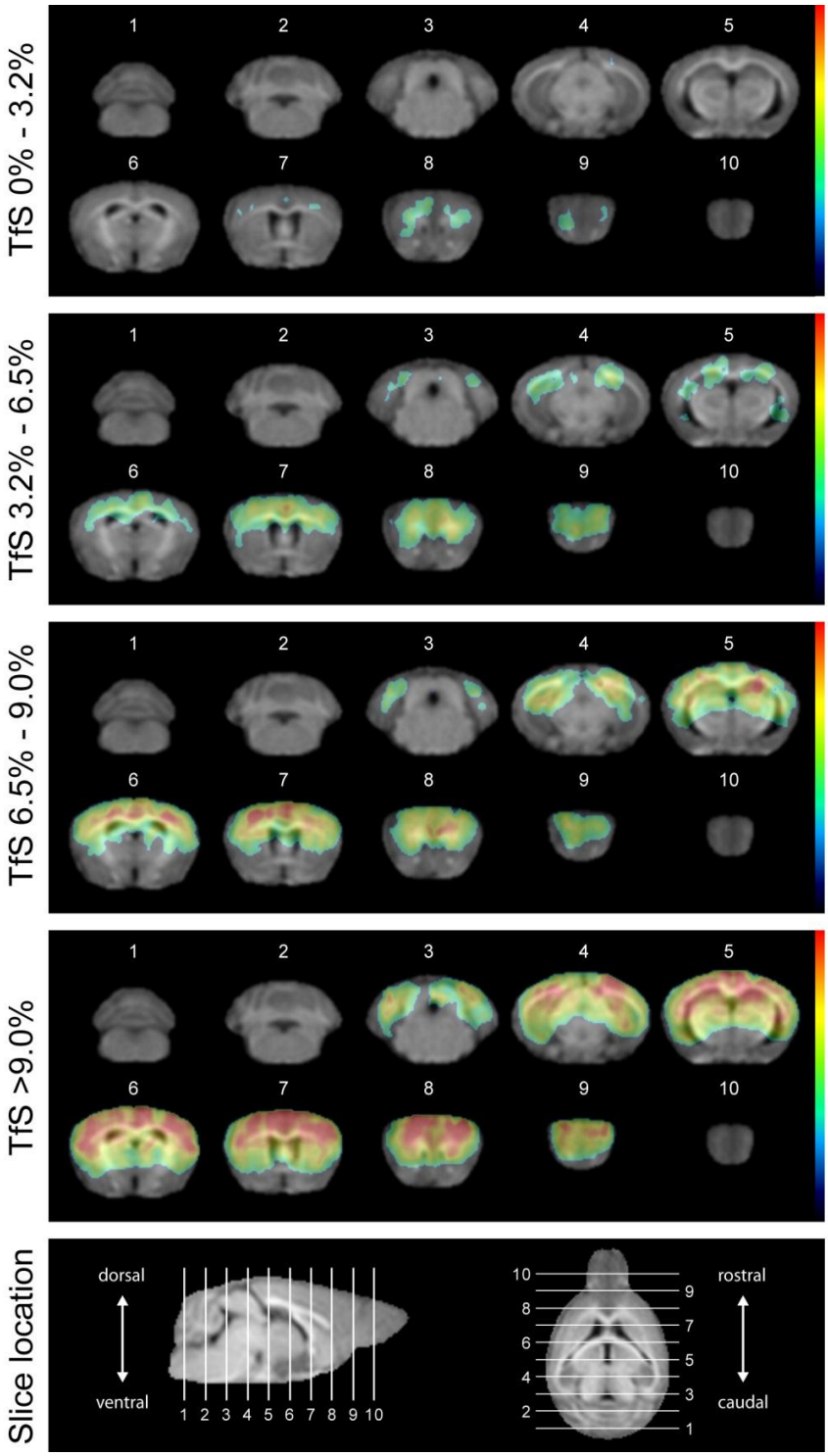

Figure 15. Voxel-based analysis of PET tracer retention. Transgenic animals were stratified by Thioflavin S plaque load into 4 groups and tested against wildtype animals (n=17). Images represent resulting t-map superimposed to a brain extracted MRI template of all ARTE10 tg animals. Rows from top to bottom: Group 1 (0% to 3.2%, n=14), Group 2 (>3.2% to 6.5%, n=15), Group 3 (>6.5% to 9.0%, n=15), Group 4 (>9.0%, n =15), last row depicts location of numbered coronal slices used in row 1 to 4. Colour scale bar represents t value from 0 to 15 (black to red). Applied t-contrast is thresholded with pFWE ≤ 0.05.

be identified anymore but most caudal parts of the neocortex showed the lowest t-values still regarded as significant.
In all groups, the cerebellum and most of the olfactory bulb showed no significant voxels.

3.2.3 Voxel-based regression analysis with plaque load

In order to further establish a relation between the voxel-based signal and histological findings, we performed a voxel-based regression analysis with Thioflavin S plaque load in all transgenic animals. Figure 16 on page 54 illustrates the resulting t-map, thresholded at $p \leq 0.05$ with FWE correction. Significant voxels covered almost the entire neocortex and hippocampus and large parts of the dorsal thalamus. Highest t-values were found mostly in the frontal and parietal parts of the neocortex and dorsal regions of the hippocampus. The cerebellum and most of the olfactory bulb showed no significant voxels.

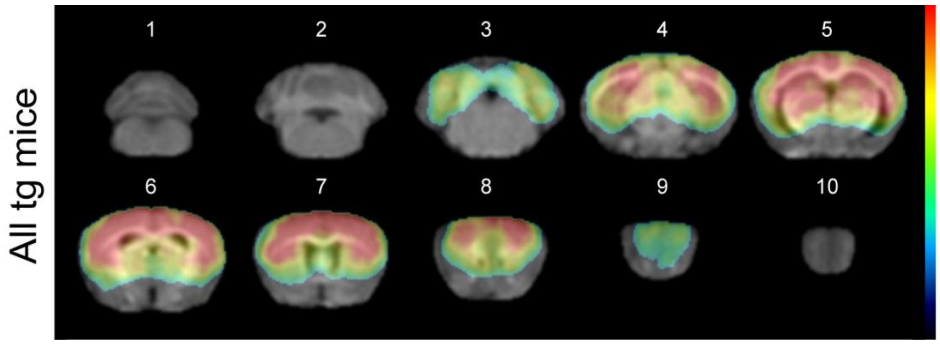

Figure 16. Voxel-based regression analysis with Thioflavin S plaque load for all transgenic mice (n=59). Images represent resulting t-map superimposed to a brain extracted MRI template of all ARTE10 animals. Numbered coronal slices are at the same location as in Figure 13. Colour scale bar represents t value from 0 to 15 (black to red). Applied t-contrast is thresholded with pFWE ≤ 0.05.

4. Discussion

4.1 Summary

4.1.1 Summary of the results

In this study, we employed two different mouse models of AD: the single APP transgenic Tg2576 and the APP/PS1 double transgenic ARTE10 mouse model. We performed in-vivo Aβ PET imaging with PiB, followed by a histopathologic analysis of the Aβ plaque pathology with three different stainings: immunofluorescence (IF) against full length Aβ peptide (N1-Aβ), immunofluorescence against N3-pyroglutamate-Aβ peptide (N3pE-Aβ) and Thioflavin S (TfS). Aβ pathology was quantified using a special script for the digital image analysis software Acapella. PiB PET images were analysed with a ROI-ratio-based and a voxel-based approach.

PiB PET imaging in all transgenic study groups resulted in cortex-to-cerebellum ROI-ratios of greater 1.0 compared to wildtype animals with ratios mostly less than 1.0. However our results suggest a potential overlap of PET ratio values between wildtype animals and transgenic animals with low amounts of Aβ plaque load.

Generally speaking, PET results corresponded well to the histological findings in matters of signal intensity as well as signal distribution among brain regions. On average, transgenic animals of higher age (young homozygous ARTE10 vs. old homozygous ARTE10), double transgenic animals instead of single transgenic (ARTE10 vs. Tg2576) and animals with two transgenic alleles instead of one (old homozygous ARTE10 vs. old hemizygous ARTE10) showed a higher amount of Aβ deposits and accordingly higher PET ratios. Aβ deposits were found not exclusively but concentrated in cortical and hippocampal brain regions. Analogously, visual inspection of PET images suggested higher PiB retention in cortical and hippocampal regions than in any other brain region.

The correlation of PET signal intensity as well as PET signal distribution with Aβ deposits was further established by voxel based analysis. The pattern of

significant voxels (transgenic tested against wildtype animals) resembled the pattern of the distribution of Aβ deposits in the brain. Furthermore, voxel based regression analysis of PET signal with Aβ plaque load identified brain regions in which Aβ deposits preferably concentrate with increasing plaque load.

On further analysis of our histologic findings, we found that age as well as transgenic configuration of a mouse model influences how the accumulating Aβ peptides deposit within the brain parenchyma. Although high in N1-Aβ plaque load, Tg2576 tg animals turned a lower fraction of its N1-Aβ plaque load into TfS positive plaque load. This was of particular interest with respect to the correlation of histological findings with PET results. We found that the correlation of TfS plaque load with PET ratios was higher than the correlation of N1-Aβ plaque load with PET ratios, but both correlations were significant. Furthermore, our data indicates that the relation of plaque count to plaque size might influence the yield of PET signal per plaque load.

N3pE-Aβ takes an exceptional position among the histological findings. First of all, we found that the N3pE-Aβ plaque load constituted only a minor fraction of N1-Aβ plaque load reaching about 10 to 15% in old homozygous ARTE10. But most importantly, we found some transgenic animals, mainly Tg2576 tg animals, with only unspecific N3pE-Aβ values despite the presence of high N1-Aβ plaque load and high PiB PET ratios.

4.1.2 Key interpretations of our results

Overall our data suggests the following interpretations:

(1) ROI-ratio-based analysis of PiB PET images of transgenic mouse models of AD gives a reliable estimation of the amount of Aβ deposits in the brain.

(2) The best quantitative relationship of PiB binding and Aβ plaque pathology in mouse models of AD was established for highly-dense TfS positive plaques.

(3) The ability to distinguish a transgenic from a control mouse by PiB PET imaging requires a certain amount of accumulated highly-dense Aβ deposits.

(4) The fraction of N3pE-Aβ varies between mouse models of AD. But if at all, post-translational modified Aβ peptides such as N3pE-Aβ play only a minor role for PiB binding.
(5) Voxel-based analysis of PiB PET images of transgenic mouse models of AD allows to identify brain regions with a high density of Aβ deposits without regional a priori hypothesis.

4.2 Aβ pathology and Aβ imaging

4.2.1 Plaque nomenclature and plaque spectrum detected in this study

In order to discuss Aβ pathology and its relationship to PiB PET imaging results, one has to clarify the employed nomenclature, as literature provides different classifications of plaques with a varying number of different types of plaques being distinguished[38,181]. In general, all types of cerebral, nonvascular Aβ deposits are typically referred to as “senile plaques” regardless of their morphology[182], whereas cerebral vascular plaques are usually referred to as cerebrovascular amyloid-angiopathy (CAA). Senile plaques can be further classified according to a number of different features e.g. morphology, inclusions of other proteins than Aβ such as ApoE, presence of dystrophic neurites, reactive astrocytes or microglial cells. This leads to a high number of different plaques being distinguished[183]. However, in our approach using TfS and immunofluorescence (IF) against Aβ peptide, we adopted staining techniques and a simplified classification that has been used in several human and preclinical studies to study Aβ plaque morphology before[38,166,181]. According to these studies, our stainings were able to discriminate between plaques that contain densely packed Aβ fibrils being positive for TfS and N1-Aβ, and diffuse plaques positive for N1-Aβ and not or only weakly for TfS[184]. Theoretically, our stainings would have allowed to further classify TfS positive plaques into purely fibrillar plaques being entirely TfS positive (often called compact plaques) and plaques with a fibrillar TfS positive core and a diffuse TfS negative corona

(usually called dense-cored plaques)[181]. However, such a discrimination requires an analysis of corresponding sections in order to co-localise the TfS and N1-Aβ staining. We did not perform such an analysis for two reasons. First, we were mainly interested in the overall plaque load of highly-dense plaques, diffuse plaques and N3pE-Aβ positive plaques. Second, studies analysing plaque types in mouse models of AD reported that dense-core plaques are only occasionally encountered in mouse models of AD, even at an advanced age[166]. The prevalent types of plaques are diffuse or compact, in contrast to human AD patients, where mostly diffuse and dense-core plaques are found[166].

The two monoclonal antibodies employed in this study showed high specificity towards specific types of Aβ peptide[179]. The D129 antibody is highly specific for the pyroglutamate form of the N3-truncated Aβ40/42 peptide (N3pE-Aβ). The cross reactivity with unmodified N3-truncated Aβ40/42 or full length Aβ40/42 was minimal. Whereas the 3A5 antibody is highly specific for the full length Aβ40/42 peptide, i.e. unmodified at the N-terminus (N1-Aβ)[179]. It was shown that the majority of Aβ peptide in mouse models of AD is not N-truncated[185,186]. Therefore, we expect 3A5 to sensitively detect virtually all deposits of Aβ peptide present in our mouse models.

As outlined above, we found that each staining covered a different spectrum of the deposited Aβ. The N1-Aβ staining visualised diffuse low-dense plaques as well as highly-dense plaques, TfS visualised mostly highly-dense plaques. N3pE-Aβ was found mostly in the centre of highly-dense plaques and represented only relatively small amount of the overall detected Aβ plaque load with the other two stainings.

4.2.2 Aβ pathology and PiB imaging studies in mouse models of AD

So far, the literature provides five studies using in-vivo PiB PET in mouse models of AD[162-164,168,187]. Although more recent studies reported to detect specific PiB binding to Aβ deposits[164,168], our knowledge about this field of Aβ imaging is still hampered due to the following reasons: methodological aspects strongly vary[162,164,168], almost every study employed a different mouse model at

a different age[163,164,168], in studies with related mouse models (same transgenes but different mutations, genetic background and age) contradicting results were reported[162,168], and Aβ pathology of the mice were mostly reported but not always quantified[163]. After initial failures to image Aβ in mouse models of AD, the prevalent hypothesis was that Aβ deposits in mouse models do not provide sufficient high affinity binding sites for PiB. A recent study[168] and our results in Tg2576 that was determined not suitable for preclinical Aβ imaging[163] argue against this hypothesis. In the following, we discuss our results with respect to the previously reported results and argue for a general suitability of mouse models for preclinical Aβ imaging based on the exhibited Aβ pathology.

We employed ARET10 mice in similar age groups as previously done by Manook et al. Taking into account that their young homozygous ARTE10 were 9 months old and ours 12 months, our results broadly resemble their findings of a gradation of plaque load and PiB results from young homozygous (lowest), to old hemizygous (middle), to old homozygous (highest).
Regarding Tg2576 mice, Toyama et al. reported higher PiB PET ratios than controls at a mean age of 22 months[163]. However, they concluded that their study could not prove specific binding of PiB to Aβ plaques due to a smaller amount of PiB binding sites or a lower affinity of these binding sites. Albeit their oppositional conclusion, we regard our findings also in line with the study of Toyama et al. Importantly, the results of both studies are comparable based on the very high age of the Tg2576 in both studies (Toyama et al: 22 months, this study: 25 months). Also their cortex-to-cerebellum analysis approach is analogue to our ROI-ratio-based analysis. We postulate that their significant results for the frontal-cortex- and parietal-cortex-to-cerebellum ratios in transgenic mice compared to controls indeed originated from a specific binding of PiB to Aβ. The present study employed 16 mice with several of them showing only a rather low TfS plaque load with PET ratios similar to those observed by Toyama. Thus, the small difference between transgenic and wildtype mice in the study of Toyama et al. might be a statistical effect, as Toyama employed only six Tg2576 mice. Toyama et al. histologically confirmed the presence of Aβ

plaques with TfS stainings but unfortunately did not quantify the plaque load. Of note, also their findings in aged matched wildtype mice are in line with our results. Both studies observed ratios in wildtype mice of mostly less than 1.0, but with few mice ranging close to or within the values of transgenic animals with low PET ratios. However, the reasons behind these outliers among wildtype mice are not known.

Maeda et al.[164] reported successful Aβ detection with PiB imaging in an aged single APP transgenic mouse model named APP23. On the one hand, they concluded that the specific activity employed in our study would lead to the detection of mostly dense Aβ deposits, which is in line with our results. On the other hand, our results disagree with their conclusion that N3pE-Aβ would be necessary to form high affinity binding sites on Aβ deposits.

Maeda et al. held the employment of a very high specific activity responsible for their ability to detect the Aβ deposits. They concluded that using high specific activity would increase the exploitation of high affinity binding sites on mouse Aβ. Based on repetitive scans with varying specific activity, they postulated that the detection of diffuse Aβ deposits is highly sensitive to the specific activity with high specific activity values being necessary to detect diffuse plaques, whereas dense clusters of Aβ deposits can be detected regardless of the specific activity. Their results regarding the effect of high specific activities have not been reproduced in our study, as the high specific activity used in their study is a magnitude higher than what is achievable in most clinical PET centres, including ours. Our study employed a specific activity for which Maeda et al. assumed that PiB binding is mainly driven by dense Aβ deposits. Indeed, several findings in our study indicate that the amount of TfS positive plaque load provided the essential structures for PiB binding and TfS was shown to stain mainly dense fibrillar Aβ deposits and only weakly diffuse plaques[184]. PET ratios showed a higher correlation to TfS plaque load than to N1-Aβ plaque load. Furthermore, the correlation of N1-Aβ plaque load is mainly driven by the N1-Aβ plaque size, which in turn shows a close association with TfS plaque load. For this interpretation, two aspects have to be considered. First, the difference in correlation between the TfS staining and N1-Aβ staining could have had

methodological reasons. Indeed, we observed a higher background staining in wildtype mice for N1-Aβ than for TfS. However the signal-to-noise ratios in transgenic animals with a low plaque load were about the same for both stainings. Second, the interpretation of the correlations is hindered as there is a concordant increase of N1-Aβ plaque load and TfS plaque load in a given mouse model in a relative constant relation to each other (e.g. TfS plaque load in all ARTE10 animals correlated well with N1-Aβ plaque load with r=0.85). However, the direct comparison between the two mouse models provided important information for the interpretation of our histological findings. The first striking finding is the sharp discrepancy between mean PET ratios and N1-Aβ plaque load across our study groups. This is most evident for young homozygous ARTE10 compared with Tg2576. Tg2576 has about the same N1-Aβ plaque load as young homozygous ARTE10 but clearly lower PET ratios and lower TfS plaque load. Analysing individual correlations, we observed a separation of Tg2576 animals from ARTE10 animals in the scatter plots for N1-Aβ plaque findings plotted against TfS plaque findings. Overall, this separation indicated that Tg2576 turns less of its N1-Aβ plaque load into TfS positive plaque load. Furthermore, calculating the relative yield of PiB signal in the cortex and hippocampus per TfS plaque load percentage point, we observed similar values across all study groups. This finding was corroborated by correlating the relative PiB signal increase with the amount of N1-Aβ plaque load which was not TfS positive (non-TfS Aβ plaque load). The association was minimal, despite a large spread of non-TfS Aβ plaque load across our study groups. Taken together, the most coherent measure explaining our PET results was the amount of TfS positive Aβ deposits.

Maeda's conclusion of the necessary presence of N3pE-Aβ is based on a quantified autoradiographic experiment with in-vitro [^{11}C]PiB labelled brain tissue sections. They correlated this signal with plaque load values calculated from immunofluorescence stainings of the same sections. They employed tissue from a single Tg2576 mouse, a single young APP/PS1, five APP23 mice and a single human AD patient. They measured the plaque load for N3pE-Aβ, Aβ40, Aβ42 and untruncated Aβ at the N-terminus (AβN1D). N3pE-Aβ was the

only measure that correlated well with the PiB signal. However, the low correlations for the other stainings were mainly caused by the single human AD data set. If that would have been left out and only transgenic mice were considered, the graphs provided by Maeda et al. suggest high correlations for all stainings. Therefore, it is possible that N3pE-Aβ positivity is merely a surrogate marker for another quality of human AD Aβ plaques that caused the higher PiB binding in their experiment. There are several reasons for such an interpretation. Our Tg2576 showed only unspecific or very low amounts of N3pE-Aβ. This was also shown in histological and biochemical evaluations of this mouse model before[167,186]. N3pE-Aβ seems generally decreased in mouse models of AD compared to human AD patients[185,188], but can be detected in an age dependent manner in APP/PS1 transgenic mice[189]. However, contrary to Maeda's conclusion that N3pE-Aβ is the major source of target structures for high-affinity PIB binding, we found high PET ratios of up to 1.4 in our Tg2576 mice despite basically undetectable amounts of N3pE-Aβ. As outlined above, our data suggests that dense TfS positive plaque load is the main provider for PiB binding sites. Hereby, N3pE-Aβ positivity might be a surrogate marker for these mature dense fibrillar Aβ plaques. Indeed, in our study, N3pE-Aβ plaque load correlated well with TfS plaque load in ARTE10 mice in our study and also TfS plaque size, which is a rough estimate of the age of a plaque (young homozygous ARTE10 had in general smaller TfS plaques than old homozygous ARTE10). Several studies in human and mouse tissue support this notion. It was shown that diffuse plaques contain only low to none N3pE-Aβ in mouse models as well as in AD patients[166], but substantial amounts in dense cored plaques of human AD tissue[166]. Diffuse plaques are thought to occur early in the disease process[190] and are believed to proceed towards typical cored plaques[191]. This implies that N3pE-Aβ formation is a late process involved in the maturation of plaques[189] and that the presence of N3pE-Aβ and other N-truncated forms of Aβ is related to proteolytic processes that take place over prolonged time[166]. This would also explain that mouse models in general show lower levels of N3pE-Aβ than human AD patients, because the assumed period of Aβ accumulation in pre-symptomatic patients is several-fold longer than the

natural life span of any mouse model. Analogously, our finding that ARTE10 in contrast to Tg2576 mice show relevant amounts of N3pE-Aβ plaque load could be due to the earlier onset of plaque depositing in ARTE10 (homozygous mice around 3 months[174]) compared to Tg2576 (appreciable number of diffuse plaques around 12 months[167]).

Maeda et al. corroborated their conclusion of the importance of N3pE-Aβ for PiB binding with in-vitro binding assays. They found a higher PiB binding to synthetic fibrils of N3pE-Aβ than to Aβ42 without N-terminus modification. However, this result is not necessarily inconsistent with the notion that high fibrillarity of Aβ is important for PiB binding. Several in-vitro studies reported enhanced oligomerisation and fibril formation of N-truncated Aβ compared to Aβ1-42[192], which was particularly demonstrated for N3pE-Aβ[185,193-196].

Based on in-vitro PiB binding assays of brain tissue homogenates, Klunk et al. suggested that high affinity PiB binding sites are generally sparse on mouse Aβ compared to human AD Aβ (less than 1 compared to 500 per 1000 molecules Aβ). This finding was contrasted by a study from our group[168] employing a similar in-vitro assay. Hereby, Manook et al. reported high affinity binding sites on Aβ deposits of ARTE10 and a binding potential (BP) comparable to human AD tissue, even exceeding human AD tissue in old homozygous ARTE10. In our study, Tg2576 mice and ARTE10 mice show the same in-vivo PiB signal relative to TfS plaque load. Therefore it is reasonable to assume that the findings from Manook et al. can be transferred in some extend to Tg2576, at least to those with a relevant amount of TfS positive plaque load.

However, it is important to note that in our study, we did not investigate the difference between TfS positive plaques in mice and TfS positive plaques in human AD patients. It might not be true that mouse Aβ lacks relevant amounts of high-affinity PiB binding sites, but this does not rule out differences of mouse to human Aβ deposits. For instance, Manook et al. reported differing binding kinetics for mouse brain tissue compared to human AD tissue in their in-vitro binding assay. A potential molecular basis for such differences was suggested in a study by Ye et al.[197] comparing the properties of rodent Aβ (endogenous mouse Aβ, not derived from the cleavage of the human APP transgene) and

human Aβ. This study found that fibrils formed by rodent Aβ do not differ greatly from those formed by human Aβ. However, it was previously shown that Aβ deposits in transgenic mice generally contain relevant amounts of endogenous rodent Aβ[198] and Ye et al. demonstrated that unlike pure rodent or human Aβ fibrils, Aβ fibrils formed by rodent-human copolymers show altered binding properties for various Aβ ligands including PiB.

4.2.3 Analogies of our findings to human data

In-vitro PiB binding studies on human AD tissue are ambiguous about the selectivity of PiB to different types of Aβ pathology. However, in analogy to our results, case studies of in-vivo-post-mortem correlation in AD patients suggest that Aβ pathology exists that remains undetected by PiB PET imaging.
An in-vitro study on human AD tissue by Lockhart et al.[135] reported that [^{3}H]PiB binds to all kinds of senile plaques, particularly including diffuse plaques. In order to better emulate the in-vivo situation of tracer binding, they applied tracer concentration relevant to imaging studies (i.e. low nM range) on fresh, frozen brain tissues that were not pre-treated otherwise. They concluded that PiB is primarily a non-specific marker of Aβ peptide related cerebral amyloidosis. However, their autoradiographic approach provided a rather bimodal information (labelled / not labelled) and the [^{3}H]PiB signal was not quantified. Their finding was contrasted by a study from Ikonomovic et al.[137]. They conducted an in-vitro study of 6-CN-PiB binding (a fluorescent analogue of PiB) on AD tissue sections from autopsy cases. Importantly, they reported that the plaque pattern visualised with 6-CN-PiB closely resembled the one visualised with TfS. Furthermore, 6-CN-PiB binding as well as TfS binding could be abolished by destroying the fibrillar character of Aβ deposits, e.g. by treating the tissue sections with formic acid. Furthermore 6-CN-PiB robustly labelled compact and dense-cored plaques, while diffuse and amorphous plaques were only weakly labelled. Interestingly, in contrast to cortical diffuse plaques with weak 6-CN-PiB labelling, they found diffuse plaques occurring in the cerebellum which were detected by antibody stainings, but not by 6-CN-PiB. In summary,

Ikonomovic et al. concluded that the intensity of 6-CN-PiB labelling reflected the density of Aβ fibrils.

Interesting findings were reported from in-vivo PiB studies with subsequent post-mortem histopathologic analysis[136-140,143-145]. So far, the literature provides 27 cases of which 10 cases were frontal cortex biopsies in patients that underwent intra-ventricular pressure monitoring for suspected normal-pressure hydrocephalus[145]. Generally speaking, it was shown that PiB retention in various brain regions reflects the amount of present Aβ plaque pathology. However, in 4 cases (one of them in the biopsy study), a relevant amount of Aβ pathology but a negative PiB scan was observed (of note, these cases met only the criteria for possible AD by CERAD[146]).

Sojkova et al. reported[143] a PiB negative case with a post-mortem analysis 2.4 years after the PiB scan. Neuropathological analysis showed moderate numbers of neuritic plaques in the parietal and temporal lobe and sparse numbers in the frontal lobe. However, the overall amount of immunoreactive Aβ plaque load was determined to be low.

Cairns et al. reported[138] a symptomatic case (mild cognitive impairment) with a negative PiB scan and a post-mortem neuropathological analysis 2.5 years after the PiB PET scan. The post-mortem analysis showed foci of frequent neocortical diffuse plaques, but more mature neuritic plaques were scarce. The authors suggested that PiB may be unable to detect AD variants that are characterized predominantly by diffuse Aβ plaques.

Leinonen et al. reported that the patients with the highest Aβ load (antibody staining) in a biopsy specimen from the frontal cortex had also the highest PiB uptake in PET imaging. However they identified one patient with diffuse Aβ plaques but negative PiB scan, but the small amount of tissue derived from biopsy specimen prevented further histological analyses.

Ikonomovic et al. reported a PiB negative case that was clinically diagnosed with dementia with Lewy bodies (DLB) and possible AD[144]. They detected cortical Aβ plaques on post-mortem analysis 17 months after the PiB scan. However these plaques were infrequent, primarily diffuse and stained only weakly with Thioflavin S. Of note, the authors concluded that PiB negativity was

likely not the result of an unusual profile of proteolytically modified Aβ species, as the plaques found in the PiB negative case showed a similar pattern of labelling by antibodies generated against different Aβ subtypes including N3pE-Aβ. Furthermore, Ikonomovic et al. suggested the possibility that a low Aβ42 to Aβ40 ratio could lead to decreased in-vivo PiB binding. Rosen et al. also suggested that insoluble Aβ40 may present in high quantities without significant PiB binding[147], although no in-vivo PiB data exists for their case. This hypothesis is particular interesting as several in-vitro studies reported equal binding of PiB to synthetic Aβ40 and Aβ42 fibrils[137].

Further evidence that PiB does not bind to every kind of Aβ deposit comes from a study by Schöll et al.[199]. They measured low PiB retention in AD patients that carry the "arctic" APP mutation (APParc), despite the presence of AD-typical pathologic changes such as CSF biomarkers, cerebral glucose metabolism, and medial temporal lobe atrophy as well as severe cognitive impairment. Autopsy studies of APParc carriers reported highly immunoreactive Aβ deposits that showed a characteristic ring-like character and were weakly congophilic. Overall the neuropathologic findings were regarded as consistent with the diagnosis of AD[200].

Taken together, these in-vivo-post-mortem correlation studies as well as the results of our study indicate that in-vivo PiB PET imaging might be less sensitive to diffuse, less fibrillar Aβ deposits. Furthermore, regardless of the type of Aβ deposits, a threshold of Aβ pathology for PiB positivity probably exists and has yet to be determined.

4.3 Voxel-based analysis of PiB data

Often, clinical Aβ imaging PET studies in AD relied on traditional region-of-interest (ROI) based analysis[124,201-203]. This approach has been adopted for all small animal Aβ imaging PET studies published so far. However, an alternative approach is the voxel-based statistical analysis. This approach has been evaluated for human PiB PET data[204-206] and was also applied in clinical Aβ PET imaging studies[207-212]. In mouse models of AD, voxel-based analysis has

been only employed to study ex-vivo cerebral tracer retention[213]. Whereas in-vivo small animal PET studies analysed on a voxel-basis employed mostly rats[214-217], but not yet mice. In our study, we aimed to investigate the feasibility of a voxel-based analysis of cerebral PiB retention in our study groups. Two main questions had to be answered in advance: the method of signal normalisation across individuals and the need of spatial normalisation as we included mice with different transgenic configuration and of different transgenic background.

We chose a reference-tissue-normalisation and normalised the PiB data to the individual mean cerebellum value acquired in the ROI-ratio-based analysis as the cerebellum was free of Aβ deposits in all animals. This approach has been used in clinical PiB studies before[218]. Extra-cranial structures seemed unsuitable to serve as reference region because we observed unsteady tracer retention patterns. An alternative approach would have been to normalise to the injected activity and body weight (%ID-kg/g). However, we observed intense hotspots at the point of tracer injection. Therefore, the amount of activity that was trapped in the extracellular space of the tail was difficult to estimate, thus making a normalisation to injected activity prone to error.

After comparing anatomical measures of the brains of our study groups, we came to the conclusion that a spatial normalisation was necessary to account for differences between brain measures of ARTE10 animals and Tg2576 animals. Interestingly, the variation between animals of the same genetic background was minimal. It is important to note that our approach to spatially normalise based on created brain masks was motivated through the relatively low contrast in our MRI images, allowing manual but not automated delineation of brain regions. High-contrast MRI images acquired with high-field small animal MRI scanner would make this analysis step unnecessary[219].

Our results suggest that voxel-based analysis of in-vivo Aβ PET imaging studies in mouse models of AD is feasible and significant voxels are indicative of Aβ deposits in the brain. However, our group comparison between transgenic animals with low TfS plaque load (< 3.0%) and wildtype animals suggests that a certain plaque load level is necessary in order to detect a significant PiB

retention on the voxel-level. In this group, only few significant voxels were found in the frontal parts of the neocortex. Although this is a brain region where Aβ plaque deposits emerge early and generally show higher plaque load values than other regions[174], this finding should be interpreted with caution since these few significant voxels extended over an area that was less than the intrinsic spatial resolution of the small animal PET scanner.

In one aspects the findings of our in-vivo imaging analyses did not correspond to the histopathological evaluation. The voxel-based group comparison analysis as well as the regression analysis did not identified significant voxels in the olfactory bulb, although we found Aβ plaque deposits in this region. This discrepancy may be linked to the high unspecific tracer uptake in neighbouring structures in both study groups. This applies especially for orbital structures such as the Harderian glands. Unspecific tracer uptake in these structures is also known for other tracers too and represents a common challenge in small animal PET imaging studies of cerebral tracer uptake[220-223]. Hereby, the olfactory bulb is located between the two orbitae, separated only by a thin bone lamination. The relatively low intrinsic spatial resolution of small animal PET probably results in partial volume effects masking potential PiB retention in the olfactory bulb.

Although a voxel-based analysis might contain multiple advantages over a traditional ROI-based analysis, a voxel-based analysis introduces errors of its own. Strict statistical thresholding and correction for multiple testing potentially leads to false negative findings. By choosing FWE correction we decided on a more conservative approach in analogy to an evaluation study of voxel-based analysis of human PiB data[205]. Small animal Aβ imaging PET studies aiming at detecting smaller differences in signal, a more liberal approach might be necessary. Smoothing is another potential source of error. Preprocessing of human PET data usually includes heavy smoothing. Smoothing potentially masks significant signals in brain structures whose size lies within the resolution of the PET scanner[224]. We chose not to smooth the images as this would have increased the effects of partial volume with extra-cranial structures with high unspecific binding.

4.4 Limitations

Most of our conclusions rely on our measurement of histological plaque load for which some limitations have to be considered. We quantified Aβ pathology by calculating stained area per area of a given region of a histological section. Although this approach is often applied in histological analysis of mouse brain tissue[164,171,174] as well as post-mortem analysis of human AD tissue[137], it is potentially not a valid estimate of the amount of deposited Aβ peptide. It was shown that the histological quantification of plaque load correlates tightly with the amount of insoluble Aβ peptide[174], but this was measured over a range of Aβ plaque load of four magnitudes.

Reasons for a potential discrepancy between histological determined plaque load and amount of Aβ peptide lie mainly in the bimodal nature of detection. Acapella determines an analysed pixel either as belonging to a plaque or not. It does not account for potential differences in density or intensity of the staining. The potential error would be minor if the relation of highly-dense to low-dense deposits would be relatively constant across analysed sections. However, our conclusions rely on the difference of TfS positive plaque load across different mouse models of AD. There is the possibility that TfS positive plaque load does not represent the determining structure for PiB binding, but only a better measure for the overall Aβ peptide deposited and that PiB binds to all kinds of deposited Aβ peptide in mouse models of AD. Nevertheless, even if it turns out that TfS plaque load is a better representative of Aβ peptide and does not imply the presence of structures important for PiB binding, it seems to pose a valid tool to assess the in-vivo PiB signal determining Aβ plaque pathology.

As outlined in the discussion, findings in in-vitro studies on AD tissue and a limited number of in-vivo case studies support our conclusion. However, these findings might not be transferable across species. Although Aβ deposits in mouse models are generally thought to resemble those found in human AD tissue, also marked differences in the composition were found[186]. For the same reasons, the transferability of our results to a human setting might be limited.

4.5 Is there a future for Aβ imaging?

It is important to put our findings into a broader context as recent research questions more and more the importance of Aβ for the progression of the disease in AD patients. While writing this thesis, a drug in which great hope was placed, the monoclonal antibody Bapineuzumab directed against Aβ deposits, was halted in development due to a missing effect on patients outcome in large phase 3 clinical trials. Solanezumab, another promising candidate and also a monoclonal antibody, missed the endpoints of two phase 3 clinical trials a few weeks later. So far, no decision on the future of this drug has been made as the data of these two phase 3 clinical trials suggests a delay in progression in a subgroup of the enrolled patients with mild AD. However, critical voices can be heard about the soundness of such a subgroup analysis. Importantly, both drugs did fairly what they were designed to do: lowering the Aβ plaque burden in AD patients. These failures provide further evidence for the increasing popular hypothesis that, in order to be effective, anti-Aβ therapy strategies have to be employed very early in the disease process, possibly long before symptoms occur. Furthermore, these failures fuel doubts on the significance of Aβ for the disease progression.

Aβ PET imaging is currently mainly employed to evaluate symptomatic patients. Not only the focus of disease modifying drug development shifts towards early intervention, also the potential that lies in Aβ imaging receives increasing attention in this context. There is growing evidence that the cognitive normal PiB positive individuals are indeed in the pre-symptomatic stage of AD. However hopes for Aβ imaging being a powerful screening tool shouldn't get up too soon. As suggested in this study and preliminary human data, Aβ imaging might not be sensitive enough for none- or low-fibrillar diffuse deposits. However, these diffuse deposits are regarded as an early event in the disease process and the initial deposition of insoluble Aβ peptide[225]. Furthermore, the failures in recent drug development render the possibility that by the time a level of Aβ deposits is reached that is detectable by PiB imaging, Aβ might not be the disease driving pathogen anymore.

In addition, Aβ imaging as screening tool might get an easy-to-perform and inexpensive competitor which is already broadly available and routinely performed. If it turns out that it will be only necessary to screen for the presence of Aβ pathology and not to localize or quantify it (which are particular strengths of Aβ imaging), cerebrospinal fluid (CSF) analysis might provide enough information to indicate a prophylactic treatment, once it is available. Aβ42 in the CSF seems to decrease very early in the disease process and might be sufficient for the identification of individuals at risk of developing symptomatic AD. One study suggested even a moderate negative association between PiB retention and CSF Aβ42 levels[226]. However, the decline in CSF Aβ42 is thought to reach an early plateau and might also be rather unspecific as decreased levels were also reported for frontotemporal dementia, vascular dementia, Creutzfeldt-Jacob disease and dementia with Lewy bodies[227-229]. But it was suggested that the specificity of CSF biomarkers can be increased through subtype specification of increased tau protein[230].

What does all that potentially mean for preclinical Aβ imaging? Arguments that are brought forward in favour of preclinical Aβ imaging often include the chance to in-vivo monitor longitudinal anti-Aβ therapies experiments in animal models of AD. Additional, for Aβ tracer development, preclinical imaging could be an ideal complement to the other screening tests used to identify optimal lead imaging agents[231]. But if it turns out that Aβ deposits are not a favourable drug target and that Aβ imaging is not the first choice for an early detection of AD pathology, the scope of future applications of preclinical Aβ imaging would be limited. However, as long as Aβ deposits at levels detectable with Aβ imaging has not definitely been ticked off as still important pathogen for the progression of early AD, one should not forget the unique advantages that Aβ imaging provides compared to biochemical tests such as blood or CSF analysis. Advantages are primarily the ability of PET imaging to allow to draw conclusions about the quantity and spatial distribution of a traced molecular structure. Furthermore, PiB and similarly F-18 labelled Aβ tracers in development are probably not the end of the story. A major advantage of PET imaging is the flexibility in designing imaging agents. This offers the possibility of targeting

different molecules in the same individual, e.g. non-fibrillar Aβ deposits or other aspects of AD pathology. Additional, there might be advances in PET technology improving spatial resolution and/or sensitivity of a (pre)clinical scanner system[232,233]. For instance, this could improve the ability to identify small brain regions with pathologic changes and thus PET imaging would be more sensitive towards early stages of the disease. Preclinical imaging might help to better understand the in-vivo binding characteristics of an imaging agent and thus might provide crucial information about the chances and limits of a given approach in humans.

4.6 Conclusion

In this study we further added evidence for the feasibility of small animal PiB PET imaging in mouse models of AD. Our results suggest that Thioflavin S positive Aβ deposits are a reliable indicator for structures relevant for specific PiB binding as we found a quantitative relationship between measured PiB PET signal and the amount of Thioflavin S positive Aβ deposits.

At least in mouse models of AD, the composition of these Thioflavin S positive structures by different types of Aβ peptide seems to be of minor importance, based on our finding that the yield of in-vivo PET signal relative to the Thioflavin S plaque load is approximately equal across our study groups despite marked differences in N3pE-Aβ plaque load. Therefore, the presence of truncated or otherwise modified Aβ peptides such as N3pE-Aβ is not obligatory for the formation of such structures, but might still be relevant in the sense that they enhance the formation of those.

Our study further suggests that voxel-based analysis is a valid approach to analyse differences in intensity and distribution of PiB binding throughout the mouse brain, which could remain undiscovered by predefined ROI analyses. In our study, the results of the voxel-based analysis reliably indicated brain regions with high concentration of Aβ deposits. Voxel-based analyses might facilitate preclinical studies such as tracer comparison studies, longitudinal studies, or systematic comparisons between different mouse models of AD.

5. Appendix

5.1 Abbreviations

°C	degrees Celsius
AD	Alzheimer's disease
APP	amyloid precursor protein
Aqua dest.	distilled and deionised water (Millipore water)
Aβ	amyloid-β
N1-Aβ	not truncated amyloid-β
N3pE-Aβ	N3-truncated pyroglutamate amyloid-β
Bq	Becquerel
DAPI	4',6-diamidino-2-phenylindole
FBP	filtered back projection
FOV	field of view
FWHM	full width at half maximum
ID	injected dose
IF	immunofluorescence
MRI	magnetic resonance imaging
PBS	phosphate buffered saline solution
PET	positron emission tomography
PiB	Pittsburgh compound B
PS1	presenilin 1
ROI(s)	region(s) of interest
SD	standard deviation
SPM	statistical parametric mapping
tg	transgenic
tg/-	hemizygous
tg/tg	homozygous
TI	inversion time
TR	repetition time
wt	wildtype

5.2 List of figures

5.3 List of tables

5.4 Publications within the scope of the thesis

A Novel F-18-Labeled Imidazo[2,1-b]benzothiazole (IBT) for High-Contrast PET Imaging of beta-Amyloid Plaques.

Authors: Yousefi, Behrooz H.; Drzezga, Alexander**; von Reutern, Boris**; et al.

Acs Medicinal Chemistry Letters. DOI: 10.1021/ml200123w. Published: 2011.

Data not part of the thesis.

Development of an improved radioiodinated phenyl-imidazo[1,2-a]pyridine for non-invasive imaging of amyloid plaques.

Authors: Yousefi, Behrooz H.; **von Reutern, Boris**; Schwaiger, Markus; et al.

Journal of Labelled Compounds & Radiopharmaceuticals. Published: 2011

Data not part of the thesis.

Synthesis and Evaluation of C-11-Labeled Imidazo[2,1-b]benzothiazoles (IBTs) as PET Tracers for Imaging beta-Amyloid Plaques in Alzheimer's Disease.

Authors: Yousefi, Behrooz H.; Manook, Andre; Drzezga, Alexander; **von Reutern, Boris**; et al.

Journal of Medicinal Chemistry. DOI: 10.1021/jm101129a. Published: 2011.

Data not part of the thesis.

Voxel-based analysis of Amyloid-burden measured with [11C]PiB PET in a double transgenic mouse model of Alzheimer's disease.

Authors: **Boris von Reutern**, Barbara Grünecker, Behrooz Yousefi, Gjermund Henriksen, Michael Czisch, Alexander Drzezga

submitted

Direct comparison of two mouse models of AD regarding their suitability for in-vivo [11C]PiB PET imaging. PiB signal correlates well with dense amyloid-β deposits.

Authors: **von Reutern, Boris**, Yousefi, Behrooz H.; Gjermund Henriksen; et al.

in preparation

6. References

1. Przedborski S, Vila M, Jackson-Lewis V. Neurodegeneration: what is it and where are we? J Clin Invest 2003;111(1):3-10.
2. Shastry BS. Neurodegenerative disorders of protein aggregation. Neurochem Int 2003;43(1):1-7.
3. Lill CM, Bertram L. Towards unveiling the genetics of neurodegenerative diseases. Semin Neurol 2011;31(5):531-41.
4. Katsuno M, Tanaka F, Sobue G. Perspectives on molecular targeted therapies and clinical trials for neurodegenerative diseases. J Neurol Neurosurg Psychiatry 2012;83(3):329-35.
5. Forman MS, Trojanowski JQ, Lee VM. Neurodegenerative diseases: a decade of discoveries paves the way for therapeutic breakthroughs. Nat Med 2004;10(10):1055-63.
6. Bouchard M, Suchowersky O. Tauopathies: one disease or many? Can J Neurol Sci 2011;38(4):547-56.
7. Hardy J, Gwinn-Hardy K. Genetic classification of primary neurodegenerative disease. Science 1998;282(5391):1075-9.
8. Williams DR. Tauopathies: classification and clinical update on neurodegenerative diseases associated with microtubule-associated protein tau. Intern Med J 2006;36(10):652-60.
9. Bence NF, Sampat RM, Kopito RR. Impairment of the ubiquitin-proteasome system by protein aggregation. Science 2001;292(5521):1552-5.
10. Bucciantini M, Giannoni E, Chiti F, Baroni F, Formigli L, Zurdo J, Taddei N, Ramponi G, Dobson CM, Stefani M. Inherent toxicity of aggregates implies a common mechanism for protein misfolding diseases. Nature 2002;416(6880):507-11.
11. Gandy S. Will "cerebral proteopathy" be a useful construct for discovering one drug that shows efficacy against multiple neurodegenerative diseases? Neurobiol Aging 2000;21(4):565; discussion 567.
12. Naeem A, Fazili NA. Defective protein folding and aggregation as the basis of neurodegenerative diseases: the darker aspect of proteins. Cell Biochem Biophys 2011;61(2):237-50.
13. Cummings JL. Toward a molecular neuropsychiatry of neurodegenerative diseases. Ann Neurol 2003;54(2):147-54.
14. Strong MJ, Kesavapany S, Pant HC. The pathobiology of amyotrophic lateral sclerosis: a proteinopathy? J Neuropathol Exp Neurol 2005;64(8):649-64.
15. Jucker M, Walker LC. Pathogenic protein seeding in Alzheimer disease and other neurodegenerative disorders. Ann Neurol 2011;70(4):532-40.
16. Jucker M, Beyreuther K, Haass C, Nithsch R, Christen Y. Alzheimer: 100 Years and Beyond. Springer-Verlag Berlin Heidelberg; 2006.
17. Tomlinson BE, Blessed G, Roth M. Observations on the brains of demented old people. J Neurol Sci 1970;11(3):205-42.

18. Tomlinson BE, Blessed G, Roth M. Observations on the brains of non-demented old people. J Neurol Sci 1968;7(2):331-56.
19. Katzman R. The prevalence and malignancy of Alzheimer's disease: a major killer. Arch Neurol 1976;33:217-218.
20. Cupers P, Sautter J, Vanvossel A. European Union research policy and funding for Alzheimer disease. Nat Med 2006;12(7):774-5.
21. Tomlinson BE. The pathology of dementia. Contemp Neurol Ser 1977;15:113-53.
22. Thies W, Bleiler L. 2011 Alzheimer's disease facts and figures. Alzheimers Dement 2011;7(2):208-44.
23. Fratiglioni L, Launer LJ, Andersen K, Breteler MM, Copeland JR, Dartigues JF, Lobo A, Martinez-Lage J, Soininen H, Hofman A. Incidence of dementia and major subtypes in Europe: A collaborative study of population-based cohorts. Neurologic Diseases in the Elderly Research Group. Neurology 2000;54(11 Suppl 5):S10-5.
24. Wadman M. US government sets out Alzheimer's plan. Nature 2012;485(7399):426-7.
25. Genin E, Hannequin D, Wallon D, Sleegers K, Hiltunen M, Combarros O, Bullido MJ, Engelborghs S, De Deyn P, Berr C and others. APOE and Alzheimer disease: a major gene with semi-dominant inheritance. Mol Psychiatry 2011;16(9):903-7.
26. Kukull WA, Higdon R, Bowen JD, McCormick WC, Teri L, Schellenberg GD, van Belle G, Jolley L, Larson EB. Dementia and Alzheimer disease incidence: a prospective cohort study. Arch Neurol 2002;59(11):1737-46.
27. Evans DA, Funkenstein HH, Albert MS, Scherr PA, Cook NR, Chown MJ, Hebert LE, Hennekens CH, Taylor JO. Prevalence of Alzheimer's disease in a community population of older persons. Higher than previously reported. JAMA 1989;262(18):2551-6.
28. Ferri CP, Prince M, Brayne C, Brodaty H, Fratiglioni L, Ganguli M, Hall K, Hasegawa K, Hendrie H, Huang Y and others. Global prevalence of dementia: a Delphi consensus study. Lancet 2005;366(9503):2112-7.
29. Wimo A, Jonsson L, Gustavsson A, McDaid D, Ersek K, Georges J, Gulacsi L, Karpati K, Kenigsberg P, Valtonen H. The economic impact of dementia in Europe in 2008-cost estimates from the Eurocode project. Int J Geriatr Psychiatry 2011;26(8):825-32.
30. Sousa RM, Ferri CP, Acosta D, Albanese E, Guerra M, Huang Y, Jacob KS, Jotheeswaran AT, Rodriguez JJ, Pichardo GR and others. Contribution of chronic diseases to disability in elderly people in countries with low and middle incomes: a 10/66 Dementia Research Group population-based survey. Lancet 2009;374(9704):1821-30.
31. Fitzpatrick AL, Kuller LH, Lopez OL, Kawas CH, Jagust W. Survival following dementia onset: Alzheimer's disease and vascular dementia. J Neurol Sci 2005;229-230:43-9.
32. Ganguli M, Dodge HH, Shen C, Pandav RS, DeKosky ST. Alzheimer disease and mortality: a 15-year epidemiological study. Arch Neurol 2005;62(5):779-84.
33. Eaker ED, Vierkant RA, Mickel SF. Predictors of nursing home admission and/or death in incident Alzheimer's disease and other dementia cases

compared to controls: a population-based study. J Clin Epidemiol 2002;55(5):462-8.
34. Jones AL, Dwyer LL, Bercovitz AR, Strahan GW. The National Nursing Home Survey: 2004 overview. Vital Health Stat 13 2009(167):1-155.
35. Wimo A, Prince M. World Alzheimer Report. Alzheimer's Disease International. London2010.
36. Stefanacci RG. The costs of Alzheimer's disease and the value of effective therapies. Am J Manag Care 2011;17 Suppl 13:S356-62.
37. Hampel H, Prvulovic D, Teipel S, Jessen F, Luckhaus C, Frolich L, Riepe MW, Dodel R, Leyhe T, Bertram L and others. The future of Alzheimer's disease: the next 10 years. Prog Neurobiol 2011;95(4):718-28.
38. Perl DP. Neuropathology of Alzheimer's disease. Mt Sinai J Med 2010;77(1):32-42.
39. Niedowicz DM, Nelson PT, Murphy MP. Alzheimer's disease: pathological mechanisms and recent insights. Curr Neuropharmacol 2011;9(4):674-84.
40. Walsh DM, Selkoe DJ. Deciphering the molecular basis of memory failure in Alzheimer's disease. Neuron 2004;44(1):181-93.
41. Gamblin TC, Chen F, Zambrano A, Abraha A, Lagalwar S, Guillozet AL, Lu M, Fu Y, Garcia-Sierra F, LaPointe N and others. Caspase cleavage of tau: linking amyloid and neurofibrillary tangles in Alzheimer's disease. Proc Natl Acad Sci U S A 2003;100(17):10032-7.
42. Kawabata S, Higgins GA, Gordon JW. Amyloid plaques, neurofibrillary tangles and neuronal loss in brains of transgenic mice overexpressing a C-terminal fragment of human amyloid precursor protein. Nature 1992;356(6366):265.
43. Hardy J. Has the amyloid cascade hypothesis for Alzheimer's disease been proved? Curr Alzheimer Res 2006;3(1):71-3.
44. Braak H, Braak E. Neuropathological stageing of Alzheimer-related changes. Acta Neuropathol 1991;82(4):239-59.
45. Braak H, Braak E. Evolution of neuronal changes in the course of Alzheimer's disease. J Neural Transm Suppl 1998;53:127-40.
46. McKhann GM, Knopman DS, Chertkow H, Hyman BT, Jack CR, Jr., Kawas CH, Klunk WE, Koroshetz WJ, Manly JJ, Mayeux R and others. The diagnosis of dementia due to Alzheimer's disease: recommendations from the National Institute on Aging-Alzheimer's Association workgroups on diagnostic guidelines for Alzheimer's disease. Alzheimers Dement 2011;7(3):263-9.
47. Faber-Langendoen K, Morris JC, Knesevich JW, LaBarge E, Miller JP, Berg L. Aphasia in senile dementia of the Alzheimer type. Ann Neurol 1988;23(4):365-70.
48. Swearer JM, Drachman DA, O'Donnell BF, Mitchell AL. Troublesome and disruptive behaviors in dementia. Relationships to diagnosis and disease severity. J Am Geriatr Soc 1988;36(9):784-90.
49. Ropacki SA, Jeste DV. Epidemiology of and risk factors for psychosis of Alzheimer's disease: a review of 55 studies published from 1990 to 2003. Am J Psychiatry 2005;162(11):2022-30.

50. Morris JC, Drazner M, Fulling K, Grant EA, Goldring J. Clinical and pathological aspects of parkinsonism in Alzheimer's disease. A role for extranigral factors? Arch Neurol 1989;46(6):651-7.
51. Querfurth HW, LaFerla FM. Alzheimer's disease. N Engl J Med 2010;362(4):329-44.
52. Hardy J. The amyloid hypothesis for Alzheimer's disease: a critical reappraisal. J Neurochem 2009;110(4):1129-34.
53. Jonsson T, Atwal JK, Steinberg S, Snaedal J, Jonsson PV, Bjornsson S, Stefansson H, Sulem P, Gudbjartsson D, Maloney J and others. A mutation in APP protects against Alzheimer's disease and age-related cognitive decline. Nature 2012;488(7409):96-9.
54. Frost B, Jacks RL, Diamond MI. Propagation of tau misfolding from the outside to the inside of a cell. J Biol Chem 2009;284(19):12845-52.
55. Extance A. Alzheimer's failure raises questions about disease-modifying strategies. Nat Rev Drug Discov 2010;9(10):749-51.
56. Arriagada PV, Growdon JH, Hedley-Whyte ET, Hyman BT. Neurofibrillary tangles but not senile plaques parallel duration and severity of Alzheimer's disease. Neurology 1992;42(3 Pt 1):631-9.
57. Santacruz K, Lewis J, Spires T, Paulson J, Kotilinek L, Ingelsson M, Guimaraes A, DeTure M, Ramsden M, McGowan E and others. Tau suppression in a neurodegenerative mouse model improves memory function. Science 2005;309(5733):476-81.
58. Gomez-Isla T, Hollister R, West H, Mui S, Growdon JH, Petersen RC, Parisi JE, Hyman BT. Neuronal loss correlates with but exceeds neurofibrillary tangles in Alzheimer's disease. Ann Neurol 1997;41(1):17-24.
59. Alves L, Correia AS, Miguel R, Alegria P, Bugalho P. Alzheimer's disease: a clinical practice-oriented review. Front Neurol 2012;3:63.
60. Goldman JS, Hahn SE, Catania JW, LaRusse-Eckert S, Butson MB, Rumbaugh M, Strecker MN, Roberts JS, Burke W, Mayeux R and others. Genetic counseling and testing for Alzheimer disease: joint practice guidelines of the American College of Medical Genetics and the National Society of Genetic Counselors. Genet Med 2011;13(6):597-605.
61. Cruts M, Theuns J, Van Broeckhoven C. Locus-specific mutation databases for neurodegenerative brain diseases. Hum Mutat 2012;33(9):1340-4.
62. Bertram L, Tanzi RE. The genetic epidemiology of neurodegenerative disease. J Clin Invest 2005;115(6):1449-57.
63. Campion D, Dumanchin C, Hannequin D, Dubois B, Belliard S, Puel M, Thomas-Anterion C, Michon A, Martin C, Charbonnier F and others. Early-onset autosomal dominant Alzheimer disease: prevalence, genetic heterogeneity, and mutation spectrum. Am J Hum Genet 1999;65(3):664-70.
64. Sherrington R, Froelich S, Sorbi S, Campion D, Chi H, Rogaeva EA, Levesque G, Rogaev EI, Lin C, Liang Y and others. Alzheimer's disease associated with mutations in presenilin 2 is rare and variably penetrant. Hum Mol Genet 1996;5(7):985-8.

65. Coon KD, Myers AJ, Craig DW, Webster JA, Pearson JV, Lince DH, Zismann VL, Beach TG, Leung D, Bryden L and others. A high-density whole-genome association study reveals that APOE is the major susceptibility gene for sporadic late-onset Alzheimer's disease. J Clin Psychiatry 2007;68(4):613-8.
66. Nussbaum RL, Ellis CE. Alzheimer's disease and Parkinson's disease. N Engl J Med 2003;348(14):1356-64.
67. Naj AC, Jun G, Beecham GW, Wang LS, Vardarajan BN, Buros J, Gallins PJ, Buxbaum JD, Jarvik GP, Crane PK and others. Common variants at MS4A4/MS4A6E, CD2AP, CD33 and EPHA1 are associated with late-onset Alzheimer's disease. Nat Genet 2011;43(5):436-41.
68. Morgan K. The three new pathways leading to Alzheimer's disease. Neuropathol Appl Neurobiol 2011;37(4):353-7.
69. Lambert JC, Amouyel P. Genetics of Alzheimer's disease: new evidences for an old hypothesis? Curr Opin Genet Dev 2011;21(3):295-301.
70. Mawuenyega KG, Sigurdson W, Ovod V, Munsell L, Kasten T, Morris JC, Yarasheski KE, Bateman RJ. Decreased clearance of CNS beta-amyloid in Alzheimer's disease. Science 2010;330(6012):1774.
71. Fotenos AF, Mintun MA, Snyder AZ, Morris JC, Buckner RL. Brain volume decline in aging: evidence for a relation between socioeconomic status, preclinical Alzheimer disease, and reserve. Arch Neurol 2008;65(1):113-20.
72. Rentz DM, Locascio JJ, Becker JA, Moran EK, Eng E, Buckner RL, Sperling RA, Johnson KA. Cognition, reserve, and amyloid deposition in normal aging. Ann Neurol 2010;67(3):353-64.
73. Wingo TS, Lah JJ, Levey AI, Cutler DJ. Autosomal recessive causes likely in early-onset Alzheimer disease. Arch Neurol 2012;69(1):59-64.
74. Gatz M, Pedersen NL, Berg S, Johansson B, Johansson K, Mortimer JA, Posner SF, Viitanen M, Winblad B, Ahlbom A. Heritability for Alzheimer's disease: the study of dementia in Swedish twins. J Gerontol A Biol Sci Med Sci 1997;52(2):M117-25.
75. Gatz M, Reynolds CA, Fratiglioni L, Johansson B, Mortimer JA, Berg S, Fiske A, Pedersen NL. Role of genes and environments for explaining Alzheimer disease. Arch Gen Psychiatry 2006;63(2):168-74.
76. Games D, Adams D, Alessandrini R, Barbour R, Berthelette P, Blackwell C, Carr T, Clemens J, Donaldson T, Gillespie F and others. Alzheimer-type neuropathology in transgenic mice overexpressing V717F beta-amyloid precursor protein. Nature 1995;373(6514):523-7.
77. Van Dam D, De Deyn PP. Drug discovery in dementia: the role of rodent models. Nat Rev Drug Discov 2006;5(11):956-70.
78. Radde R, Duma C, Goedert M, Jucker M. The value of incomplete mouse models of Alzheimer's disease. Eur J Nucl Med Mol Imaging 2008;35 Suppl 1:S70-4.
79. Lewis J, Dickson DW, Lin WL, Chisholm L, Corral A, Jones G, Yen SH, Sahara N, Skipper L, Yager D and others. Enhanced neurofibrillary degeneration in transgenic mice expressing mutant tau and APP. Science 2001;293(5534):1487-91.

80. Harvey BK, Richie CT, Hoffer BJ, Airavaara M. Transgenic animal models of neurodegeneration based on human genetic studies. J Neural Transm 2011;118(1):27-45.
81. Van Dam D, De Deyn PP. Animal models in the drug discovery pipeline for Alzheimer's disease. Br J Pharmacol 2011;164(4):1285-300.
82. Spires TL, Hyman BT. Transgenic models of Alzheimer's disease: learning from animals. NeuroRx 2005;2(3):423-37.
83. McGowan E, Eriksen J, Hutton M. A decade of modeling Alzheimer's disease in transgenic mice. Trends Genet 2006;22(5):281-9.
84. Frolich L. The cholinergic pathology in Alzheimer's disease--discrepancies between clinical experience and pathophysiological findings. J Neural Transm 2002;109(7-8):1003-13.
85. Schneider LS, Insel PS, Weiner MW. Treatment with cholinesterase inhibitors and memantine of patients in the Alzheimer's Disease Neuroimaging Initiative. Arch Neurol 2011;68(1):58-66.
86. Raschetti R, Albanese E, Vanacore N, Maggini M. Cholinesterase inhibitors in mild cognitive impairment: a systematic review of randomised trials. PLoS Med 2007;4(11):e338.
87. Schneider LS, Dagerman KS, Higgins JP, McShane R. Lack of evidence for the efficacy of memantine in mild Alzheimer disease. Arch Neurol 2011;68(8):991-8.
88. Petersen RC, Thomas RG, Grundman M, Bennett D, Doody R, Ferris S, Galasko D, Jin S, Kaye J, Levey A and others. Vitamin E and donepezil for the treatment of mild cognitive impairment. N Engl J Med 2005;352(23):2379-88.
89. Feldman HH, Ferris S, Winblad B, Sfikas N, Mancione L, He Y, Tekin S, Burns A, Cummings J, del Ser T and others. Effect of rivastigmine on delay to diagnosis of Alzheimer's disease from mild cognitive impairment: the InDDEx study. Lancet Neurol 2007;6(6):501-12.
90. Ballard C, Khan Z, Clack H, Corbett A. Nonpharmacological treatment of Alzheimer disease. Can J Psychiatry 2011;56(10):589-95.
91. Hort J, O'Brien JT, Gainotti G, Pirttila T, Popescu BO, Rektorova I, Sorbi S, Scheltens P. EFNS guidelines for the diagnosis and management of Alzheimer's disease. Eur J Neurol 2010;17(10):1236-48.
92. "Drugs In Clinical Trials". The Alzheimer Research Forum.
93. Watson GS, Cholerton BA, Reger MA, Baker LD, Plymate SR, Asthana S, Fishel MA, Kulstad JJ, Green PS, Cook DG and others. Preserved cognition in patients with early Alzheimer disease and amnestic mild cognitive impairment during treatment with rosiglitazone: a preliminary study. Am J Geriatr Psychiatry 2005;13(11):950-8.
94. Paris D, Bachmeier C, Patel N, Quadros A, Volmar CH, Laporte V, Ganey J, Beaulieu-Abdelahad D, Ait-Ghezala G, Crawford F and others. Selective antihypertensive dihydropyridines lower Abeta accumulation by targeting both the production and the clearance of Abeta across the blood-brain barrier. Mol Med 2011;17(3-4):149-62.
95. Ghosh AK, Gemma S, Tang J. beta-Secretase as a therapeutic target for Alzheimer's disease. Neurotherapeutics 2008;5(3):399-408.

96. Schor NF. What the halted phase III gamma-secretase inhibitor trial may (or may not) be telling us. Ann Neurol 2011;69(2):237-9.
97. Town T. Alternative Abeta immunotherapy approaches for Alzheimer's disease. CNS Neurol Disord Drug Targets 2009;8(2):114-27.
98. Gervais F, Paquette J, Morissette C, Krzywkowski P, Yu M, Azzi M, Lacombe D, Kong X, Aman A, Laurin J and others. Targeting soluble Abeta peptide with Tramiprosate for the treatment of brain amyloidosis. Neurobiol Aging 2007;28(4):537-47.
99. Walsh DM, Selkoe DJ. A beta oligomers - a decade of discovery. J Neurochem 2007;101(5):1172-84.
100. Tariot PN, Aisen PS. Can lithium or valproate untie tangles in Alzheimer's disease? J Clin Psychiatry 2009;70(6):919-21.
101. Oz M, Lorke DE, Petroianu GA. Methylene blue and Alzheimer's disease. Biochem Pharmacol 2009;78(8):927-32.
102. Allen SJ, Watson JJ, Dawbarn D. The neurotrophins and their role in Alzheimer's disease. Curr Neuropharmacol 2011;9(4):559-73.
103. Su B, Wang X, Bonda D, Perry G, Smith M, Zhu X. Abnormal mitochondrial dynamics--a novel therapeutic target for Alzheimer's disease? Mol Neurobiol 2010;41(2-3):87-96.
104. Sabbagh MN, Agro A, Bell J, Aisen PS, Schweizer E, Galasko D. PF-04494700, an oral inhibitor of receptor for advanced glycation end products (RAGE), in Alzheimer disease. Alzheimer Dis Assoc Disord 2011;25(3):206-12.
105. Laxton AW, Tang-Wai DF, McAndrews MP, Zumsteg D, Wennberg R, Keren R, Wherrett J, Naglie G, Hamani C, Smith GS and others. A phase I trial of deep brain stimulation of memory circuits in Alzheimer's disease. Ann Neurol 2010;68(4):521-34.
106. Salomone S, Caraci F, Leggio GM, Fedotova J, Drago F. New pharmacological strategies for treatment of Alzheimer's disease: focus on disease modifying drugs. Br J Clin Pharmacol 2012;73(4):504-17.
107. Ji W, Ha I. Drug development for Alzheimer's disease: recent progress. Exp Neurobiol 2010;19(3):120-31.
108. Vellas B, Aisen PS, Sampaio C, Carrillo M, Scheltens P, Scherrer B, Frisoni GB, Weiner M, Schneider L, Gauthier S and others. Prevention trials in Alzheimer's disease: an EU-US task force report. Prog Neurobiol 2011;95(4):594-600.
109. Albert MS, DeKosky ST, Dickson D, Dubois B, Feldman HH, Fox NC, Gamst A, Holtzman DM, Jagust WJ, Petersen RC and others. The diagnosis of mild cognitive impairment due to Alzheimer's disease: recommendations from the National Institute on Aging-Alzheimer's Association workgroups on diagnostic guidelines for Alzheimer's disease. Alzheimers Dement 2011;7(3):270-9.
110. Sperling RA, Aisen PS, Beckett LA, Bennett DA, Craft S, Fagan AM, Iwatsubo T, Jack CR, Jr., Kaye J, Montine TJ and others. Toward defining the preclinical stages of Alzheimer's disease: recommendations from the National Institute on Aging-Alzheimer's Association workgroups on diagnostic guidelines for Alzheimer's disease. Alzheimers Dement 2011;7(3):280-92.

111. Marchesi VT. Alzheimer's disease 2012: the great amyloid gamble. Am J Pathol 2012;180(5):1762-7.
112. McKhann G, Drachman D, Folstein M, Katzman R, Price D, Stadlan EM. Clinical diagnosis of Alzheimer's disease: report of the NINCDS-ADRDA Work Group under the auspices of Department of Health and Human Services Task Force on Alzheimer's Disease. Neurology 1984;34(7):939-44.
113. Diagnostic and Statistical Manual of Mental disorders, 4th Edition, Washington DC.: American Psychiatric Association; 2000.
114. Knopman DS, DeKosky ST, Cummings JL, Chui H, Corey-Bloom J, Relkin N, Small GW, Miller B, Stevens JC. Practice parameter: diagnosis of dementia (an evidence-based review). Report of the Quality Standards Subcommittee of the American Academy of Neurology. Neurology 2001;56(9):1143-53.
115. Cummings JL. Biomarkers in Alzheimer's disease drug development. Alzheimers Dement 2011;7(3):e13-44.
116. Petersen RC, Negash S. Mild cognitive impairment: an overview. CNS Spectr 2008;13(1):45-53.
117. Dubois B, Feldman HH, Jacova C, Dekosky ST, Barberger-Gateau P, Cummings J, Delacourte A, Galasko D, Gauthier S, Jicha G and others. Research criteria for the diagnosis of Alzheimer's disease: revising the NINCDS-ADRDA criteria. Lancet Neurol 2007;6(8):734-46.
118. Jack CR, Jr., Knopman DS, Jagust WJ, Shaw LM, Aisen PS, Weiner MW, Petersen RC, Trojanowski JQ. Hypothetical model of dynamic biomarkers of the Alzheimer's pathological cascade. Lancet Neurol 2010;9(1):119-28.
119. Nelson PT, Alafuzoff I, Bigio EH, Bouras C, Braak H, Cairns NJ, Castellani RJ, Crain BJ, Davies P, Del Tredici K and others. Correlation of Alzheimer disease neuropathologic changes with cognitive status: a review of the literature. J Neuropathol Exp Neurol 2012;71(5):362-81.
120. Jack CR, Jr., Vemuri P, Wiste HJ, Weigand SD, Aisen PS, Trojanowski JQ, Shaw LM, Bernstein MA, Petersen RC, Weiner MW and others. Evidence for ordering of Alzheimer disease biomarkers. Arch Neurol 2011;68(12):1526-35.
121. Klunk WE, Wang Y, Huang GF, Debnath ML, Holt DP, Mathis CA. Uncharged thioflavin-T derivatives bind to amyloid-beta protein with high affinity and readily enter the brain. Life Sci 2001;69(13):1471-84.
122. Agdeppa ED, Kepe V, Liu J, Flores-Torres S, Satyamurthy N, Petric A, Cole GM, Small GW, Huang SC, Barrio JR. Binding characteristics of radiofluorinated 6-dialkylamino-2-naphthylethylidene derivatives as positron emission tomography imaging probes for beta-amyloid plaques in Alzheimer's disease. J Neurosci 2001;21(24):RC189.
123. Ono M, Wilson A, Nobrega J, Westaway D, Verhoeff P, Zhuang ZP, Kung MP, Kung HF. 11C-labeled stilbene derivatives as Abeta-aggregate-specific PET imaging agents for Alzheimer's disease. Nucl Med Biol 2003;30(6):565-71.
124. Klunk WE, Engler H, Nordberg A, Wang Y, Blomqvist G, Holt DP, Bergstrom M, Savitcheva I, Huang GF, Estrada S and others. Imaging

brain amyloid in Alzheimer's disease with Pittsburgh Compound-B. Ann Neurol 2004;55(3):306-19.
125. Rowe CC, Ackerman U, Browne W, Mulligan R, Pike KL, O'Keefe G, Tochon-Danguy H, Chan G, Berlangieri SU, Jones G and others. Imaging of amyloid beta in Alzheimer's disease with 18F-BAY94-9172, a novel PET tracer: proof of mechanism. Lancet Neurol 2008;7(2):129-35.
126. Koole M, Lewis DM, Buckley C, Nelissen N, Vandenbulcke M, Brooks DJ, Vandenberghe R, Van Laere K. Whole-body biodistribution and radiation dosimetry of 18F-GE067: a radioligand for in vivo brain amyloid imaging. J Nucl Med 2009;50(5):818-22.
127. Kung HF, Choi SR, Qu W, Zhang W, Skovronsky D. 18F stilbenes and styrylpyridines for PET imaging of A beta plaques in Alzheimer's disease: a miniperspective. J Med Chem 2010;53(3):933-41.
128. Klunk WE. Amyloid imaging as a biomarker for cerebral beta-amyloidosis and risk prediction for Alzheimer dementia. Neurobiol Aging 2011;32 Suppl 1:S20-36.
129. Mayeux R, Saunders AM, Shea S, Mirra S, Evans D, Roses AD, Hyman BT, Crain B, Tang MX, Phelps CH. Utility of the apolipoprotein E genotype in the diagnosis of Alzheimer's disease. Alzheimer's Disease Centers Consortium on Apolipoprotein E and Alzheimer's Disease. N Engl J Med 1998;338(8):506-11.
130. Hansson O, Zetterberg H, Buchhave P, Londos E, Blennow K, Minthon L. Association between CSF biomarkers and incipient Alzheimer's disease in patients with mild cognitive impairment: a follow-up study. Lancet Neurol 2006;5(3):228-34.
131. Mitchell AJ, Shiri-Feshki M. Rate of progression of mild cognitive impairment to dementia--meta-analysis of 41 robust inception cohort studies. Acta Psychiatr Scand 2009;119(4):252-65.
132. Ganguli M, Dodge HH, Shen C, DeKosky ST. Mild cognitive impairment, amnestic type: an epidemiologic study. Neurology 2004;63(1):115-21.
133. Larrieu S, Letenneur L, Orgogozo JM, Fabrigoule C, Amieva H, Le Carret N, Barberger-Gateau P, Dartigues JF. Incidence and outcome of mild cognitive impairment in a population-based prospective cohort. Neurology 2002;59(10):1594-9.
134. Morris JC, Roe CM, Grant EA, Head D, Storandt M, Goate AM, Fagan AM, Holtzman DM, Mintun MA. Pittsburgh compound B imaging and prediction of progression from cognitive normality to symptomatic Alzheimer disease. Arch Neurol 2009;66(12):1469-75.
135. Lockhart A, Lamb JR, Osredkar T, Sue LI, Joyce JN, Ye L, Libri V, Leppert D, Beach TG. PIB is a non-specific imaging marker of amyloid-beta (Abeta) peptide-related cerebral amyloidosis. Brain 2007;130(Pt 10):2607-15.
136. Bacskai BJ, Frosch MP, Freeman SH, Raymond SB, Augustinack JC, Johnson KA, Irizarry MC, Klunk WE, Mathis CA, Dekosky ST and others. Molecular imaging with Pittsburgh Compound B confirmed at autopsy: a case report. Arch Neurol 2007;64(3):431-4.
137. Ikonomovic MD, Klunk WE, Abrahamson EE, Mathis CA, Price JC, Tsopelas ND, Lopresti BJ, Ziolko S, Bi W, Paljug WR and others. Post-

mortem correlates of in vivo PiB-PET amyloid imaging in a typical case of Alzheimer's disease. Brain 2008;131(Pt 6):1630-45.
138. Cairns NJ, Ikonomovic MD, Benzinger T, Storandt M, Fagan AM, Shah AR, Reinwald LT, Carter D, Felton A, Holtzman DM and others. Absence of Pittsburgh compound B detection of cerebral amyloid beta in a patient with clinical, cognitive, and cerebrospinal fluid markers of Alzheimer disease: a case report. Arch Neurol 2009;66(12):1557-62.
139. Villemagne VL, McLean CA, Reardon K, Boyd A, Lewis V, Klug G, Jones G, Baxendale D, Masters CL, Rowe CC and others. 11C-PiB PET studies in typical sporadic Creutzfeldt-Jakob disease. J Neurol Neurosurg Psychiatry 2009;80(9):998-1001.
140. Burack MA, Hartlein J, Flores HP, Taylor-Reinwald L, Perlmutter JS, Cairns NJ. In vivo amyloid imaging in autopsy-confirmed Parkinson disease with dementia. Neurology 2010;74(1):77-84.
141. Kantarci K, Yang C, Schneider JA, Senjem ML, Reyes DA, Lowe VJ, Barnes LL, Aggarwal NT, Bennett DA, Smith GE and others. Ante mortem amyloid imaging and beta-amyloid pathology in a case with dementia with Lewy bodies. Neurobiol Aging 2012;33(5):878-85.
142. Kadir A, Marutle A, Gonzalez D, Scholl M, Almkvist O, Mousavi M, Mustafiz T, Darreh-Shori T, Nennesmo I, Nordberg A. Positron emission tomography imaging and clinical progression in relation to molecular pathology in the first Pittsburgh Compound B positron emission tomography patient with Alzheimer's disease. Brain 2011;134(Pt 1):301-17.
143. Sojkova J, Driscoll I, Iacono D, Zhou Y, Codispoti KE, Kraut MA, Ferrucci L, Pletnikova O, Mathis CA, Klunk WE and others. In vivo fibrillar beta-amyloid detected using [11C]PiB positron emission tomography and neuropathologic assessment in older adults. Arch Neurol 2011;68(2):232-40.
144. Ikonomovic MD, Abrahamson EE, Price JC, Hamilton RL, Mathis CA, Paljug WR, Debnath ML, Cohen AD, Mizukami K, DeKosky ST and others. Early AD pathology in a [C-11]PiB-negative case: a PiB-amyloid imaging, biochemical, and immunohistochemical study. Acta Neuropathol 2012;123(3):433-47.
145. Leinonen V, Alafuzoff I, Aalto S, Suotunen T, Savolainen S, Nagren K, Tapiola T, Pirttila T, Rinne J, Jaaskelainen JE and others. Assessment of beta-amyloid in a frontal cortical brain biopsy specimen and by positron emission tomography with carbon 11-labeled Pittsburgh Compound B. Arch Neurol 2008;65(10):1304-9.
146. Mirra SS, Heyman A, McKeel D, Sumi SM, Crain BJ, Brownlee LM, Vogel FS, Hughes JP, van Belle G, Berg L. The Consortium to Establish a Registry for Alzheimer's Disease (CERAD). Part II. Standardization of the neuropathologic assessment of Alzheimer's disease. Neurology 1991;41(4):479-86.
147. Rosen RF, Ciliax BJ, Wingo TS, Gearing M, Dooyema J, Lah JJ, Ghiso JA, LeVine H, 3rd, Walker LC. Deficient high-affinity binding of Pittsburgh compound B in a case of Alzheimer's disease. Acta Neuropathol 2010;119(2):221-33.

148. Roher AE, Lowenson JD, Clarke S, Wolkow C, Wang R, Cotter RJ, Reardon IM, Zurcher-Neely HA, Heinrikson RL, Ball MJ and others. Structural alterations in the peptide backbone of beta-amyloid core protein may account for its deposition and stability in Alzheimer's disease. J Biol Chem 1993;268(5):3072-83.
149. Naslund J, Haroutunian V, Mohs R, Davis KL, Davies P, Greengard P, Buxbaum JD. Correlation between elevated levels of amyloid beta-peptide in the brain and cognitive decline. JAMA 2000;283(12):1571-7.
150. Dong J, Revilla-Sanchez R, Moss S, Haydon PG. Multiphoton in vivo imaging of amyloid in animal models of Alzheimer's disease. Neuropharmacology 2010;59(4-5):268-75.
151. Bacskai BJ, Hickey GA, Skoch J, Kajdasz ST, Wang Y, Huang GF, Mathis CA, Klunk WE, Hyman BT. Four-dimensional multiphoton imaging of brain entry, amyloid binding, and clearance of an amyloid-beta ligand in transgenic mice. Proc Natl Acad Sci U S A 2003;100(21):12462-7.
152. Jack CR, Jr., Garwood M, Wengenack TM, Borowski B, Curran GL, Lin J, Adriany G, Grohn OH, Grimm R, Poduslo JF. In vivo visualization of Alzheimer's amyloid plaques by magnetic resonance imaging in transgenic mice without a contrast agent. Magn Reson Med 2004;52(6):1263-71.
153. Meadowcroft MD, Connor JR, Smith MB, Yang QX. MRI and histological analysis of beta-amyloid plaques in both human Alzheimer's disease and APP/PS1 transgenic mice. J Magn Reson Imaging 2009;29(5):997-1007.
154. Jack CR, Jr., Marjanska M, Wengenack TM, Reyes DA, Curran GL, Lin J, Preboske GM, Poduslo JF, Garwood M. Magnetic resonance imaging of Alzheimer's pathology in the brains of living transgenic mice: a new tool in Alzheimer's disease research. Neuroscientist 2007;13(1):38-48.
155. Jack CR, Jr., Wengenack TM, Reyes DA, Garwood M, Curran GL, Borowski BJ, Lin J, Preboske GM, Holasek SS, Adriany G and others. In vivo magnetic resonance microimaging of individual amyloid plaques in Alzheimer's transgenic mice. J Neurosci 2005;25(43):10041-8.
156. Higuchi M, Iwata N, Matsuba Y, Sato K, Sasamoto K, Saido TC. 19F and 1H MRI detection of amyloid beta plaques in vivo. Nat Neurosci 2005;8(4):527-33.
157. Jack CR, Jr. Alzheimer disease: new concepts on its neurobiology and the clinical role imaging will play. Radiology 2012;263(2):344-61.
158. Flood DG, Lin YG, Lang DM, Trusko SP, Hirsch JD, Savage MJ, Scott RW, Howland DS. A transgenic rat model of Alzheimer's disease with extracellular Abeta deposition. Neurobiol Aging 2009;30(7):1078-90.
159. Bugos O, Bhide M, Zilka N. Beyond the rat models of human neurodegenerative disorders. Cell Mol Neurobiol 2009;29(6-7):859-69.
160. Woodruff-Pak DS. Animal models of Alzheimer's disease: therapeutic implications. J Alzheimers Dis 2008;15(4):507-21.
161. Howlett DR. APP transgenic mice and their application to drug discovery. Histol Histopathol 2011;26(12):1611-32.
162. Klunk WE, Lopresti BJ, Ikonomovic MD, Lefterov IM, Koldamova RP, Abrahamson EE, Debnath ML, Holt DP, Huang GF, Shao L and others. Binding of the positron emission tomography tracer Pittsburgh

compound-B reflects the amount of amyloid-beta in Alzheimer's disease brain but not in transgenic mouse brain. J Neurosci 2005;25(46):10598-606.

163. Toyama H, Ye D, Ichise M, Liow JS, Cai L, Jacobowitz D, Musachio JL, Hong J, Crescenzo M, Tipre D and others. PET imaging of brain with the beta-amyloid probe, [11C]6-OH-BTA-1, in a transgenic mouse model of Alzheimer's disease. Eur J Nucl Med Mol Imaging 2005;32(5):593-600.
164. Maeda J, Ji B, Irie T, Tomiyama T, Maruyama M, Okauchi T, Staufenbiel M, Iwata N, Ono M, Saido TC and others. Longitudinal, quantitative assessment of amyloid, neuroinflammation, and anti-amyloid treatment in a living mouse model of Alzheimer's disease enabled by positron emission tomography. J Neurosci 2007;27(41):10957-68.
165. Saido TC, Iwatsubo T, Mann DM, Shimada H, Ihara Y, Kawashima S. Dominant and differential deposition of distinct beta-amyloid peptide species, A beta N3(pE), in senile plaques. Neuron 1995;14(2):457-66.
166. Guntert A, Dobeli H, Bohrmann B. High sensitivity analysis of amyloid-beta peptide composition in amyloid deposits from human and PS2APP mouse brain. Neuroscience 2006;143(2):461-75.
167. Kawarabayashi T, Younkin LH, Saido TC, Shoji M, Ashe KH, Younkin SG. Age-dependent changes in brain, CSF, and plasma amyloid (beta) protein in the Tg2576 transgenic mouse model of Alzheimer's disease. J Neurosci 2001;21(2):372-81.
168. Manook A, Yousefi BH, Willuweit A, Platzer S, Reder S, Voss A, Huisman M, Settles M, Neff F, Velden J and others. Small-Animal PET Imaging of Amyloid-Beta Plaques with [C]PiB and Its Multi-Modal Validation in an APP/PS1 Mouse Model of Alzheimer's Disease. PLoS One 2012;7(3):e31310.
169. Yousefi BH, Manook A, Drzezga A, von Reutern B, Schwaiger M, Wester HJ, Henriksen G. Synthesis and evaluation of 11C-labeled imidazo[2,1-b]benzothiazoles (IBTs) as PET tracers for imaging beta-amyloid plaques in Alzheimer's disease. J Med Chem 2011;54(4):949-56.
170. Poisnel G, Dhilly M, Moustie O, Delamare J, Abbas A, Guilloteau D, Barre L. PET imaging with [18F]AV-45 in an APP/PS1-21 murine model of amyloid plaque deposition. Neurobiol Aging 2012;33(11):2561-71.
171. Kim TK, Lee JE, Park SK, Lee KW, Seo JS, Im JY, Kim ST, Lee JY, Kim YH, Lee JK and others. Analysis of differential plaque depositions in the brains of Tg2576 and Tg-APPswe/PS1dE9 transgenic mouse models of Alzheimer disease. Exp Mol Med 2012;44(8):492-502.
172. Wolf DS, Gearing M, Snowdon DA, Mori H, Markesbery WR, Mirra SS. Progression of regional neuropathology in Alzheimer disease and normal elderly: findings from the Nun study. Alzheimer Dis Assoc Disord 1999;13(4):226-31.
173. Morris JC, Storandt M, McKeel DW, Jr., Rubin EH, Price JL, Grant EA, Berg L. Cerebral amyloid deposition and diffuse plaques in "normal" aging: Evidence for presymptomatic and very mild Alzheimer's disease. Neurology 1996;46(3):707-19.
174. Willuweit A, Velden J, Godemann R, Manook A, Jetzek F, Tintrup H, Kauselmann G, Zevnik B, Henriksen G, Drzezga A and others. Early-

onset and robust amyloid pathology in a new homozygous mouse model of Alzheimer's disease. PLoS One 2009;4(11):e7931.
175. Hsiao K, Chapman P, Nilsen S, Eckman C, Harigaya Y, Younkin S, Yang F, Cole G. Correlative memory deficits, Abeta elevation, and amyloid plaques in transgenic mice. Science 1996;274(5284):99-102.
176. Mullan M, Crawford F, Axelman K, Houlden H, Lilius L, Winblad B, Lannfelt L. A pathogenic mutation for probable Alzheimer's disease in the APP gene at the N-terminus of beta-amyloid. Nat Genet 1992;1(5):345-7.
177. Clark RF, Hutton M, Fuldner M, Froelich S. The structure of the presenilin 1 (S182) gene and identification of six novel mutations in early onset AD families. Alzheimer's Disease Collaborative Group. Nat Genet 1995;11(2):219-22.
178. Visser EP, Disselhorst JA, Brom M, Laverman P, Gotthardt M, Oyen WJ, Boerman OC. Spatial resolution and sensitivity of the Inveon small-animal PET scanner. J Nucl Med 2009;50(1):139-47.
179. Mandler M, Rockenstein E, Ubhi K, Hansen L, Adame A, Michael S, Galasko D, Santic R, Mattner F, Masliah E. Detection of peri-synaptic amyloid-beta pyroglutamate aggregates in early stages of Alzheimer's disease and in AbetaPP transgenic mice using a novel monoclonal antibody. J Alzheimers Dis 2012;28(4):783-94.
180. Paxinos G, Franklin KBJ. The mouse brain in stereotaxic coordinates. San Diego: Academic Press; 2001. xxv, 1 v. (various pagings) p.
181. Dickson TC, Vickers JC. The morphological phenotype of beta-amyloid plaques and associated neuritic changes in Alzheimer's disease. Neuroscience 2001;105(1):99-107.
182. Duyckaerts C, Dickson DW. Neurodegeneration: The Molecular Pathology of Dementia and Movement Disorders. ISN Neuropath Press, Basel; 2003.
183. Thal DR, Capetillo-Zarate E, Del Tredici K, Braak H. The development of amyloid beta protein deposits in the aged brain. Sci Aging Knowledge Environ 2006;2006(6):re1.
184. Dickson DW. Required techniques and useful molecular markers in the neuropathologic diagnosis of neurodegenerative diseases. Acta Neuropathol 2005;109(1):14-24.
185. Kuo YM, Kokjohn TA, Beach TG, Sue LI, Brune D, Lopez JC, Kalback WM, Abramowski D, Sturchler-Pierrat C, Staufenbiel M and others. Comparative analysis of amyloid-beta chemical structure and amyloid plaque morphology of transgenic mouse and Alzheimer's disease brains. J Biol Chem 2001;276(16):12991-8.
186. Kalback W, Watson MD, Kokjohn TA, Kuo YM, Weiss N, Luehrs DC, Lopez J, Brune D, Sisodia SS, Staufenbiel M and others. APP transgenic mice Tg2576 accumulate Abeta peptides that are distinct from the chemically modified and insoluble peptides deposited in Alzheimer's disease senile plaques. Biochemistry 2002;41(3):922-8.
187. Serdons K, Verduyckt T, Vanderghinste D, Cleynhens J, Borghgraef P, Vermaelen P, Terwinghe C, Van Leuven F, Van Laere K, Kung H and others. Synthesis of 18F-labelled 2-(4'-fluorophenyl)-1,3-benzothiazole

and evaluation as amyloid imaging agent in comparison with [11C]PIB. Bioorg Med Chem Lett 2009;19(3):602-5.
188. Rufenacht P, Guntert A, Bohrmann B, Ducret A, Dobeli H. Quantification of the A beta peptide in Alzheimer's plaques by laser dissection microscopy combined with mass spectrometry. J Mass Spectrom 2005;40(2):193-201.
189. Wirths O, Bethge T, Marcello A, Harmeier A, Jawhar S, Lucassen PJ, Multhaup G, Brody DL, Esparza T, Ingelsson M and others. Pyroglutamate Abeta pathology in APP/PS1KI mice, sporadic and familial Alzheimer's disease cases. J Neural Transm 2010;117(1):85-96.
190. Iwatsubo T, Odaka A, Suzuki N, Mizusawa H, Nukina N, Ihara Y. Visualization of A beta 42(43) and A beta 40 in senile plaques with end-specific A beta monoclonals: evidence that an initially deposited species is A beta 42(43). Neuron 1994;13(1):45-53.
191. Hefendehl JK, Wegenast-Braun BM, Liebig C, Eicke D, Milford D, Calhoun ME, Kohsaka S, Eichner M, Jucker M. Long-term in vivo imaging of beta-amyloid plaque appearance and growth in a mouse model of cerebral beta-amyloidosis. J Neurosci 2011;31(2):624-9.
192. Pike CJ, Overman MJ, Cotman CW. Amino-terminal deletions enhance aggregation of beta-amyloid peptides in vitro. J Biol Chem 1995;270(41):23895-8.
193. He W, Barrow CJ. The A beta 3-pyroglutamyl and 11-pyroglutamyl peptides found in senile plaque have greater beta-sheet forming and aggregation propensities in vitro than full-length A beta. Biochemistry 1999;38(33):10871-7.
194. Schilling S, Lauber T, Schaupp M, Manhart S, Scheel E, Bohm G, Demuth HU. On the seeding and oligomerization of pGlu-amyloid peptides (in vitro). Biochemistry 2006;45(41):12393-9.
195. Harigaya Y, Saido TC, Eckman CB, Prada CM, Shoji M, Younkin SG. Amyloid beta protein starting pyroglutamate at position 3 is a major component of the amyloid deposits in the Alzheimer's disease brain. Biochem Biophys Res Commun 2000;276(2):422-7.
196. Schlenzig D, Manhart S, Cinar Y, Kleinschmidt M, Hause G, Willbold D, Funke SA, Schilling S, Demuth HU. Pyroglutamate formation influences solubility and amyloidogenicity of amyloid peptides. Biochemistry 2009;48(29):7072-8.
197. Ye L, Morgenstern JL, Lamb JR, Lockhart A. Characterisation of the binding of amyloid imaging tracers to rodent Abeta fibrils and rodent-human Abeta co-polymers. Biochem Biophys Res Commun 2006;347(3):669-77.
198. van Groen T, Kiliaan AJ, Kadish I. Deposition of mouse amyloid beta in human APP/PS1 double and single AD model transgenic mice. Neurobiol Dis 2006;23(3):653-62.
199. Scholl M, Wall A, Thordardottir S, Ferreira D, Bogdanovic N, Langstrom B, Almkvist O, Graff C, Nordberg A. Low PiB PET retention in presence of pathologic CSF biomarkers in Arctic APP mutation carriers. Neurology 2012;79(3):229-36.

200. Basun H, Bogdanovic N, Ingelsson M, Almkvist O, Naslund J, Axelman K, Bird TD, Nochlin D, Schellenberg GD, Wahlund LO and others. Clinical and neuropathological features of the arctic APP gene mutation causing early-onset Alzheimer disease. Arch Neurol 2008;65(4):499-505.
201. Verhoeff NP, Wilson AA, Takeshita S, Trop L, Hussey D, Singh K, Kung HF, Kung MP, Houle S. In-vivo imaging of Alzheimer disease beta-amyloid with [11C]SB-13 PET. Am J Geriatr Psychiatry 2004;12(6):584-95.
202. Price JC, Klunk WE, Lopresti BJ, Lu X, Hoge JA, Ziolko SK, Holt DP, Meltzer CC, DeKosky ST, Mathis CA. Kinetic modeling of amyloid binding in humans using PET imaging and Pittsburgh Compound-B. J Cereb Blood Flow Metab 2005;25(11):1528-47.
203. Lopresti BJ, Klunk WE, Mathis CA, Hoge JA, Ziolko SK, Lu X, Meltzer CC, Schimmel K, Tsopelas ND, DeKosky ST and others. Simplified quantification of Pittsburgh Compound B amyloid imaging PET studies: a comparative analysis. J Nucl Med 2005;46(12):1959-72.
204. Kemppainen NM, Aalto S, Wilson IA, Nagren K, Helin S, Bruck A, Oikonen V, Kailajarvi M, Scheinin M, Viitanen M and others. Voxel-based analysis of PET amyloid ligand [11C]PIB uptake in Alzheimer disease. Neurology 2006;67(9):1575-80.
205. Ziolko SK, Weissfeld LA, Klunk WE, Mathis CA, Hoge JA, Lopresti BJ, DeKosky ST, Price JC. Evaluation of voxel-based methods for the statistical analysis of PIB PET amyloid imaging studies in Alzheimer's disease. Neuroimage 2006;33(1):94-102.
206. Mikhno A, Devanand D, Pelton G, Cuasay K, Gunn R, Upton N, Lai RY, Libri V, Mann JJ, Parsey RV. Voxel-based analysis of 11C-PIB scans for diagnosing Alzheimer's disease. J Nucl Med 2008;49(8):1262-9.
207. Kemppainen NM, Aalto S, Wilson IA, Nagren K, Helin S, Bruck A, Oikonen V, Kailajarvi M, Scheinin M, Viitanen M and others. PET amyloid ligand [11C]PIB uptake is increased in mild cognitive impairment. Neurology 2007;68(19):1603-6.
208. Grimmer T, Henriksen G, Wester HJ, Forstl H, Klunk WE, Mathis CA, Kurz A, Drzezga A. Clinical severity of Alzheimer's disease is associated with PIB uptake in PET. Neurobiol Aging 2009;30(12):1902-9.
209. Shin J, Lee SY, Kim SJ, Kim SH, Cho SJ, Kim YB. Voxel-based analysis of Alzheimer's disease PET imaging using a triplet of radiotracers: PIB, FDDNP, and FDG. Neuroimage 2010;52(2):488-96.
210. Scheinin NM, Aalto S, Koikkalainen J, Lotjonen J, Karrasch M, Kemppainen N, Viitanen M, Nagren K, Helin S, Scheinin M and others. Follow-up of [11C]PIB uptake and brain volume in patients with Alzheimer disease and controls. Neurology 2009;73(15):1186-92.
211. Edison P, Archer HA, Gerhard A, Hinz R, Pavese N, Turkheimer FE, Hammers A, Tai YF, Fox N, Kennedy A and others. Microglia, amyloid, and cognition in Alzheimer's disease: An [11C](R)PK11195-PET and [11C]PIB-PET study. Neurobiol Dis 2008;32(3):412-9.
212. Jack CR, Jr., Lowe VJ, Senjem ML, Weigand SD, Kemp BJ, Shiung MM, Knopman DS, Boeve BF, Klunk WE, Mathis CA and others. 11C PiB and structural MRI provide complementary information in imaging of

Alzheimer's disease and amnestic mild cognitive impairment. Brain 2008;131(Pt 3):665-80.

213. Dubois A, Herard AS, Delatour B, Hantraye P, Bonvento G, Dhenain M, Delzescaux T. Detection by voxel-wise statistical analysis of significant changes in regional cerebral glucose uptake in an APP/PS1 transgenic mouse model of Alzheimer's disease. Neuroimage 2010;51(2):586-98.
214. Hooker JM, Patel V, Kothari S, Schiffer WK. Metabolic changes in the rodent brain after acute administration of salvinorin A. Mol Imaging Biol 2009;11(3):137-43.
215. Prieto E, Collantes M, Delgado M, Juri C, Garcia-Garcia L, Molinet F, Fernandez-Valle ME, Pozo MA, Gago B, Marti-Climent JM and others. Statistical parametric maps of (1)(8)F-FDG PET and 3-D autoradiography in the rat brain: a cross-validation study. Eur J Nucl Med Mol Imaging 2011;38(12):2228-37.
216. Casteels C, Bormans G, Van Laere K. The effect of anaesthesia on [(18)F]MK-9470 binding to the type 1 cannabinoid receptor in the rat brain. Eur J Nucl Med Mol Imaging 2010;37(6):1164-73.
217. Casteels C, Lauwers E, Baitar A, Bormans G, Baekelandt V, Van Laere K. In vivo type 1 cannabinoid receptor mapping in the 6-hydroxydopamine lesion rat model of Parkinson's disease. Brain Res 2010;1316:153-62.
218. Kemppainen NM, Aalto S, Karrasch M, Nagren K, Savisto N, Oikonen V, Viitanen M, Parkkola R, Rinne JO. Cognitive reserve hypothesis: Pittsburgh Compound B and fluorodeoxyglucose positron emission tomography in relation to education in mild Alzheimer's disease. Ann Neurol 2008;63(1):112-8.
219. Grunecker B, Kaltwasser SF, Peterse Y, Samann PG, Schmidt MV, Wotjak CT, Czisch M. Fractionated manganese injections: effects on MRI contrast enhancement and physiological measures in C57BL/6 mice. NMR Biomed 2010;23(8):913-21.
220. Brammer DW, Riley JM, Kreuser SC, Zasadny KR, Callahan MJ, Davis MD. Harderian gland adenectomy: a method to eliminate confounding radio-opacity in the assessment of rat brain metabolism by 18F-fluoro-2-deoxy-D-glucose positron emission tomography. J Am Assoc Lab Anim Sci 2007;46(5):42-5.
221. Fukuyama H, Hayashi T, Katsumi Y, Tsukada H, Shibasaki H. Issues in measuring glucose metabolism of rat brain using PET: the effect of harderian glands on the frontal lobe. Neurosci Lett 1998;255(2):99-102.
222. Kuge Y, Kawashima H, Yamazaki S, Hashimoto N, Miyake Y. [1-11C]octanoate as a potential PET tracer for studying glial functions: PET evaluation in rats and cats. Nucl Med Biol 1996;23(8):1009-12.
223. Kuge Y, Minematsu K, Hasegawa Y, Yamaguchi T, Mori H, Matsuura H, Hashimoto N, Miyake Y. Positron emission tomography for quantitative determination of glucose metabolism in normal and ischemic brains in rats: an insoluble problem by the Harderian glands. J Cereb Blood Flow Metab 1997;17(1):116-20.

224. Nestor PJ, Fryer TD, Smielewski P, Hodges JR. Limbic hypometabolism in Alzheimer's disease and mild cognitive impairment. Ann Neurol 2003;54(3):343-51.
225. Masters CL, Simms G, Weinman NA, Multhaup G, McDonald BL, Beyreuther K. Amyloid plaque core protein in Alzheimer disease and Down syndrome. Proc Natl Acad Sci U S A 1985;82(12):4245-9.
226. Grimmer T, Riemenschneider M, Forstl H, Henriksen G, Klunk WE, Mathis CA, Shiga T, Wester HJ, Kurz A, Drzezga A. Beta amyloid in Alzheimer's disease: increased deposition in brain is reflected in reduced concentration in cerebrospinal fluid. Biol Psychiatry 2009;65(11):927-34.
227. Riemenschneider M, Wagenpfeil S, Diehl J, Lautenschlager N, Theml T, Heldmann B, Drzezga A, Jahn T, Forstl H, Kurz A. Tau and Abeta42 protein in CSF of patients with frontotemporal degeneration. Neurology 2002;58(11):1622-8.
228. Sjogren M, Minthon L, Davidsson P, Granerus AK, Clarberg A, Vanderstichele H, Vanmechelen E, Wallin A, Blennow K. CSF levels of tau, beta-amyloid(1-42) and GAP-43 in frontotemporal dementia, other types of dementia and normal aging. J Neural Transm 2000;107(5):563-79.
229. Clark CM, Xie S, Chittams J, Ewbank D, Peskind E, Galasko D, Morris JC, McKeel DW, Jr., Farlow M, Weitlauf SL and others. Cerebrospinal fluid tau and beta-amyloid: how well do these biomarkers reflect autopsy-confirmed dementia diagnoses? Arch Neurol 2003;60(12):1696-702.
230. Hampel H, Buerger K, Zinkowski R, Teipel SJ, Goernitz A, Andreasen N, Sjoegren M, DeBernardis J, Kerkman D, Ishiguro K and others. Measurement of phosphorylated tau epitopes in the differential diagnosis of Alzheimer disease: a comparative cerebrospinal fluid study. Arch Gen Psychiatry 2004;61(1):95-102.
231. Yousefi B, Drzezga A, von Reutern B, Manook A, Schwaiger M. A Novel (18)F-Labeled Imidazo[2,1-b]benzothiazole (IBT) for High-Contrast PET Imaging of beta-Amyloid Plaques. Acs Medicinal Chemistry Letters 2011;2:673-677.
232. Martinez MJ, Bercier Y, Schwaiger M, Ziegler SI. PET/CT Biograph Sensation 16. Performance improvement using faster electronics. Nuklearmedizin 2006;45(3):126-33.
233. Delso G, Ziegler S. PET/MRI system design. Eur J Nucl Med Mol Imaging 2009;36 Suppl 1:S86-92.